X-692-74-52
PREPRINT

A STUDY OF THE SOLAR WIND ANGULAR MOMENTUM INCLUDING PROTON THERMAL ANISOTROPY

MARIO H. ACUÑA

FEBRUARY 1974

GODDARD SPACE FLIGHT CENTER
GREENBELT, MARYLAND

THE CATHOLIC UNIVERSITY OF AMERICA

" A STUDY OF THE SOLAR WIND ANGULAR MOMENTUM INCLUDING PROTON THERMAL ANISOTROPY "

A DISSERTATION

Submitted to the Faculty of the
School of Engineering and Architecture
Of the Catholic University of America
In Partial Fulfillment of the Requirements
For the Degree
Doctor of Philosophy

by

Mario H. Acuna
Washington, D.C.

1973

This dissertation was approved by Dr. Y.C. Whang as director and by Dr. L.F. Burlaga and Dr. T.J. Eisler as readers.

Director Y. C. Whang

Reader L. F. Burlaga

Reader _____

ACKNOWLEDGMENT

The author wishes to express his sincere appreciation to his thesis advisor, Professor Yun Chow Whang, for his encouragement and helpful suggestions during the course of this work.

It is a pleasure to acknowledge many helpful and enlightening discussions with Drs. L.F. Burlaga, F.M. Neubauer and Mr. J. Scudder.

ABSTRACT

The solution to the steady state magnetohydrodynamic equations governing the supersonic expansion of the solar corona into interplanetary space is obtained for various assumptions regarding the form in which proton thermal energy is carried away from the sun.

The one-fluid, inviscid, formulation of the MHD equations is considered first assuming that thermal energy is carried away by conduction from a heat source located at the base of the corona. The inclusion in the analysis of the angular motion of the solar wind, leads to the existence of three critical points through which the numerical solutions must pass to extend from the sun's surface to large heliocentric distances. The results show that the amount of magnetic field energy converted into kinetic energy in the solar wind is only a small fraction of the total expansion energy flux and has little effect upon the final radial expansion velocity.

The azimuthal velocity predicted by this model at 1 A.U. is 1.19 Km/sec., which is smaller that that indicated by experimental observations but in agreement with previous theoretical work in this field.

The two-fluid formulation of the MHD equations is obtained next under the assumption that the protons become collisionless and thermally anisotropic beyond a given radius. This formulation is then applied to a two-region model of the solar wind in which the flow in the inner region is described by the one-fluid equations and in the outer region

by the two-fluid formulation. It is shown that the effect of the proton thermal anisotropy upon the angular motion of the solar wind is small and cannot increase the predicted azimuthal velocities at 1 A.U. to values in better agreement with observations. Since a modified CGL theory is used in the two-fluid formulation of the magnetohydrodynamic equations, the model provides, in addition, microscopic information about the protons in the form of velocity distribution function plots at various selected heliocentric distances.

The macroscopic properties predicted by the models are in good agreement with experimental quiet-time observations at 1 A.U. The proton velocity distribution function obtained at this radius resembles closely that inferred from in-situ proton measurements. The models may be used with increased confidence to predict flow conditions at other heliocentric radii presently under experimental investigation or to be explored in the near future.

TABLE OF CONTENTS

LIST OF TABLES

LIST OF ILLUSTRATIONS

I. INTRODUCTION

I.1 The Solar Wind

The existence of a continuous high-speed outflow of corspuscular radiation from the sun, known today as the "solar wind", is a well established fact, first suggested by Biermann (1951) to explain the observed acceleration of comet tails pointing away from the sun, and later predicted by Parker (1958) as a continuous supersonic expansion of the solar corona.

In his pioneering paper Parker demonstrated that the corona cannot exist in a state of hydrostatic equilibrium. Its large extent and elevated temperature, (of the order of a few million degrees), create a pressure force distribution that cannot be balanced by the containing effects of the sun's gravitational attraction and interstellar pressure and thus expands supersonically into space. This expansion process is analogous to the flow of gas through a deLaval nozzle, as pointed out by Clauser (1960).

The existence of the solar wind was verified by the first Mariner 2 results (Neugebauer and Snyder, 1962; Snyder et al., 1963), resolving a long standing controversy between the evaporative processes proposed by Chamberlain (1960) or "solar breeze", and the hydrodynamic supersonic expansion of Parker. The history of the ideas and experimental observations that led to the solar wind concept as presently known, has been reviewed by Dessler (1967) and Spreiter and Rizzi (1972).

Today, after a decade of spacecraft observations, the large scale features of the solar wind such as its average flow speed, density,

composition, electron and proton temperatures and thermal anisotropy ratios, are relatively well known. On a smaller scale, it has been observed that the coronal expansion is a dynamic process giving rise to a multitude of magnetohydrodynamic phenomena such as shock waves, density and magnetic field discontinuities, and high-speed stream interactions. In spite of this dynamic character, a "quiet-state" of the solar wind has been associated with low-speed conditions observed at certain times to prevail for periods long compared to the expansion time (Hundhausen, 1972). The observed properties of this "quiet-state" solar wind have been summarized in Table I for future reference.

Reviews of the observational knowledge of the solar wind have been given by Ness (1967), Axford (1968) and Hundhausen (1968, 1970), while recent measurements concerning transport phenomena, pressure anisotropies and other related features, have been reported by Montgomery (1971) and Ogilvie et al. (1968).

The expanding coronal gas is an electrically neutral, highly conductive plasma and as such it is expected to carry with it the relatively weak solar magnetic field. This frozen-in flux combined with solar rotation results in the Archimedean spiral structure of the interplanetary magnetic field first suggested by Parker and later confirmed by in-situ observations by spacecraft in the Venus-Earth-Mars space. Ness and Wilcox (1967) reported a particular large scale feature of the interplanetary field; this is its sector structure associated with polarity reversals observed during the course of a solar rotation and persisting over periods of several solar rotations.

TABLE I

AVERAGE PROPERTIES OF THE LOW-SPEED (QUIET-STATE) SOLAR WIND AT 1 A.U.

Radial Component of Flow Velocity	300-325 Km/sec.
Nonradial Component of Flow Velocity	8 Km/sec.
Proton (electron) Density	$8.7\ cm^{-3}$
Electron Temperature	$1.5 \times 10^{5}\ ^{o}K$
Proton Temperature	$4 \times 10^{4}\ ^{o}K$
Magnetic Field Intensity	5 gamma
Solar Ecliptic Longitude of Field	140^{o}
Proton Thermal Anisotropy	2
Total Energy Flux Density	$0.25\ ergs\ cm^{-2}\ sec^{-1}$
Electron Heat Conduction Flux Density	$7 \times 10^{-3}\ ergs\ cm^{-2}\ sec^{-1}$

The spiral configuration of the field results in the transport of angular momentum away from the sun thus exerting a retarding torque on its outer layers. In addition, a smaller amount of angular momentum is transported by the solar wind in the form of an azimuthal velocity component in interplanetary space.

At large distances from the sun, the momentum flux and magnetic pressure associated with the solar wind become comparable to the total interstellar pressure. In this region it is expected that the solar wind will undergo a supersonic to subsonic transition generating a shock wave, (Axford et al. 1963; Dessler, 1967).

I.2 Theoretical Models of the Solar Wind

Since the early work of Parker, (1958, 1960) numerous fluid and exospheric models of the coronal expansion have been proposed. Hundhausen (1968, 1970, 1972) has reviewed the general characteristics and conditions of applicability for these models, and the accuracy with which they predict observed flow conditions at the earth's orbit.

The assumption made in most models that the solar wind behaves collectively as a ionized fluid cannot be substantiated in terms of classical plasma theory. The exospheric models of Chamberlain predicted very small expansion velocities but later refinements on these models by Brandt and Casinelli (1966), Jockers (1970), and Hollweg (1970), produced expansion speeds comparable to those obtained from fluid models. Nevertheless, other values are in considerable disagreement with observations, in particular the proton thermal anisotropy ratio and expected behavior of $^4He^{++}$ ions in the solar wind.

All of the observational evidence indicates a fluid-like behavior in the coronal expansion and therefore fluid models are expected to give results in better general agreement with observations than exospheric (or evaporative) models.

The general nature of the results obtained from hydrodynamic models is the same, that is, supersonic expansion of the coronal gas in interplanetary space. The significant differences among the models result from the particular treatment of the energy equation and the inclusion of the spiral magnetic field in the analysis. Of particular importance to the subject of this dissertation are the models of Weber and Davis (1967), Urch (1969), Whang (1971a), Wolff et al. (1971) and Whang (1972).

Weber and Davis developed a one-fluid model with a polytropic radial temperature dependence and included the effects of the frozen-in solar magnetic field. The radial expansion velocity is not affected to any large extent by the inclusion of the field but a significant retarding torque on the sun is predicted as a result of the stress produced by the spiral structure of the magnetic field.

Urch obtained a numerical solution to the magnetohydrodynamic one-fluid equations under the assumptions that heat is carried away by conduction from a heat source located at the base of the corona and that the magnetic field inhibits the transport of thermal energy at right angles to the field. The temperatures predicted by this model at 1 A.U. are too high, although other quantities are in agreement with observations. The azimuthal velocity at the earth's orbit predicted by these models lies in the range of 1-2 K/sec. in disagreement with reported observations of 6-10 Km/sec.

Whang considered a radial model of the coronal expansion including the spiral magnetic field and showed that under these assumptions, magnetic field expansion energy is continuously converted into kinetic energy and thus was able to increase the predicted radial velocity at 1 A.U. by 17%. Modisette (1972) has pointed out that although the magnetic energy conversion process described by Whang is indeed operative in the solar wind, its effect should not be as large when the azimuthal velocity component is taken into consideration in the analysis. We shall consider this problem in detail in the first part of this dissertation by incorporating the azimuthal velocity into Whang's one-fluid model and obtain numerical solutions to the resulting system of magnetohydrodynamic equations.

Wolff et al. have proposed that viscosity plays a major role in heating up the protons in the solar wind and in this fashion account for a non-thermal source required by two-fluid models to obtain reasonable proton temperatures at 1 A.U., (Hundhausen, 1970). Although their results agree quite well with observations after an empirical function for the conductivity coefficient is assumed, the role of viscosity and other transport phenomena defined in terms of classical plasma theory is not completely understood at the present time. The observational evidence points out to the existence of randomizing effects other than Coulomb collisions in solar wind but the exact nature of these interactions is not known.

A theoretical approximation to the observed proton velocity distribution function was obtained by Whang (1971b) and it allows the set of

magnetohydrodynamic equations of Chew, Goldberger and Low (1956) to be closed relating the proton temperature to the proton heat flux in the context of guiding center plasma theory rather than classical heat conduction. These results were included in a two-fluid, two-region anisotropic model (Whang, 1972), capable of providing macroscopic as well as microscopic information about the solar wind.

Weber (1967) and Weber and Davis (1970) have considered the effects of thermal anisotropies upon the angular motion of the solar wind under certain simplifying assumptions and show that the predicted azimuthal velocity at 1 A.U. is five times larger than that predicted by isotropic, one-fluid models. The second part of this dissertation will consider the solution to the magnetohydrodynamic equations for a two-fluid, two-region solar wind model which includes Whang's formulation of the proton velocity distribution function to represent proton thermal anisotropy effects upon the angular motion. The two-region formulation of the model is necessary to avoid the rapid proton cooling problem which has plagued most two-fluid models and represents only an approximation to the physical processes believed to be responsible for the observed properties of the solar wind.

II. A ONE-FLUID MAGNETOHYDRODYNAMIC MODEL OF THE SOLAR WIND

II.1 Basic Assumptions

In this section we shall obtain numerical solutions to the steady state magnetohydrodynamic equations governing the expansion of the coronal gas under the assumptions that the solar wind is a perfectly conducting fluid, heat is carried away by conduction from the base of the corona and that the solar magnetic field depends only on latitude, ignoring its sector structure.

The assumption that the solar wind behaves as a fluid is based upon observed characteristics of the coronal expansion. We shall consider this fluid to be inviscid since energy supplied by thermal conduction is much larger than that dissipated by viscosity (Parker, 1965) and the general form of the viscous stress tensor for low density plasmas in the presence of a magnetic field is not well known. Viscous models based upon the classical formulation for this tensor have shown greater disagreement with observations than inviscid models (Whang, Chang and Liu, 1966; Scarf and Noble, 1964). The gas will be assumed to be composed of fully ionized hydrogen with a 5% helium number density content.

In developing the model we shall closely follow the approach of Whang (1971a), except for the inclusion of the azimuthal component of the momentum equation in our analysis. The model will thus represent the flow of ionized gas in the sun's equatorial plane and it is further assumed that this flow is axially symmetric about the sun's rotation axis.

II.2 MHD Governing Equations for the Model

The steady state MHD equations of mass, momentum and energy conservation, assuming that charge neutrality is maintained in the plasma, may be expressed as

$$\nabla.(n\underline{u}) = 0 \tag{II.2.1}$$

$$mn(\underline{u}.\nabla)\underline{u} + \nabla.\underline{\underline{P}} - \frac{1}{c}\underline{J}\times\underline{B} - mn\underline{X} = 0 \tag{II.2.2}$$

$$\nabla.\left[\left(\frac{3}{2}nkT + \frac{1}{2}mnu^2\right)\underline{u}\right] + \nabla.\underline{N} + \nabla.\underline{Q} + \nabla.(\underline{\underline{P}}.\underline{u}) + mn\underline{X}.\underline{u} = 0 \tag{II.2.3}$$

where $\underline{\underline{P}}$ is the pressure tensor, $\underline{N}$ the Poynting vector and $\underline{X}$ an external force function. Other quantities such as the heat flux vector $\underline{Q}$, magnetic field $\underline{B}$, mass density $\rho = mn$, temperature T, are represented in standard MHD notation and gaussian units will be used throughout the development.

Maxwell's equations govern the steady state interplanetary magnetic field and may be written as

$$\nabla\times\underline{E} = 0 \tag{II.2.4}$$

$$\nabla.\underline{B} = 0 \tag{II.2.5}$$

$$\nabla\times\underline{B} = \frac{4\pi}{c}\underline{J} \tag{II.2.6}$$

$$\nabla \cdot \underline{E} = 0 \tag{II.2.7}$$

For a perfect conductor in an inertial frame of reference the electric field is given by

$$\underline{E} = -\frac{1}{c}\, \underline{u} \times \underline{B} \tag{II.2.8}$$

and the Poynting vector takes the form

$$\underline{N} = \frac{c}{4\pi}\, \underline{E} \times \underline{B} \tag{II.2.9}$$

From (II.2.4), (II.2.6) and (II.2.8) we obtain

$$\nabla \times (\underline{u} \times \underline{B}) = 0 \tag{II.2.10}$$

and

$$\frac{1}{c}\, \underline{J} \times \underline{B} = \frac{1}{4\pi} (\nabla \times \underline{B}) \times \underline{B} \tag{II.2.11}$$

We consider now the spherical coordinate system (r, ψ, ω) centered at the sun and aligned with the ecliptic plane, shown in Figure 1a. In this system we express the magnetic field $\underline{B}$ and velocity vector $\underline{u}$ as

$$\underline{u} = \underline{e}_r u_r(r,\psi) + \underline{e}_\omega u_\omega(r,\psi) \tag{II.2.12}$$

$$\underline{B} = \underline{e}_r B_r(r,\psi) + \underline{e}_\omega B_\omega(r,\psi) \tag{II.2.13}$$

The mass conservation equation (II.2.1) becomes then

$$\frac{\partial}{\partial r}(n u_r r^2) = 0$$

or

$$n u_r r^2 = \text{const.} \tag{II.2.14}$$

Since the model is assumed isotropic and one-fluid, the pressure tensor is given by

$$\underline{\underline{P}} = (2nkT)\, \underline{\underline{I}} \tag{II.2.15}$$

where n is the particle density, k Boltzmann's constant and $\underline{\underline{I}}$ the unit

Figure 1

a) The spherical coordinate system.

b) Definition of the magnetic field angle ϕ.

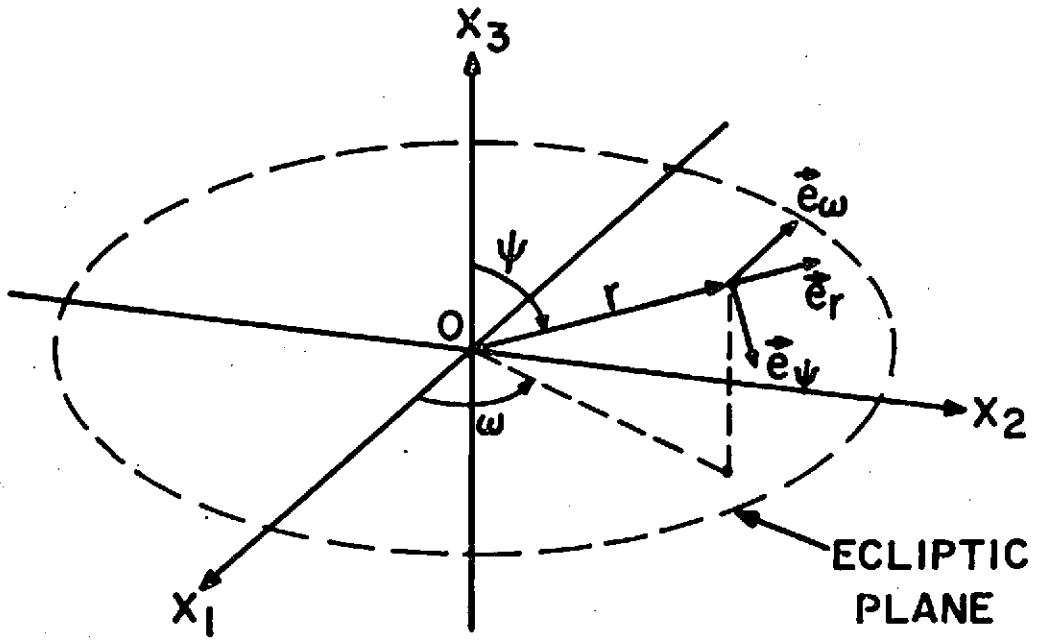
X3
X2
X1
O
ψ
r
ω
$\hat{e}_\omega$
$\hat{e}_r$
$\hat{e}_\psi$
ECLIPTIC
PLANE

(a)

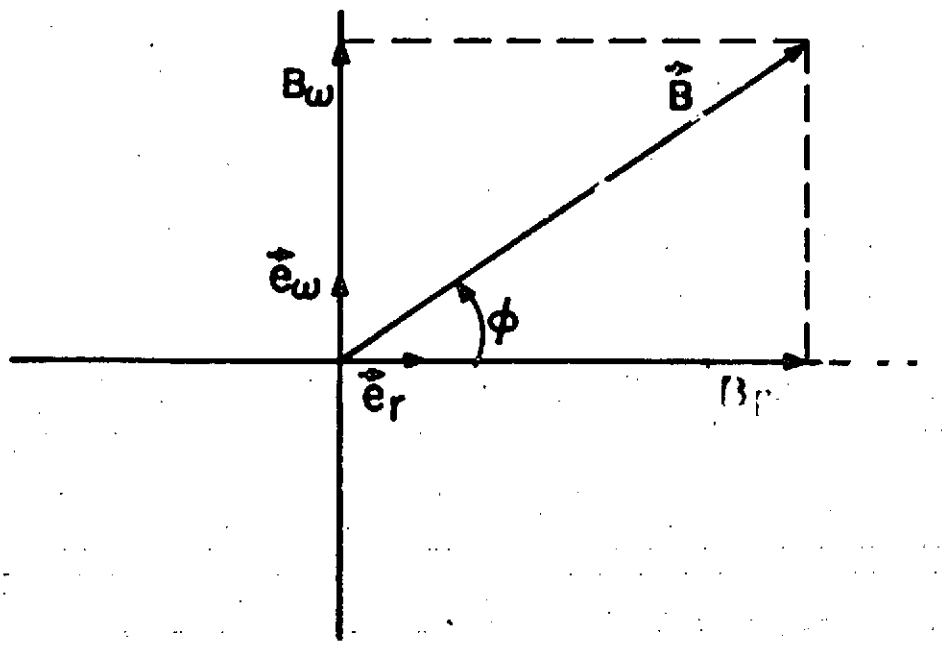
B_ω
$\hat{B}$
$\hat{e}_\omega$
ϕ
$\hat{e}_r$

(b)

tensor. It follows that

$$\nabla \cdot \underline{\underline{P}} = \nabla(2nkT) \tag{II.2.16}$$

Introducing (II.2.12) and (II.2.13) in (II.2.10) we obtain

$$\nabla \times (\underline{u} \times \underline{B}) = \frac{e\omega}{r} \frac{\partial}{\partial r} \left[r(u_r B_\omega - u_\omega B_r) \right] = 0 \tag{II.2.17}$$

which implies

$$r u_r B_\omega - r u_\omega B_r = \text{const.} = C' \tag{II.2.18}$$

An analogous procedure with (II.2.5) yields

$$\frac{\partial}{\partial r}(r^2 B_r) = 0 \tag{II.2.19}$$

or

$$r^2 B_r = \text{const.} \tag{II.2.20}$$

The radial and azimuthal components of the magnetic force may be obtained from (II.2.11) and are given by

$$\frac{4\pi}{c}(\underline{J} \times \underline{B})_r = \frac{B_\omega}{r} \frac{\partial}{\partial r}(r B_\omega) \tag{II.2.21}$$

and

$$\frac{4\pi}{c}(\underline{J} \times \underline{B})_\omega = \frac{B_r}{r} \frac{\partial}{\partial r}(r B_\omega) \tag{II.2.22}$$

where sin ψ has been taken as unity for the equatorial plane model under consideration.

The external force function $\underline{X}$ in the case of the solar wind is given by the sun's gravitational attraction

$$\underline{X} = -\underline{e}_r \frac{GM_\odot}{r^2} \tag{II.2.23}$$

where G is the universal gravitational constant and $M_\odot$ the mass of the sun. The radial and azimuthal components of the momentum equation thus take the forms

$$mn\left(u_r\frac{\partial u_r}{\partial r}-\frac{u_\omega^2}{r}\right)=-\nabla(2nkT)-\frac{B_\omega}{4\pi r}\frac{\partial}{\partial r}(rB_\omega)$$

$$-\frac{mnGM_\odot}{r^2} \qquad \text{(II.2.24)}$$

and

$$mn\frac{u_r}{r}\frac{\partial}{\partial r}(ru_\omega)=\frac{B_r}{4\pi r}\frac{\partial}{\partial r}(rB_\omega) \qquad \text{(II.2.25)}$$

Here m is the mean mass per particle and n the particle density per cm^3. In the case of the energy equation, proceeding in an analogous fashion, we obtain

$$\nabla\cdot\underline{N}=\frac{1}{4\pi r^2}\frac{\partial}{\partial r}\left[r^2B_\omega(B_\omega u_r-u_\omega B_r)\right] \qquad \text{(II.2.26)}$$

$$\nabla\cdot(\underline{\underline{P}}\cdot\underline{u})=\frac{1}{r^2}\frac{\partial}{\partial r}(2nkTu_r r^2) \qquad \text{(II.2.27)}$$

In order to obtain an adequate expression for the heat flux term $\nabla\cdot\underline{Q}$ in (II.2.3), we must take into account the inhibiting effect of the magnetic field upon the transport of thermal energy perpendicular to the field lines. Following the approach of Urch (1969), Wolff et al. (1971), Whang (1971a), Gentry and Hundhausen (1969), we express the radial component of the heat flux term as

$$(\nabla\cdot\underline{Q})_r=\frac{1}{r^2}\frac{\partial}{\partial r}\left(-r^2\kappa\cos^2\phi\frac{\partial T}{\partial r}\right) \qquad \text{(II.2.28)}$$

where ϕ is the angle between the radial direction and the magnetic field as shown in Figure 1b, and K is the thermal conductivity coefficient. The energy conservation equation (II.2.3) is thus given by

$$\frac{1}{r^2}\frac{\partial}{\partial r}\left[r^2\left(3nkT+\frac{1}{2}mnu^2\right)u_r\right]-\frac{1}{r^2}\frac{\partial}{\partial r}\left(r^2\kappa\cos^2\phi\frac{\partial T}{\partial r}\right)+$$

$$+\frac{1}{4\pi r^2}\frac{\partial}{\partial r}\left[r^2B_\omega(B_\omega u_r-u_\omega B_r)\right]=\frac{1}{r^2}\frac{\partial}{\partial r}(2nkTu_r r^2)-$$

$$mn\frac{GM_\odot}{r^2}\,u_r = 0 \qquad \text{(II.2.29)}$$

This equation may be integrated once with the result

$$nu_r r^2\left(5kT + \frac{B_\omega^2}{4\pi n} - \frac{mGM_\odot}{r} + \frac{mu^2}{2}\right) - r^2 u_\omega \frac{B_\omega B_r}{4\pi}$$

$$= r^2 \kappa \cos^2\phi \frac{dT}{dr} + F \qquad \text{(II.2.30)}$$

where F is the total energy flux per steradian. The second term on the left-hand side of (II.2.30), not included in Whang's analysis, represents the energy flux associated with the rotational motion of the gas.

The azimuthal component of the momentum equation (II.2.25) may be integrated directly (Weber and Davis, 1967) to give

$$ru_\omega - rB_\omega B_r/4\pi mn u_r = \text{const.} = C'' \qquad \text{(II.2.31)}$$

Equations (II.2.18) and (II.2.31) may now be used to calculate

$$u_\omega = \frac{1}{r}\frac{4\pi mn u_r^2 C'' + B_r C'}{4\pi mn u_r^2 - B_r^2} \qquad \text{(II.2.32)}$$

$$B_\omega = \frac{1}{r}\frac{4\pi mn u_r (C'' B_r + C')}{4\pi mn u_r^2 - B_r^2} \qquad \text{(II.2.33)}$$

The remaining terms in (II.2.24) are obtained from the above relations and the equation takes the form

$$\frac{du_r}{dr} = \frac{u_r}{r}\left[\frac{\frac{4kT}{m} - \frac{GM_\odot}{r} - \frac{2kr}{m}\frac{dT}{dr} + u_\omega^2 + \frac{2u_\omega B_\omega B_r}{4\pi mn u_r(1-A^2)}}{u_r^2 - \frac{2kT}{m} - \frac{B_\omega^2}{4\pi mn(1-A^2)}}\right] \qquad \text{(II.2.34)}$$

where

$$A^2 = \frac{1}{M_A^2} = B_r^2/4\pi mn u_r^2 \qquad \text{(II.2.35)}$$

and A is defined as the reciprocal of the radial Alfven Mach number, M_A.

It is interesting to compare (II.2.34) with the corresponding equation obtained by Whang; this will be carried out in Section II.3.

It is convenient to introduce

$$\tan\phi = B_\omega / B_r \qquad \text{(II.2.36)}$$

in equation (II.2.34). Hence

$$\frac{du_r}{dr} = \frac{u_r}{r}\left[\frac{\frac{4kT}{m} - \frac{GM_\odot}{r} - \frac{2kr}{m}\frac{dT}{dr} + u_\omega^2 + \frac{2u_\omega u_r \tan\phi A^2}{(1-A^2)}}{u_r^2\left(1 - \frac{A^2\tan^2\phi}{1-A^2}\right) - \frac{2kT}{m}}\right] \qquad \text{(II.2.37)}$$

The governing equations (II.2.30) and (II.2.37) may be cast in dimensionless form by considering the flow conditions at a particular radius. Let us denote the conditions at $r = r_3$ by the subscript indicated. The reason for choosing 3 as the subscript will become apparent as we proceed with the development.

We introduce the following dimensionless variables

$$V = u_r/u_{r_3} \; ; \; W = u_\omega/u_{\omega_3} \; ; \; \theta = T/T_3 \; ; \; Z = r/r_3 \qquad \text{(II.2.38)}$$

and dimensionless parameters γ, ξ and δ, defined by

$$\gamma = GM_\odot/r_3 u_{r_3}^2 \; ; \; \xi = mu_{r_3}^2/2kT_3 \; ; \; \delta = u_{\omega_3}/u_{r_3} \qquad \text{(II.2.39)}$$

Equation (II.2.37) may now be written in dimensionless form as follows

$$\frac{dV}{dZ} = \frac{V}{Z}\left[\frac{2\theta - \frac{\gamma\xi}{Z} - Z\frac{d\theta}{dZ} + \xi\delta^2W^2 + \frac{2\delta\xi\mu W\tan\phi}{Z^2(1-\mu/VZ^2)}}{\xi V^2 - \theta - \xi\mu V\tan^2\phi/Z^2(1-\mu/VZ^2)}\right] \qquad \text{(II.2.40)}$$

where the parameter

$$\mu = A_3^2 = B_{r_3}^2/4\pi m n_3 u_{r_3}^2 \qquad \text{(II.2.41)}$$

is defined as the reciprocal of the radial Alfven Mach number at the reference radius.

The denominator of (II.2.40)

$$\xi V^2 - \Theta - \xi \mu V \tan^2\phi / z^2 (1 - \mu/Vz^2) \qquad \text{(II.2.42)}$$

will vanish for three sets of values of the independent and dependent variables, denoted respectively as (Z_1, V_1, θ_1), (Z_2, V_2, θ_2) and (Z_3, V_3, θ_3). These three sets correspond to the critical points of (II.2.40), first studied by Weber and Davis (1967); each critical point occurs when the fluid velocity equals the characteristic propagation speed of a possible wave mode in the medium.

The first critical point, closest to the sun ($r=r_1$), corresponds approximately to Parker's critical point where the fluid velocity equals the local characteristic thermal speed of the plasma, in our case modified by the presence of the magnetic field. The second critical point represents the singularity introduced in (II.2.40) by the azimuthal component of the momentum equation. At this point the radial component of the fluid velocity equals the local Alfven speed as determined by (II.2.35) when $M_A^2 = 1$. At the third and farthest away from the sun critical point, the radial velocity is approximately equal to the local Alfven speed as determined by the total magnitude of the magnetic field. Since $\tan\phi$ is small in this region, we expect the third critical point to be located in the immediate vicinity of the second.

The general topology of the solution differs little from the one given by Weber and Davis and a solution curve extending from the sun's surface to large heliocentric distances must pass through all three critical points. A schematic representation of this topology is given in Figure 2; (V_2, Z_2) is a node point while (V_1, Z_1) and (V_3, Z_3) are saddle

Figure 2

Schematic representation of the topology of the solution for u_r near the critical points.

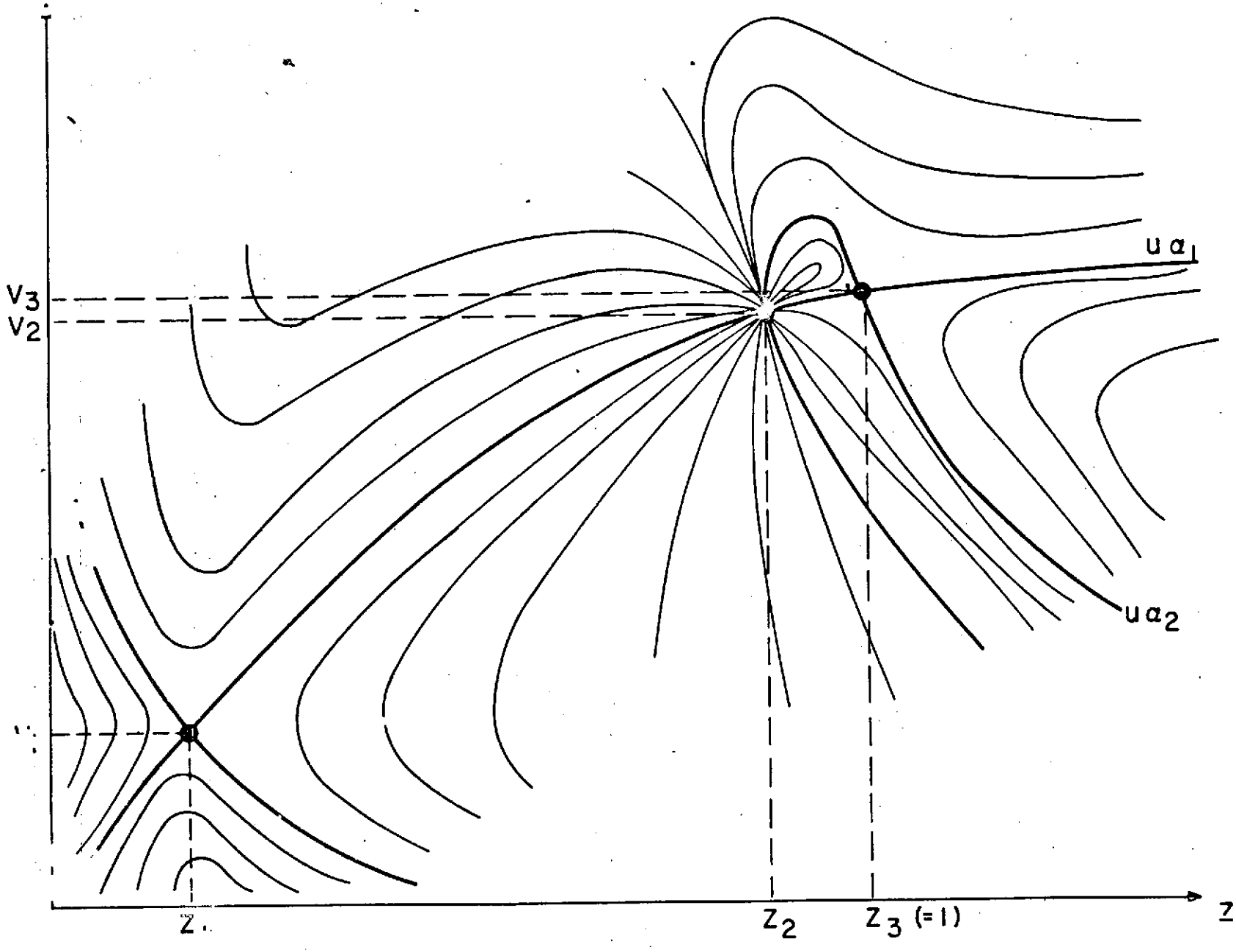
V3
V2
u α1
u α2
z
z2
z3 (=1)

points. It is then possible to determine the slope of the solution curve at the saddle points from the values assigned to the dimensionless parameters.

Because of this topology, we choose the third critical point as the reference radius for the dimensionless equations. This choice will eventually determine the success of the numerical integration scheme utilized to solve the system of differential equations. Hence, at Z = 1, (II.2.42) takes the form

$$\xi - 1 - \xi\mu \tan^2\phi_3/(1-\mu) = 0 \qquad \text{(II.2.43)}$$

from which we obtain for ξ

$$\xi = (1-\mu)/(1-\mu/\cos^2\phi_3) \qquad \text{(II.2.44)}$$

The denominator of equations (II.2.32) and (II.2.33) vanishes at the second critical point. Since u_ω and B_ω must remain finite and continuous, we require that the numerators must also vanish at this point. Hence we must have

$$4\pi m n_2 u_{r_2} C'' + B_{r_2} C' = 0 \qquad \text{(II.2.45)}$$

and C' and C'' related by

$$C'' = -C'/B_{r_2} \qquad \text{(II.2.46)}$$

where the subscript refers to the flow conditions at the Alfvenic critical point.

In a frame of reference rotating with the sun $\underline{B}$ is parallel to $\underline{u}$. In this frame (Pneuman, 1966)

$$\frac{u_r}{B_r} = \frac{u_\omega - \Omega r}{B_\omega} \qquad \text{(II.2.47)}$$

where Ω denotes the angular velocity of the outer layers of the sun. Introducing (II.2.47) in (II.2.18) we obtain

$$C' = -\Omega r^2 B_r = -\Omega r_2^2 B_{r_2} \qquad \text{(II.2.48)}$$

and

$$C'' = \Omega r_2^2 \qquad \text{(II.2.49)}$$

Introducing the dimensionless variables and defining two additional parameters σ and ζ, where

$$\sigma = r_2/r_3 \quad ; \quad \zeta = \Omega r_3/u_{r_3} \qquad \text{(II.2.50)}$$

we can write the azimuthal component of the momentum equation as

$$\delta W = \zeta Z + V \tan\phi \qquad \text{(II.2.51)}$$

where tan ϕ is given by

$$\tan\phi = \zeta(\sigma^2 - Z^2)/VZ(1-\mu/VZ^2) \qquad \text{(II.2.52)}$$

At the reference radius (Z = 1), these equations reduce to

$$\delta = \tan\phi_3 + \zeta \qquad \text{(II.2.53)}$$

and

$$\tan\phi_3 = \zeta(\sigma^2 - 1)/(1-\mu) \qquad \text{(II.2.54)}$$

We may proceed in analogous fashion with the energy equation (II.2.30). Introducing the dimensionless parameters

$$\alpha = 2n_3 u_{r_3} r_3 k/\kappa_3 \cos^2\phi_3 \qquad \text{(II.2.55)}$$

and

$$H = F/n_3 m u_{r_3}^3 r_3^2 \qquad \text{(II.2.56)}$$

with the thermal conductivity for ionized hydrogen given by (Spitzer, 1962)

$$\kappa = KT^{5/2} \qquad \text{(II.2.57)}$$

we obtain

$$\frac{d\theta}{dz} = \frac{\alpha \xi \cos^2\phi_3}{z^2 \theta^{5/2} \cos^2\phi} \left[\frac{1}{2}(V^2 + \delta^2 W^2) + \frac{\mu V}{z^2} \tan^2\phi + \frac{5}{2}\frac{\theta}{\xi} - H - \frac{\delta \mu W}{z^2} \tan\phi - \frac{\gamma}{z} \right] \tag{II.2.58}$$

The dimensionless parameters, α, β, ξ and H, measure the ratios of various energy flows at the reference radius. In addition

$$F = \left(\frac{\alpha \cos^2\phi_3 H}{\gamma^{7/2} \xi^{5/2}} \right) \left(\frac{mGM_\odot}{2kr_3} \right)^{7/2} K r_3 \tag{II.2.59}$$

that is, the total energy flux per steradian is proportional to the constant K in the thermal conductivity coefficient (Whang, 1971a). In reality K is a slowly varying function of the density and temperature of the gas (Braginskii, 1965) but in the case of the solar wind it may be assumed constant.

As shown by Whang, α is not an independent parameter. At the reference radius the numerator of (II.2.40) must vanish in order for $\frac{dv}{dz}$ to remain finite and V continuous across the critical point. Hence, from equation (II.2.58) we must have

$$\frac{d\theta}{dz} = \alpha \xi \left[\frac{1}{2}(1+\delta^2) + \mu \tan^2\phi_3 + \frac{5}{2\xi} - H - \delta\mu \tan\phi_3 - \gamma \right] \tag{II.2.60}$$

and from equation (II.2.40)

$$2 - \gamma\xi - \left(\frac{d\theta}{dz}\right)_3 + \xi\delta^2 + 2\delta\xi\mu \tan\phi_3/(1-\mu) = 0 \tag{II.2.61}$$

The parameter α is thus given by

$$\alpha = \frac{2 - \gamma\xi + \xi\delta^2 + 2\delta\xi\mu\tan\phi_3/(1-\mu)}{\xi\left[\frac{1}{2}(1+\delta^2) + \mu\tan^2\phi_3 + (5/2\xi) - H - \delta\mu\tan\phi_3 - \gamma\right]} \tag{II.2.62}$$

and the solutions for V and θ have the general form

$$V = V(z, H, \gamma, \phi_3, \xi, \mu) \quad ; \quad \theta = \theta(z, H, \gamma, \phi_3, \xi, \mu) \tag{II.2.63}$$

For convenience and future reference we summarize below the principal

equations obtained in this section and the relations among the different dimensionless parameters defined.

Radial Equation of Motion

$$\frac{dV}{dz} = \frac{V}{z}\left[\frac{2\Theta - (\gamma\xi/z) - z\,d\Theta/dz + \xi\delta^2W^2 + \dfrac{2\delta\xi\mu W\tan\phi}{z^2(1-\mu/Vz^2)}}{\xi V^2 - \Theta - \xi\mu V\tan^2\phi/z^2(1-\mu/Vz^2)}\right] \tag{II.2.64}$$

Azimuthal Equation of Motion

$$\delta W = \xi z + V\tan\phi \tag{II.2.65}$$

with

$$\tan\phi = \xi(\sigma^2 z^2)/Vz(1-\mu/Vz^2) \tag{II.2.66}$$

Energy Equation

$$\frac{d\Theta}{dz} = \frac{\alpha\xi\cos^2\phi_3}{z^2\Theta^{5/2}\cos^2\phi}\left[\frac{1}{2}(V^2+\delta^2W^2) + \frac{\mu V}{z^2}\tan^2\phi + \frac{5\Theta}{2\xi} - H - \frac{\delta\mu W}{z^2}\tan\phi - \frac{\gamma}{z}\right] \tag{II.2.67}$$

Relations Among Parameters

$$\xi = (1-\mu)/(1-\mu/\cos^2\phi_3) \tag{II.2.68}$$

$$\alpha = \frac{2-\gamma\xi+\xi\delta^2+2\delta\xi\mu\tan\phi_3/(1-\mu)}{\xi\left[\frac{1}{2}(1+\delta^2)+\mu\tan^2\phi_3+(5/2\xi)-H-\delta\mu\tan\phi_3-\gamma\right]} \tag{II.2.69}$$

$$\tan\phi_3 = \delta - \xi \tag{II.2.70}$$

$$\sigma^2 = 1 + \tan\phi_3(1-\mu)/\xi \tag{II.2.71}$$

II.3 The Case of a Purely Radial Expansion

In Section II.2 we have obtained for the radial component of the momentum equation

$$\frac{du_r}{dr} = \frac{u_r}{r}\left[\frac{\frac{4kT}{m} - \frac{GM_\odot}{r} - \frac{2kr}{m}\frac{dT}{dr} + u_\omega^2 + \frac{2u_\omega B_\omega B_r}{4\pi mn u_r (1-A^2)}}{u_r^2 - \frac{2kT}{m} - \frac{B_\omega^2}{4\pi mn(1-A^2)}}\right] \qquad \text{(II.3.1)}$$

Whang (1971a), in considering the conversion of magnetic field energy into kinetic energy in the solar wind, obtained the corresponding equation for the case of a purely radial expansion as

$$\frac{du_r}{dr} = \frac{u_r}{r}\left[\frac{\frac{4kT}{m} - \frac{GM_\odot}{r} - \frac{2kr}{m}\frac{dT}{dr}}{u_r^2 - \frac{2kT}{m} - \frac{B_\omega^2}{4\pi mn}}\right] \qquad \text{(II.3.2)}$$

We immediately observe that the assumption in (II.3.1) that $u_\omega=0$ does not reduce this equation to (II.3.2). The third term in the denominator remains divided by the factor $(1-A^2)$ which leads to the existence of three critical points rather than one, as discussed in II.2.

The mathematical source of this discrepancy lies in the assumption by Whang that the velocity vector $\underline{u}$ has the form

$$\underline{u} = \underline{e}_r u_r \qquad \text{(II.3.3)}$$

while the magnetic field vector is represented by

$$\underline{B} = \underline{e}_r B_r + \underline{e}_\omega B_\omega \qquad \text{(II.3.4)}$$

In other words, the limiting condition $u_\omega=0$ is imposed at the onset of the analytical development rather than on the final differential equation. The limits obtained in each case are different, leading to the observed discrepancy.

Physically, the exclusion of u_ω from the analysis in the manner described above, implies that transverse flow perturbations that should propagate parallel to the magnetic field as Alfven waves, are ignored.

Near the sun $u_r \gg u_\omega$, $A \gg 1$ and the third term in the denominator

of (II.3.1) is of opposite sign and smaller magnitude than the corresponding term in (II.3.2). At large heliocentric distances, A<<1 and this term reduces to that given by Whang. Consequently, the effects of the magnetic field on the flow velocity are not expected to be as large as indicated by Whang. Modisette (1972) has carried out a limited analysis of this problem and reached similar conclusions. The numerical results obtained in Section II.4 will show that the effects of the magnetic field on the flow are indeed smaller than those predicted by Whang's model. In particular the "hose angle" of the interplanetary magnetic field is well behaved in the vicinity of the sun, tending to 180° as $r \to r_\odot$

II.4 Numerical Solutions for the One-Fluid Model

At the reference radius (Z = 1) equation (II.2.64) is of the form $(\frac{0}{0})$ and may be evaluated by making use of l'Hopital's rule. The result is

$$\left(\frac{dV}{dz}\right)_3 = \left(\frac{e_1 - f_2}{2f_1}\right) \pm \left(\frac{1}{2f_1}\right)\left[(f_2 - e_1)^2 + 4f_1 e_2\right]^{1/2} \qquad \text{(II.4.1)}$$

The two solutions of (II.4.1) correspond to the two possible branches of the solution curve for the radial velocity, denoted as U_{α_1} and U_{α_2} in Weber and Davis model and indicated schematically in Figure 2. The constants e_1, e_2, f_1 and f_2 are related to the various dimensionless parameters previously defined, as follows

$$e_1 = \frac{2\delta\xi\mu\tan\phi_3}{(1-\mu)^2}\left[(1-\mu)\left(a_2 + \frac{b_2}{\delta}\right) - \mu\right] - d_1 + 2\delta\xi b_2 \qquad \text{(II.4.2)}$$

$$e_2 = \frac{2\delta\xi\mu\tan\phi_3}{(1-\mu)^2}\left[(1-\mu)\left(a_1 + \frac{b_1}{\delta}\right) - 2\right] + \left(\frac{d\theta}{dz}\right)_3 + \gamma\xi - d_2$$

$$+2\delta\xi b_1 \qquad \text{(II.4.3)}$$

$$f_1 = -\frac{\xi\mu\tan^2\phi_3}{(1-\mu)^2}\left[2(a_2-\mu a_2-\mu)+1\right]+2\xi \qquad \text{(II.4.4)}$$

$$f_2 = -\frac{2\xi\mu\tan^2\phi_3}{(1-\mu)^2}\left[a_1(1-\mu)-1\right]-\left(\frac{d\theta}{dz}\right)_3 \qquad \text{(II.4.5)}$$

where

$$d_1=\alpha\xi c_1+\frac{\alpha\xi c_2 b_2}{\delta}+a_2\left[\alpha\xi c_3\tan\phi_3+2\sin^2\phi_3\left(\frac{d\theta}{dz}\right)_3\right] \qquad \text{(II.4.6)}$$

$$d_2=(\alpha\xi c_4-2)\left(\frac{d\theta}{dz}\right)_3+\frac{\alpha\xi c_2 b_1}{\delta}+a_1\left[\alpha\xi c_3\tan\phi_3+2\sin^2\phi_3\left(\frac{d\theta}{dz}\right)_3\right]$$

$$-\frac{5}{2}\left(\frac{d\theta}{dz}\right)_3^2+\alpha\xi c_5 \qquad \text{(II.4.7)}$$

$$c_1 = 1+\mu\tan^2\phi_3 \qquad \text{(II.4.8)}$$

$$c_2 = \delta^2-\delta\mu\tan\phi_3 \qquad \text{(II.4.9)}$$

$$c_3 = 2\mu\tan\phi_3-\delta\mu \qquad \text{(II.4.10)}$$

$$c_4 = 5/2\xi \qquad \text{(II.4.11)}$$

$$c_5 = 2\delta\mu\tan\phi_3-2\mu\tan^2\phi_3+\delta \qquad \text{(II.4.12)}$$

$$b_1 = \gamma + a_1 \tan\phi_3 = -\delta(1+\mu)/(1-\mu) \qquad \text{(II.4.13)}$$

$$b_2 = (1+a_2)\tan\phi_3 = -\mu\tan\phi_3/(1-\mu) \qquad \text{(II.4.14)}$$

$$a_1 = \left[3\mu - 1 - \sigma^2(1+\mu)\right]/(\sigma^2-1)(1-\mu) \qquad \text{(II.4.15)}$$

$$a_2 = -1/(1-\mu) \qquad \text{(II.4.16)}$$

The correct solution of (II.4.1) is given by the (+) sign and corresponds to a positive slope at the reference radius.

It is convenient to express the general solutions for V and θ as functions of commonly used plasma parameters, rather than those given in (II.2.63). For this purpose we introduce β, the ratio of the thermal pressure 2nkT, to the total magnetic field pressure $B^2/8\pi$. Thus at the reference radius

$$\beta_3 = \frac{2n_3 kT_3}{B_3^2/8\pi} = \frac{2\cos^2\phi_3}{\xi\mu} \qquad \text{(II.4.17)}$$

and in general

$$\beta = \beta_3 \cos^2\phi\, \Theta z^2/V\cos^2\phi_3 \qquad \text{(II.4.18)}$$

Making use of (II.2.68) it follows that the parameter ξ will be given by

$$\xi = \left(\frac{1}{2}+\frac{1}{\beta_3}\right) \pm \left[\left(\frac{1}{2}+\frac{1}{\beta_3}\right)^2 - \frac{2\cos^2\phi_3}{\beta_3}\right]^{1/2} \qquad \text{(II.4.19)}$$

once β_3 and ϕ_3 are specified. The two solutions of (II.4.19) represent two possible choices for the reference radius. The (+) sign corresponds to the outer critical point $r=r_3$ where $\xi \gg 1$, while the (-) sign corresponds to the solution that should have been used if we had chosen $r=r_1$, ($\beta=\beta_1$, $\phi=\phi_1$) as the reference radius where $\xi \sim 1$. Thus the general solutions for V and θ depend on five independent, dimensionless parameters, namely β_3, ζ, H, ϕ_3 and γ. Hence we may write

$$V = V(z, \beta_3, \phi_3, \xi, \gamma, H) \; ; \; \Theta = \Theta(z, \beta_3, \phi_3, \xi, \gamma, H) \tag{II.4.19}$$

From the values assigned to these parameters we can compute the physical location of the outer critical point or reference radius, and the flow velocity at this point. The results are given by

$$r_3 = \left(\frac{GM_\odot \xi^2}{\Omega^2 \gamma}\right)^{1/3} \tag{II.4.20}$$

$$u_{r_3} = \left(\frac{GM_\odot \Omega}{\gamma \xi}\right)^{1/3} \tag{II.4.21}$$

We observe that these quantities are uniquely determined by the particular values chosen for the parameters in a given model. Once a solution has been obtained, it is not possible to adjust the location of the critical point to obtain a best compromise between the predicted temperature and flow velocity at 1 A.U., as the case of strictly radial flow (Whang, 1971a, 1972). In this sense, we expect the solutions to our system of equations to be unique for the particular set of parameters chosen.

Since the reference radius is located at a certain distance from the sun's surface, two numerical integrations of the differential equations starting at the reference radius are required to obtain a complete solution: a) An inward (towards the sun) integration from the outer critical point, and b) An outward integration to large heliocentric distances.

The inward integration must pass through two additional critical points and presents the most difficult computational problem. Nevertheless, the proximity of the Alfvenic critical point to the reference radius

considerably simplifies this problem. An inward numerical integration starting at the outer critical point will always pass through the Alfvenic critical point since this is a node point (Fig. 2) and the integration error accumulated over such a short distance is extremely small and does not affect the solution in the vicinity of Z_2. Thus, the inward integration problem reduces to that of finding a solution curve starting at the reference radius and passing through the inner critical point. This simplification is the most important reason for choosing the location of the outer critical point as the reference radius.

Further insight into the behavior of the solutions as a function of the values assigned to the parameters in (II.4.20), may be obtained by considering certain approximations. The five parameters are expected to interact to some degree upon the final solution due to the non-linear character of the equations. The purpose of the following approximate analysis is to find an optimum strategy for the selection of parameter values which will satisfy observed conditions in the solar wind, and at the same time generate solutions passing through all three critical points and satisfying conditions at infinity.

At the inner critical point (Z_1, V_1, θ_1), the numerator and denominator of (II.2.64) must vanish simultaneously for u_r to remain continuous across the point. Hence we must have

$$(\xi V_1^2 - \theta_1)(Z_1^2 - \mu/V_1) - \xi \mu V_1 \tan^2\phi_1 = 0 \qquad \text{(II.4.22)}$$

and

$$\left[2\theta_1 - \frac{\gamma\xi}{z_1} - z_1\left(\frac{d\theta}{dz}\right)_1 + W_1^2\delta^2\xi\right]\left(z_1^2 - \mu/V_1\right) + 2\delta W_1 \xi\mu\tan\phi_1 = 0 \qquad \text{(II.4.23)}$$

The energy equation (II.2.67), at the same point, has the form

$$\left(\frac{d\theta}{dz}\right)_1 = \frac{\alpha\xi\cos^2\phi_3}{z_1^2\theta_1^{5/2}\cos^2\phi_1}\left[\frac{1}{2}\left(V_1^2 + \delta^2 W_1^2\right) + \frac{\mu V_1}{z_1^2}\tan^2\phi_1 + \frac{5\theta_1}{2\xi} - H - \frac{\delta\mu W_1}{z_1^2}\tan\phi_1 - \frac{\gamma}{z_1}\right] \qquad \text{(II.4.24)}$$

Thus we only have two independent equations to compute three unknowns z_1, V_1, θ_1 and unless we make some assumptions regarding one of the unknowns the location of the critical point cannot be determined without actually integrating the differential equations. Equations (II.4.23) through (II.4.25) may be normalized to the flow conditions at the inner critical point by introducing the following parameters

$$\xi_1 = \xi V_1^2/\theta_1 \;;\; \mu_1 = \mu/V_1 z_1^2 \;;\; H_1 = H/V_1^2 \;;\; \gamma_1 = \gamma/V_1^2 z_1 \qquad \text{(II.4.25)}$$

$$\zeta_1 = \zeta z_1/V_1 \;;\; \delta_1 = \delta W_1/V_1 \qquad \text{(II.4.26)}$$

and from (II.4.23) through (II.4.25) we obtain

$$(\xi_1 - 1)(1 - \mu_1) - \xi_1\mu_1\tan^2\phi_1 = 0 \qquad \text{(II.4.27)}$$

and

$$\left[2 - \gamma_1\xi_1 - \left(\frac{d\theta}{dz}\right)_1 + \xi_1\delta_1^2\right](1 - \mu_1) + 2\delta_1\xi_1\mu_1\tan\phi_1 = 0 \qquad \text{(II.4.28)}$$

Hence

$$\left(\frac{d\theta}{dz}\right)_1 = \frac{\alpha\xi_1\theta_1\cos^2\phi_3}{z_1^2\theta_1^{5/2}\cos^2\phi_1}\left[\frac{1}{2}\left(1 + \delta_1^2\right) + \mu_1\tan^2\phi_1 + \frac{5}{2\xi_1} - H_1 - \delta_1\mu_1\tan\phi_1\right] \qquad \text{(II.4.29)}$$

These equations are analogous to those obtained for the outer critical point and we may write

$$\alpha_1 = \frac{2 - \gamma_1\xi_1 + \xi_1\delta_1^2 + 2\delta_1\xi_1\mu_1\tan^2\phi_1/(1-\mu_1)}{\xi_1\left[\frac{1}{2}\left(1 + \delta_1^2\right) + \mu_1\tan^2\phi_1 + (5/2\xi_1) - H_1 - \delta_1\mu_1\tan\phi_1 - \gamma_1\right]} \qquad \text{(II.4.30)}$$

hence, from (II.4.25)

$$\alpha_1 = \alpha \cos^2\phi_3 / Z_1 \theta_1^{5/2} \cos^2\phi_1 \qquad \text{(II.4.31)}$$

We now make the assumption that in this region the temperature variation as a function of radius is given by

$$\theta = Z^m \qquad \text{(II.4.32)}$$

Hence

$$\frac{d\theta}{dz} = m Z^{m-1} \quad ; \quad \left(\frac{d\theta}{dz}\right)_3 = m \qquad \text{(II.4.33)}$$

This assumption is approximately true in the region considered, for most solar wind models (Hundhausen, 1972); we introduce it here for the sole purpose of estimating bounds for $(\frac{d\theta}{dz})$ at the reference radius. Introducing (II.4.32) in (II.4.31), we obtain

$$Z_1 = \left(\frac{\alpha \cos^2\phi_3}{\alpha_1 \cos^2\phi_1}\right)^{0.4/m+0.4} \qquad \text{(II.4.34)}$$

Since $(\alpha\cos^2\phi_3/\alpha_1\cos^2\phi_1)>1$ and Z_1 must be less than one to represent the inner critical point, we must have

$$\left(\frac{d\theta}{dz}\right)_3 < -0.4 \qquad \text{(II.4.35)}$$

In addition $\xi_1 \simeq 1$, hence

$$\xi V_1^2 \simeq \theta_1 \qquad \text{(II.4.36)}$$

and neglecting the effects of the azimuthal velocity, from (II.4.24) we may write

$$2\theta_1 - \frac{\gamma \xi}{Z_1} - Z_1 \left(\frac{d\theta}{dz}\right)_1 \simeq 0 \qquad \text{(II.4.37)}$$

Introducing (II.4.32) in this expression, it follows that

$$Z_1 \simeq \left(\frac{\gamma \xi}{2-m}\right)^{1/m+1} \qquad \text{(II.4.38)}$$

The term in parenthesis may be estimated from previous solar wind models and expected conditions at the critical radius and we find that it is

less than one. Thus, if $Z_1<1$, we must have $m>-1$. Equation (II.4.35) can then be expanded to include this lower bound,

$$-1 < \left(\frac{d\theta}{dz}\right)_3 < -0.4 \qquad \text{(II.4.39)}$$

At the Alfvenic critical point, equation (II.2.64) reduces to

$$\left(\frac{dV}{dz}\right)_2 = -2\delta W_2/Y_2 \tan\phi_2 \qquad \text{(II.4.40)}$$

Because of the proximity of this point to the reference radius, we may write

$$\left(\frac{dV}{dz}\right)_2 \simeq \left(\frac{dV}{dz}\right)_3 \simeq -2\delta/\tan\phi_3 \qquad \text{(II.4.41)}$$

Introducing (II.2.70), it follows that

$$\left(\frac{dV}{dz}\right)_3 \simeq -2\left(1 + \zeta/\tan\phi_3\right) \qquad \text{(II.4.42)}$$

Thus for a given angle ϕ_3, $(\frac{dv}{dz})_3$ depends almost exclusively on the value assigned to the parameter ζ.

It is now possible to formulate an optimum integration procedure based on the above results which will generate the desired solutions. The numerical integration process is optimized by introducing a new independent variable X such that

$$X = z^{-1} \qquad \text{(II.4.43)}$$

The governing equations may now be written in terms of this new variable as follows

$$\frac{dV}{dX} = -\frac{V}{X}\,\frac{f(X,V,\theta)}{g(X,V,\theta)} \qquad \text{(II.4.44)}$$

where

$$f(X,V,\theta) = 2\theta - \gamma\xi X + X\frac{d\theta}{dX} + \xi\zeta^2 X^2\left(\frac{\sigma^2-\mu/V}{1-\mu X^2/V}\right)^2 + \frac{2\xi\mu\zeta^2}{V}\left[\frac{(1-\sigma X^2)^2}{(1-\mu X^2/V)^3} - \frac{(1-\sigma^2X^2)}{(1-\mu X^2/V)^3}\right] \qquad \text{(II.4.45)}$$

and

$$g(X,V,\theta) = \xi V^2 - \theta - \frac{\xi\mu\zeta^2}{V}\frac{(1-\sigma^2X^2)^2}{(1-\mu X^2/V)^3} \qquad \text{(II.4.46)}$$

In addition

$$\frac{d\theta}{dX} = -\frac{\alpha\xi\cos^2\phi_3}{\theta^{5/2}}\left(1+\tan^2\phi\right)h(X,V,\theta) \qquad \text{(II.4.47)}$$

where

$$h(X,V,\theta) = \frac{1}{2}(V-V_\infty)(V+V_\infty) + \frac{\zeta^2X^2}{2}\left(\frac{\sigma^2-\mu/V}{1-\mu X^2/V}\right)^2 + \mu\zeta^2\left[\frac{(1-\sigma^2X^2)}{V(1-\mu X^2/V)} - \frac{1}{V_\infty}\right] + \frac{5\theta}{2\xi} - \gamma X \qquad \text{(II.4.48)}$$

and V_∞ is given by equation (II.4.50) below.

Given an initial set of values for the parameters consistent with expected solar wind conditions at the reference radius and such that equation (II.4.39) is satisfied, equations (II.4.44) and (II.4.47) are integrated inwards for $X>1+\varepsilon$ by means of a fourth-order, Runge-Kutta algorithm. This integration is carried out several times, each time adjusting $(\frac{dv}{dz})_3$ by varying ζ, such that the numerator and denominator of (II.4.44) vanish simultaneously or within a small fraction of an integration step at the inner critical point. Once this condition has been achieved, the integration is allowed to continue towards the sun's surface. The solution thus obtained is valid in the range $r_\odot<r<r_3$ but not beyond. Whang (1971c) has shown that once H is specified, the behavior of the solution for θ for large values of Z is governed by the value assigned to the parameter γ. We now integrate equations (II.4.44) and (II.4.47) in the outward direction ($X<1-\varepsilon$) utilizing the value of ζ determined by the inward integration. Again, the process is repeated several times, each time adjusting γ such that $\theta \to 0$ as $Z \to \infty$. The value

of γ thus obtained, is used to find a new value of ζ by the inward integration procedure previously described and then the equations are once more integrated in the outward direction to find the corresponding value of γ.

This iterative procedure is necessary because of the non-linear character of the equations; it is repeated enough times until the inner and outer solutions match across the reference radius with typically .01% accuracy. The outward integration is then continued to the limits imposed by the available computational accuracy and type of computer used to perform the calculation.

For the problems considered in this work, we have utilized Iverson's (1962) APL/360 language because of its unique characteristics, accuracy and conversational nature. A listing of the computer programs developed to obtain the numerical solution to the one-fluid MHD equations is given in Appendix A.

A problem that has plagued all models that numerically integrate the energy equation, is the extreme accuracy required to specify parameter values. This is due to the form of the equations when magnetic field inhibited heat conduction is assumed in the analysis and the requirement that the solutions must pass through one or more critical points. Our model is no exception, although the formulation of the equations in the form given by (II.4.44) and (II.4.47) was found to reduce the accuracy requirements by several orders of magnitude. To obtain a solution that passes through all critical points, ζ must be determined with typically 8-digit accuracy; to extend this solution to approximately 3.5 A.U., γ

must be determined with 12-digit accuracy, although this figure is strongly dependent upon the value assigned to H. If we try to obtain numerical solutions beyond this region, the computation time becomes prohibitive and other mathematical methods must be considered to obtain the desired solutions for the differential equations.

For large heliocentric distances, it is possible to find approximate analytical solutions for our equations in the form of asymptotic series. At large r, the direction of conduction heat flow is dominated by the spiral angle of the magnetic field and the conduction heat flux decreases much faster than the thermal energy flux. Hundhausen (1971, 1972) and Durney (1971) have shown that in this case the flow at large r corresponds to an adiabatic expansion with

$$\Theta \sim Z^{-4/3} \tag{II.4.49}$$

On the other hand, the velocity is expected to approach the limiting value $V=V_\infty$; hence in the limit, W, $\theta \to o$ and $V \to V_\infty$. Equation (II.2.67) reduces then to

$$H = \frac{V_\infty^2}{2} + \frac{\mu \xi^2}{V_\infty} \tag{II.4.50}$$

For large r we may neglect the azimuthal velocity component and write the governing equations in the simplified form that follows. Thus

$$\frac{dV}{dz} \simeq \frac{V}{z}\left(\frac{2\theta - \frac{\gamma\xi}{2} - z\frac{d\theta}{dz}}{\xi V^2 - \theta - \xi\mu\xi^2/V}\right) \tag{II.4.51}$$

and

$$\frac{d\theta}{dz} \simeq \frac{\alpha\xi\cos^2\phi_3}{z^2\theta^{5/2}}(1+\tan^2\phi)\left(\frac{1}{2}V^2 + \frac{\mu\xi^2}{V} + \frac{5\theta}{2\xi} - H - \frac{\gamma}{z}\right) \tag{II.4.52}$$

The formal asymptotic expansions of Whang (1972) can now be used to obtain a solution for these equations valid for large Z. Thus we write

$$V = V_\infty \left(1 + \varepsilon^3 \sum_0^\infty C_{1j}\, \varepsilon^j\right)$$
$$\theta = A\varepsilon^4 \left(1 + \sum_1^\infty C_{2j}\, \varepsilon^j\right) \qquad \text{(II.4.53)}$$

where $\varepsilon = Z^{-1/3}$. The leading terms in (II.4.47) represent the expected behavior of V and θ as $Z \to \infty$.

It follows that

$$\frac{dV}{dz} = -\frac{V_\infty}{3}\, \varepsilon^6 \sum_0^\infty (j+3)\, C_{1j}\, \varepsilon^j \qquad \text{(II.4.54)}$$

and

$$\frac{d\theta}{dz} = -\frac{A}{3}\, \varepsilon^7 \left[4 + \sum_1^\infty (j+4)\, C_{2j}\, \varepsilon^j\right] \qquad \text{(II.4.55)}$$

The coefficients C_{ij} are obtained by introducing (II.4.53) trough (II.4.55) in (II.4.51), and (II.4.52) and setting the coefficient of every power of ε equal to zero. For the one-fluid model under study we have calcualted the first few coefficients as follows

$$C_{10} = \gamma/P \quad ; \quad C_{11} = -5A/2\xi P \quad ; \quad C_{12} = 0$$
$$C_{13} = -5C_{10}\,(SC_{10} - \gamma)/2P \qquad \text{(II.4.56)}$$
$$C_{14} = \left[15\gamma\xi C_{11} - 35\, C_{10}\,(\xi S C_{11} + A)\right]/9\xi P$$

and

$$C_{21} = 0 \quad ; \quad C_{22} = \xi C_{10}\,(SC_{10} - \gamma)/A \quad ; \quad C_{23} = \left[14\, C_{10}\,(\xi S C_{11} + A) - 6\gamma\xi C_{11}\right]/4A \qquad \text{(II.4.57)}$$

where

$$\Gamma = \frac{3}{2} V_\infty^2 - H$$

and (II.4.58)

$$\Sigma = \frac{1}{2} V_\infty + H$$

The constant A in (II.4.53) is determined from the conditions obtained

at the point ϵ_o from the numerical integration such that both solutions join smoothly at this point. Hence

$$A = \frac{\theta_o - \frac{5}{3}C_{10}(5C_{10} - \gamma)\epsilon_o^6}{\epsilon_o^4 + \epsilon_o^7(29\gamma - 355C_{10})/9P} \qquad \text{(II.4.59)}$$

Once the solutions for V and θ have been obtained, we can compute

$$\delta W = \frac{5}{3}\epsilon^{-3} + V\tan\phi \qquad \text{(II.4.60)}$$

and

$$\tan\phi = \frac{5}{3}(\sigma^2 \epsilon^{-6})/V\epsilon^{-3}(1 - \mu\epsilon^{-6}/V) \qquad \text{(II.4.61)}$$

Two solutions to the one-fluid MHD equations have been obtained in the manner described above. The parameter values used in each solution are given in Table II with the corresponding dependent parameter values and flow conditions at the outer critical point.

We observe that the location of the three critical points in each solution is not very different from that given by the polytropic model of Weber and Davis. The numerical solutions pass smoothly through all critical points and approach the conditions $V=V_\infty$, $W=0$ and $\theta=0$ for $Z\to\infty$. Although both solutions give reasonable values for $\underline{u}$ and T at 1 A.U. those corresponding to Solution #2 are in better agreement with quiet time solar wind observations; numerical values for this solution are given in Table III for $1.08 \le r/r_\odot \le 2086$.

II.5 Discussion of Results and Physical Interpretations

Figures 3 and 4 show the results obtained for u_r, u_ω, T, β, and ϕ, for values of the parameters corresponding to Solution #1; Figures 5 and 6 show the corresponding results obtained for Solution #2.

TABLE II

Parameters	Solution #1	Solution #2
H	0.8	0.85
ϕ_3	169.8^o	169.8^o
ζ	0.19481	0.19531
β_3	0.2	0.2
γ	0.10924	0.097751
Related constants:		
α	0.46509	0.31673
μ	0.96529	0.96529
ξ	10.035	10.035
δ	0.014885	0.01538
σ	0.98384	0.98388
u_{r_3}	263.28 Km/sec.	272.98 Km/sec.
u_{ω_3}	3.91 Km/sec.	4.198 Km/sec.
r_3	25.237	26.234
r_2	24.829	25.81
r_1	3.74	3.96
T_3	$5.01 \times 10^5 {}^oK$	$5.39 \times 10^5 {}^oK$
u_∞	326.83 Km/sec.	349.86 Km/sec.
$(\frac{d\theta}{dZ})_3$	-0.588	-0.523
$(\frac{dV}{d\tau})_3$	0.167	0.173

TABLE III

ONE-FLUID MODEL. NUMERICAL SOLUTION #2

$r/r_\odot$	u_r (Km/sec.)	u_ψ (Km/sec.)	T (^oK)	$\frac{d\theta}{dZ}$	ϕ (deg)	β	A^2	V_a (Km/sec.)
1.084	22.29	1.99	2.68×10^6	-62.78	179.5	.0189	6101	1975
1.494	47.61	2.50	2.28 "	-37.70	179.3	.0162	1704	1966
2.065	76.05	3.03	1.93 "	-22.75	179.1	.0165	558.8	1798
2.851	107.2	3.53	1.65 "	-13.83	178.7	.0190	208.0	1546
3.944	138.3	3.98	1.41 "	- 8.54	178.3	.0240	84.20	1270
5.465	167.4	4.39	1.19 "	- 5.30	177.7	.0323	36.25	1009
7.603	195.2	4.65	1.01 "	- 3.26	176.8	.0454	16.06	783.8
10.70	220.8	4.77	8.54×10^5	- 1.97	175.6	.0669	7.16	592.8
14.99	242.8	4.70	7.20 "	- 1.21	173.9	.1000	3.32	445.1
21.86	263.9	4.42	5.93 "	-.700	171.3	.1593	1.43	320.1
29.15	277.8	4.05	5.10 "	-.446	168.7	.2280	.768	248.2
39.16	290.2	3.62	4.36 "	-.288	165.3	.3277	.407	191.5
52.47	300.8	3.14	3.72 "	-.187	161.0	.4631	.218	148.8
71.89	310.6	2.62	3.12 "	-.118	155.2	.6518	.112	115.0
97.19	318.7	2.16	2.63 "	-7.70×10^{-2}	148.4	.8607	6.02×10^{-2}	91.74
131.2	325.5	1.74	2.18 "	-5.11 "	140.8	1.057	3.23 "	75.48
181.0	331.7	1.36	1.75 "	-3.36 "	132.1	1.186	1.66 "	63.84
262.6	337.4	1.00	1.30 "	-2.08 "	122.3	1.155	7.79×10^{-3}	55.66
375.3	341.6	.735	9.44×10^4	-1.36 "	114.1	.9893	3.76 "	51.25
499.5	344.4	.569	6.47	-8.32×10^{-3}	108.7	.7366	2.10 "	49.21
664.8	346.2	.435	4.44 "	-4.29 "	104.3	.5309	1.18 "	47.99
884.9	347.4	.331	3.04 "	-2.21 "	100.9	.3747	6.66×10^{-4}	47.28
1177	348.2	.251	2.08 "	-1.14 "	98.2	.2610	3.75 "	46.86
1567	348.7	.189	1.42 "	-5.87×10^{-4}	96.2	.1804	2.11 "	46.61
2086	349.1	.143	9.73×10^3	-3.01 "	94.7	.1241	1.19 "	46.47

Figure 3

The temperature, radial and azimuthal velocities obtained for Solution #1 of the one-fluid model, as a function of heliocentric distance.

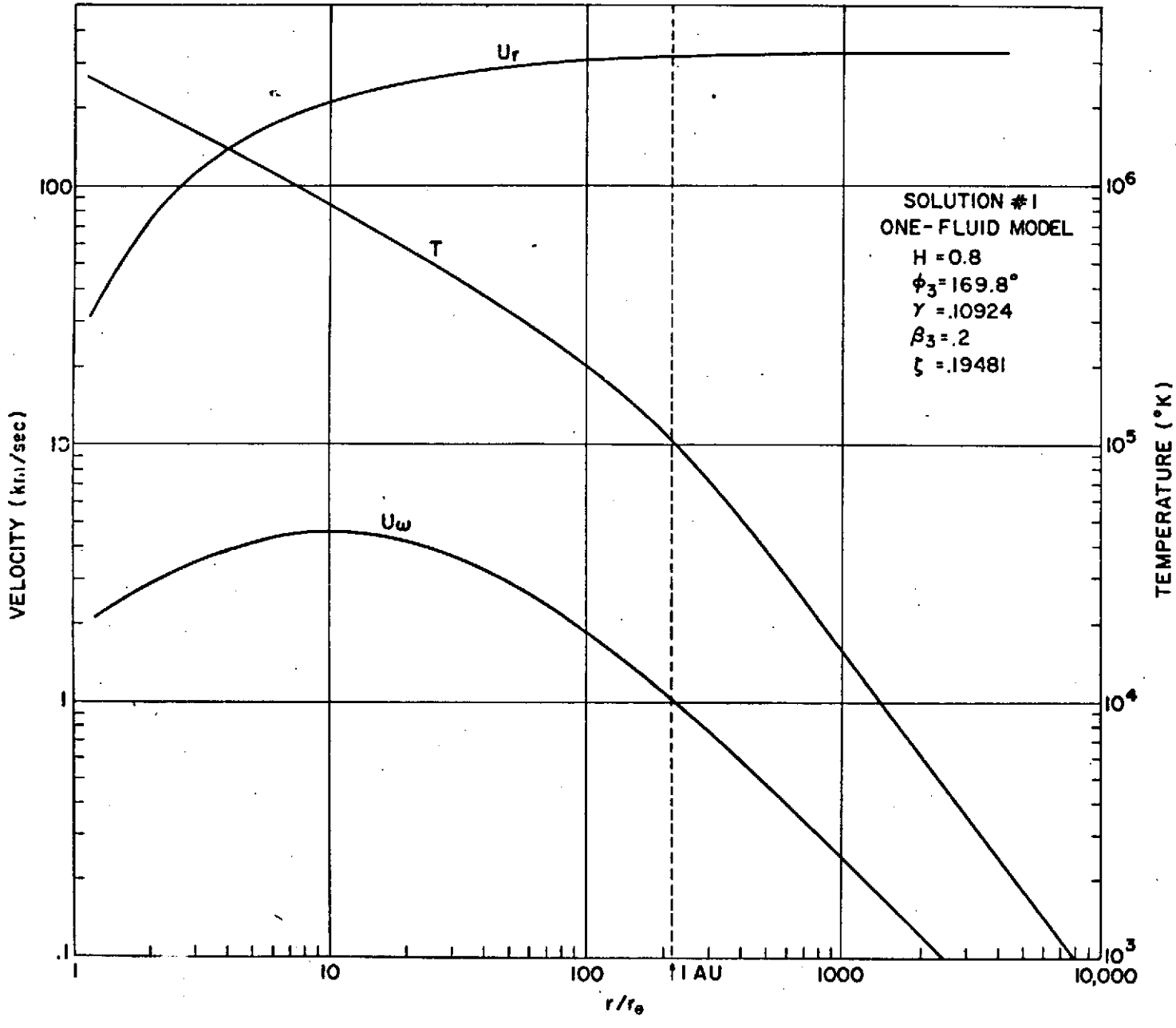
U_r
T
U_ω
SOLUTION #1
ONE-FLUID MODEL
H = 0.8
ϕ_3 = 169.8°
γ = .10924
β_3 = .2
ζ = .19481
VELOCITY (km/sec)
TEMPERATURE (°K)
100
10
1
.1
10^6
10^5
10^4
10^3
1
10
100
1 AU
1000
10,000
$r/r_\odot$

Figure 4

The plasma β and magnetic field angle ϕ as a function of heliocentric distance for Wolution #1, one-fluid model.

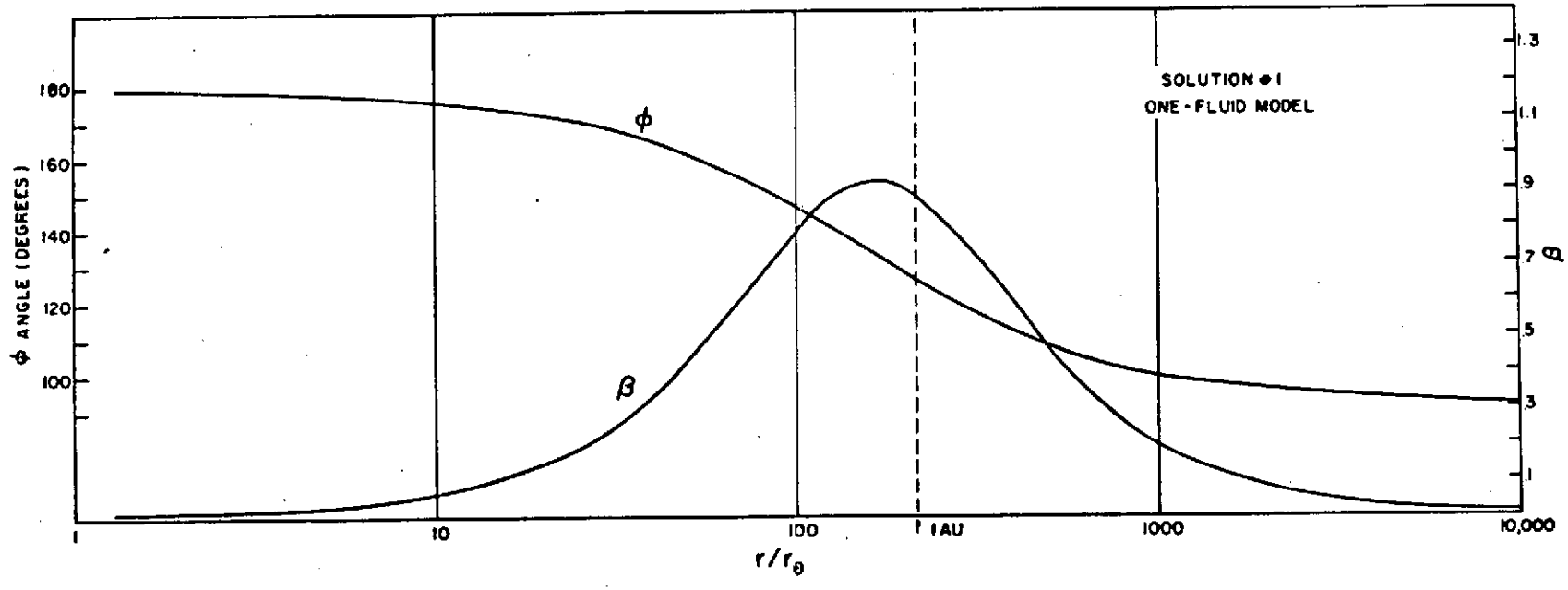
SOLUTION # 1
ONE-FLUID MODEL
φ
β
φ ANGLE (DEGREES)
180
160
140
120
100
1.3
1.1
.9
.7
.5
.3
.1
β
1
10
100
1 AU
1000
10,000
r/r0

Figure 5

The temperature, radial and azimuthal velocities obtained for Solution #2 of the one-fluid model, as a function of heliocentric distance.

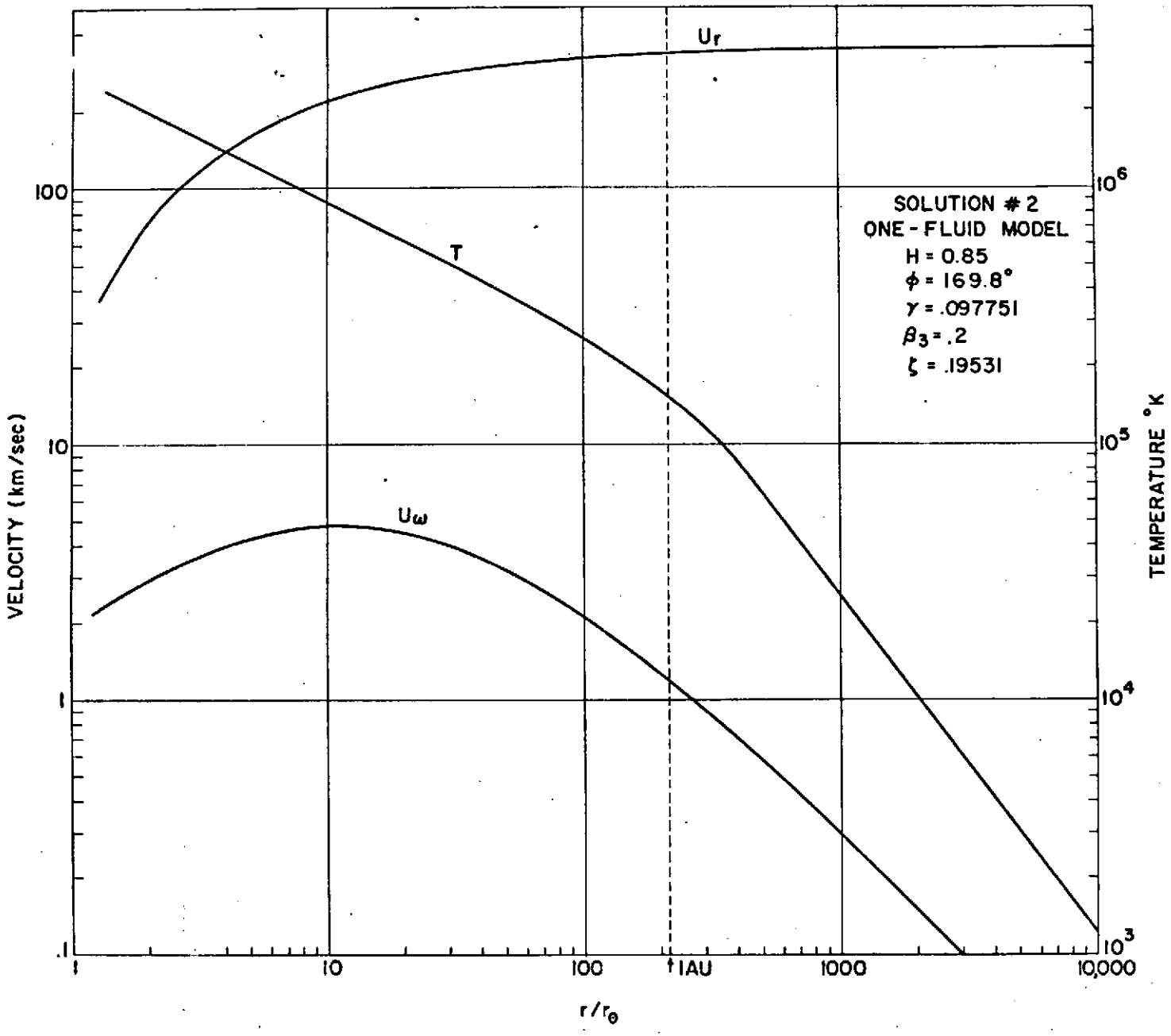
U_r
T
U_ω
SOLUTION # 2
ONE-FLUID MODEL
H = 0.85
ϕ = 169.8°
γ = .097751
β_3 = .2
ζ = .19531
VELOCITY (km/sec)
TEMPERATURE °K
100
10
1
.1
10^6
10^5
10^4
10^3
1
10
100
1AU
1000
10,000
$r/r_\odot$

Figure 6

The plasma β and magnetic field angle ϕ as a function of heliocentric distance for Solution #2, one-fluid model.

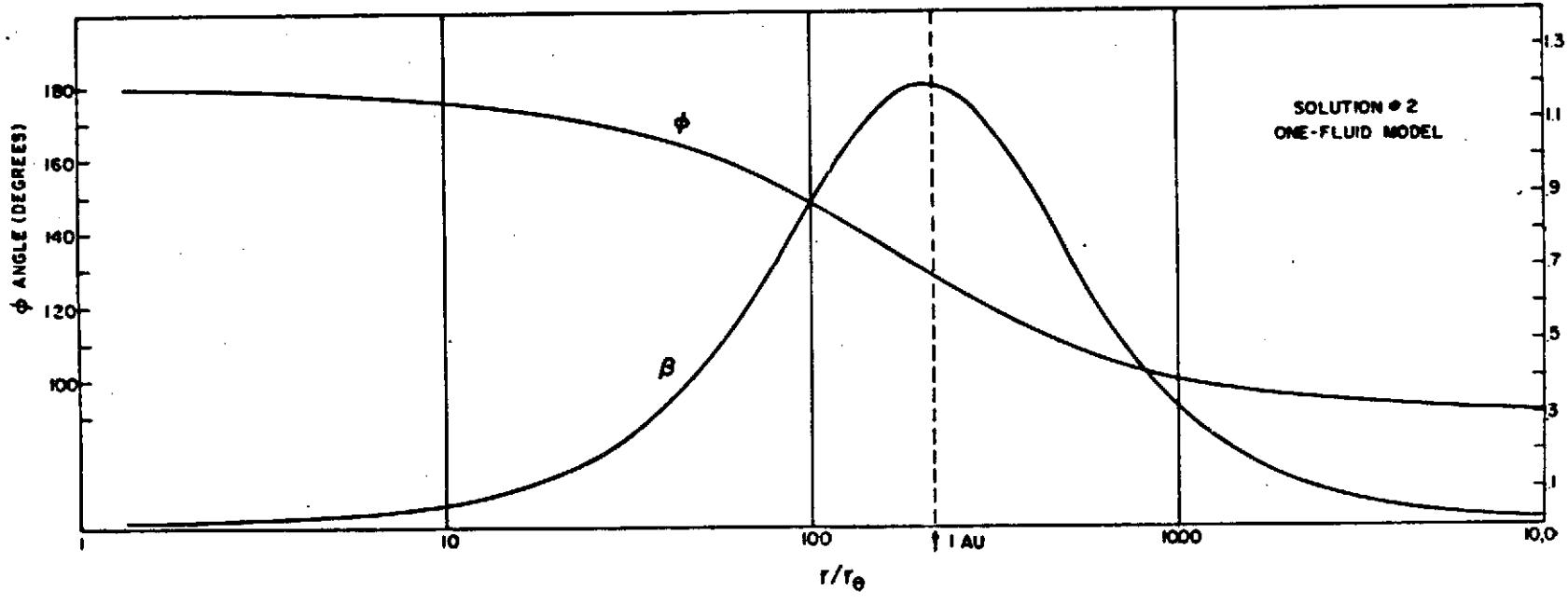
φ ANGLE (DEGREES)
180
160
140
120
100
φ
β
SOLUTION # 2
ONE-FLUID MODEL
1.3
1.1
.9
.7
.5
.3
.1
1
10
100
1 AU
1000
10,0
r/r⊙

The radial component of the expansion velocity is continuous across the critical points and increases monotonically from a few tens of Km/sec. near the sun, to a few hundred Km/sec. at large heliocentric distances. Solution #2 gives 334 Km/sec. at 1 A.U., in good agreement with observations during quiet times.

The azimuthal velocity component first increases with increasing distance from the sun's surface due to the tendency of the plasma to corotate with the sun. It reaches a maximum around $10r_{\odot}$ and then decreases monotonically with increasing distance. The predicted azimuthal velocity at the Earth's orbit for Solution #2 is 1.19 Km/sec., which is of the same magnitude as the azimuthal velocities predicted by Weber and Davis, Urch and Wolff et al.

This value of u_{ω} disagrees with reported observations of 6-10 Km/sec for the azimuthal speed; nevertheless the uncertainty in these measurements is of the same order of magnitude and further work in this area is necessary to resolve this conflict.

Weber and Davis have shown that the characteristic deceleration time for the sun due to the torque produced by the magnetic field and angular momentum loss can be written as

$$\tau = -J_{\odot} \Big/ \frac{2}{3}\Omega r_z^2 \frac{dM_{\odot}}{dt} \qquad \text{(II.5.1)}$$

If we take $\frac{dM_{\odot}}{dt} = -1.25\times10^{12}$ gm sec^{-1} we obtain $\tau = 7.9\times10^{9}$ years as the characteristic deceleration time for Solution #2. As expected this value agrees with previous results obtained by other authors.

Figure 7 shows the variation of the radial Alfven Mach number as a function of heliocentric distance. Near the sun $A^2 = M_A^{-2}$ is very large

Figure 7

The radial Alfven Mach number $M_A = \frac{u_r}{B_r}\sqrt{4\pi mn}$ as a function of heliocentric distance. Near the sun $M_A \ll 1$ reducing the effect of the magnetic field upon the radial component of the expansion velocity.

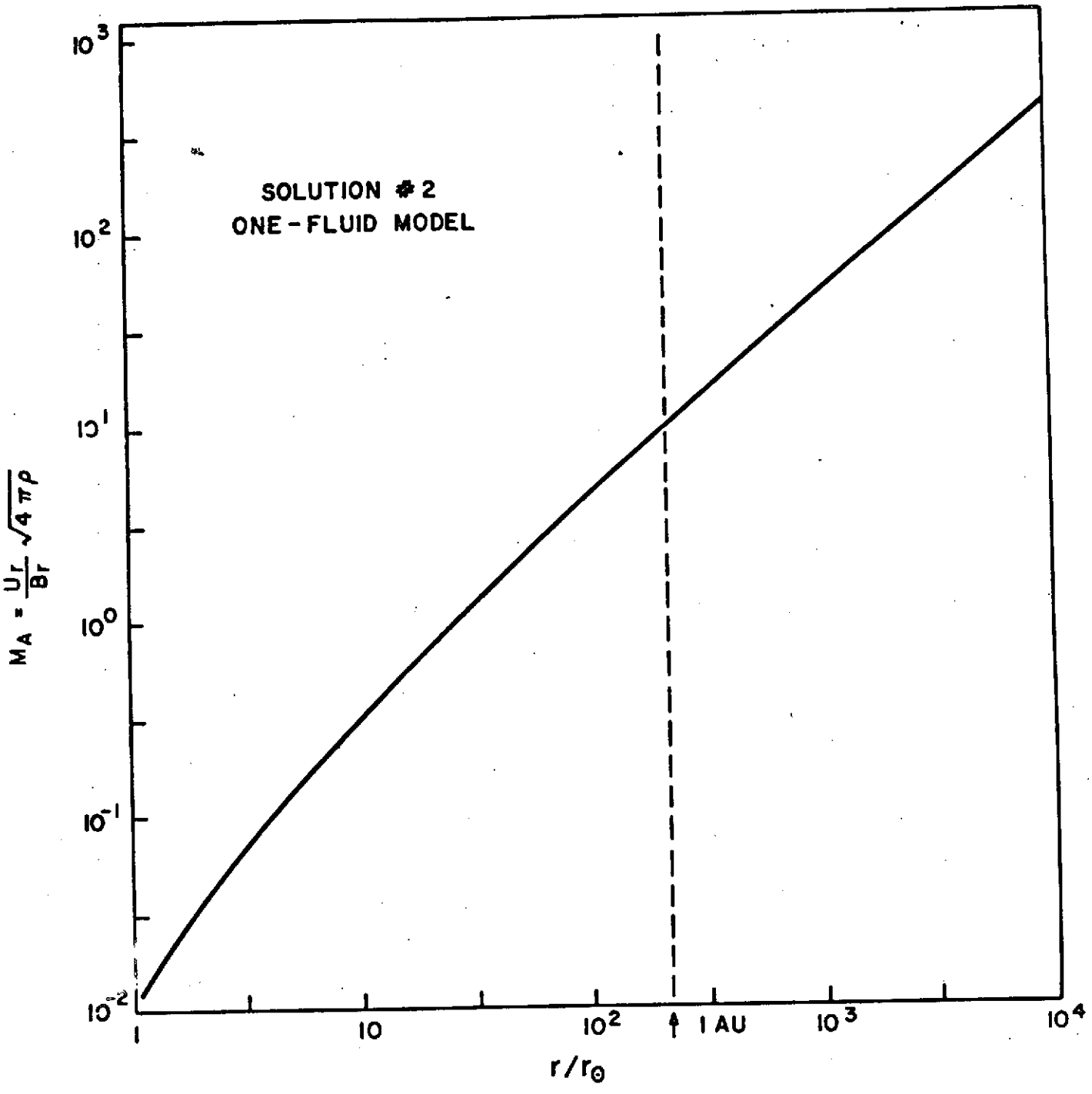
SOLUTION #2
ONE-FLUID MODEL
$M_A = \frac{U_r}{B_r}\sqrt{4\pi\rho}$
10^3
10^2
10^1
10^0
10^{-1}
10^{-2}
1
10
10^2
1 AU
10^3
10^4
$r/r_\odot$

reducing the effect of the magnetic field upon the radial expansion velocity as discussed in II.3. The magnetic field angle ϕ given in Figures 4 and 6 remains well behaved in the vicinity of the sun and tends to 180° for $r \to r_{\odot}$. A plot of the characteristic Alfven speed $B/\sqrt{4\pi\rho}$ for Solution #2 is given in Figure 8, while Figure 9 shows the radial component of V_A.

The predicted temperatures at 1 A.U. are $1.04 \times 10^5 {}^{o}K$ for Solution #1 and $1.54 \times 10^5 {}^{o}K$ for Solution #2, while the plasma β values are .89 and 1.19 respectively, in good agreement with observations. Table IV summarizes the flow conditions predicted by this model at 1 A.U. and for reference we have included the predictions of previous one-fluid models as reviewed by Hundhausen (1972).

The values of u_r, u_ω, T, $\frac{dT}{dr}$, β, ϕ, M_A and V_A calculated, are independent of the value assigned to the constant K in (II.2.57). To determine the particle number density, heat flux, magnetic field, kinetic and total energy flux, we must assign a value to K. From (II.2.55) it follows that

$$n = \frac{K}{v z^2}\left(\frac{\alpha T_3^{5/2}\cos^2\phi_3}{2 r_3 k u_{r_3}}\right) \qquad \text{(II.5.2)}$$

$$q = -\frac{K T_3}{r_3} T^{5/2}\frac{d\theta}{dz} \qquad \text{(II.5.3)}$$

and

$$B = (4\pi m n_3 \mu)^{1/2} u_{r_3} / z^2 \cos\phi \qquad \text{(II.5.4)}$$

The magnetic and kinetic energy flows per steradian are respectively

$$\frac{r^2 B^2}{4\pi}\left(u_r \sin^2\phi - u_\omega \sin\phi\cos\phi\right) \quad \text{and} \quad m n u_r r^2 \left(\frac{u^2}{\cdot\cdot}\right) \qquad \text{(II.5.5)}$$

We find that it is not possible to assign a unique value to K that will

Figure 8

The characteristic Alfven velocity $V_A = B/\sqrt{4\pi mn}$, as a function of heliocentric distance for Solution #2, one-fluid model.

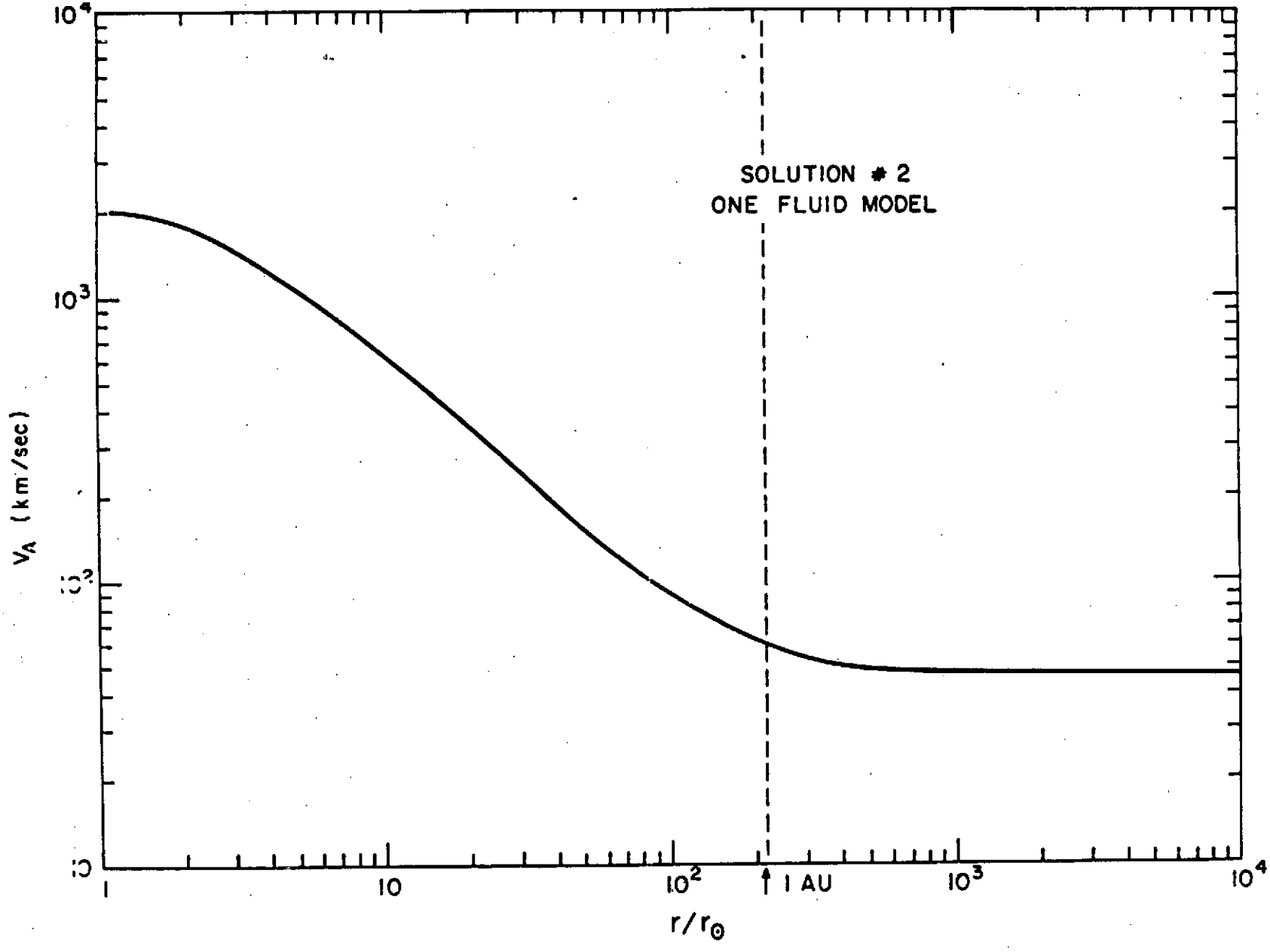
SOLUTION # 2
ONE FLUID MODEL
V_A (km/sec)
10^4
10^3
10^2
10
1
10^2
1 AU
10^3
10^4
$r/r_\odot$

Figure 9

The radial component of the characteristic Alfven velocity, V_{AR} as a function of heliocentric distance for Solution #2, one-fluid model.

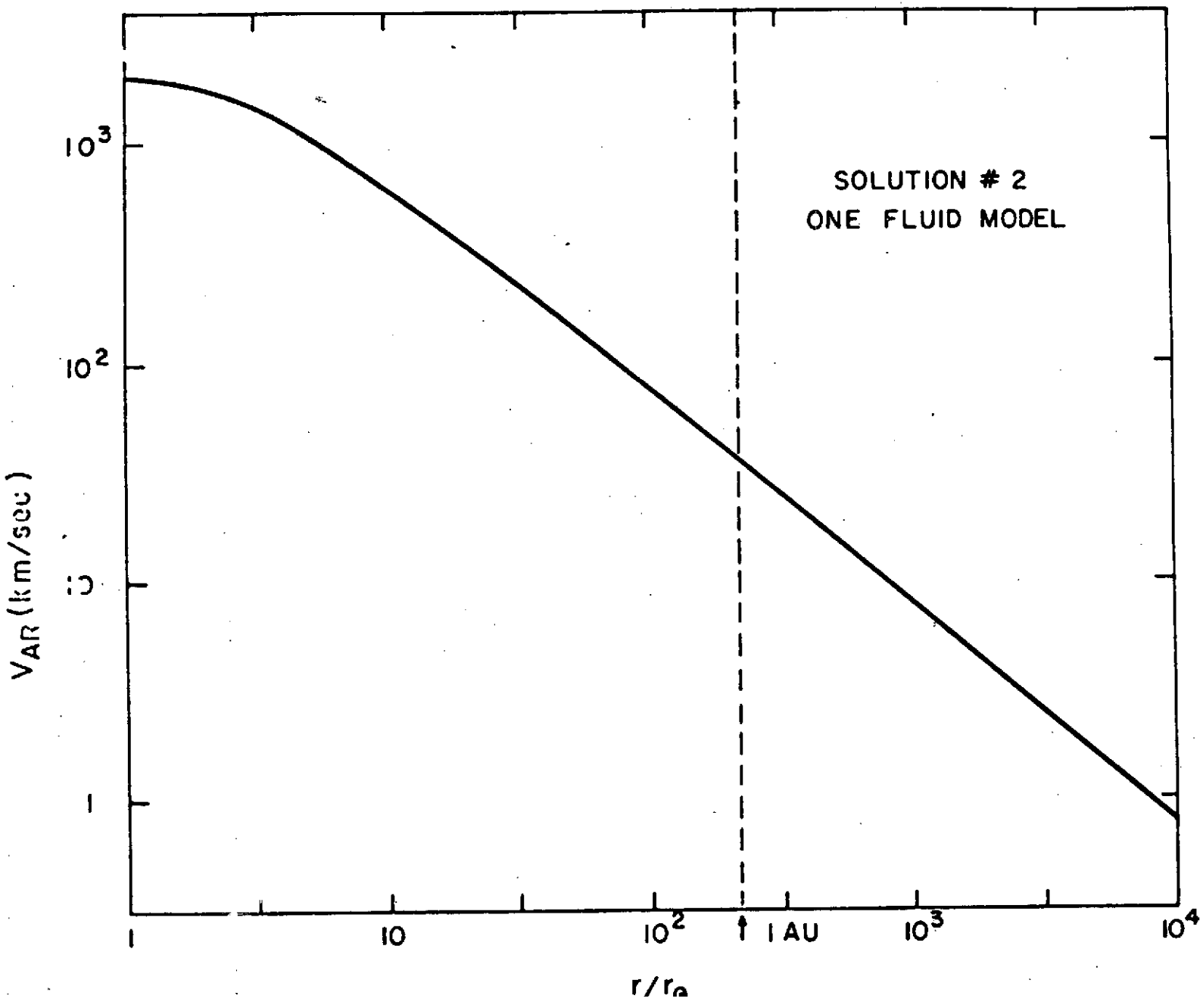
SOLUTION # 2
ONE FLUID MODEL
10^3
10^2
10
1
V_{AR} (km/sec)
1
10
10^2
1 AU
10^3
10^4
r/r_o

TABLE IV

PREDICTED FLOW CONDITIONS AT 1 A.U. - ONE-FLUID MODELS

	Sol. #1	Sol. #2	Whang (1971)	Urch (1969)	Whang & Chang (1965)	Noble & Scarf (1963)	Weber & (Davis (1967)
Radial velocity (Km/sec.)	317.6	334.4	302	371	260	352	~400
Azimuthal velocity (Km/sec.)	1.02	1.19	-	.623	-	-	1.0
Temperature (deg. K)	1.04×10^5	1.54×10^5	1.5×10^5	4.39×10^5	1.6×10^5	2.77×10^5	2×10^5
Magnetic field angle (deg.)	126.2	127.7	129.5	-	-	-	135°
Plasma Beta	.890	1.19	1.58	-	-	-	-

give reasonable values for these quantities at 1 A.U. and in the vicinity of the sun simultaneously. This would imply that the assumption K=const. is not valid throughout the region considered. In Figure 10 we show the density and magnetic field intensity obtained from Solution #2 for two extreme values of $K=8\times10^{-8}$ and $K=6\times10^{-7}$(ergs $cm^{-1}sec^{-1}deg^{-3.5}$). Analogous results are given in Figure 11 for the thermal energy flux q.

The best agreement with observations at 1 A.U. is obtained when we choose $K=1.0\times10^{-7}$(ergs $cm^{-1}sec^{-1}deg^{-3.5}$). Table V shows the values obtained for these quantities at 1 A.U. for different values of K between the two extreme values considered above.

In Figures 12 and 13 we have plotted the kinetic and magnetic energy fluxes per steradian as functions of heliocentric distance for $K=8\times10^{-8}$ ergs $cm^{-1}sec^{-1}deg^{-3.5}$. It is immediately apparent that only a small amount of magnetic field energy is converted into kinetic energy, in contrast to the results obtained by Whang. The principal factor responsible for the 17% increase in radial flow speed obtained by Whang is the introduction of magnetic field inhibited heat conduction in the energy equation. Thermal energy piles up behind the obstruction represented by the field, raising the temperature and increasing the velocity, (Parker, 1971; Hundhausen, 1972).

The value of the constant K which gives best agreement with observations at 1 A.U. is 0.16 of the classical Spitzer's value for ionized hydrogen. Recent observations of radio-star scintillations indicate that the solar wind is highly turbulent, (Jokipii, 1972). These fluctuations and waves are an essential aspect of the solar wind and affect the transpo

Figure 10

The particle number density and magnetic field intensity as a function of a heliocentric distance, for $K=8\times10^{-8}$ and 6×10^{-7} ergs cm^{-1} $sec^{-1}deg^{-3.5}$. Solution #2, one-fluid model.

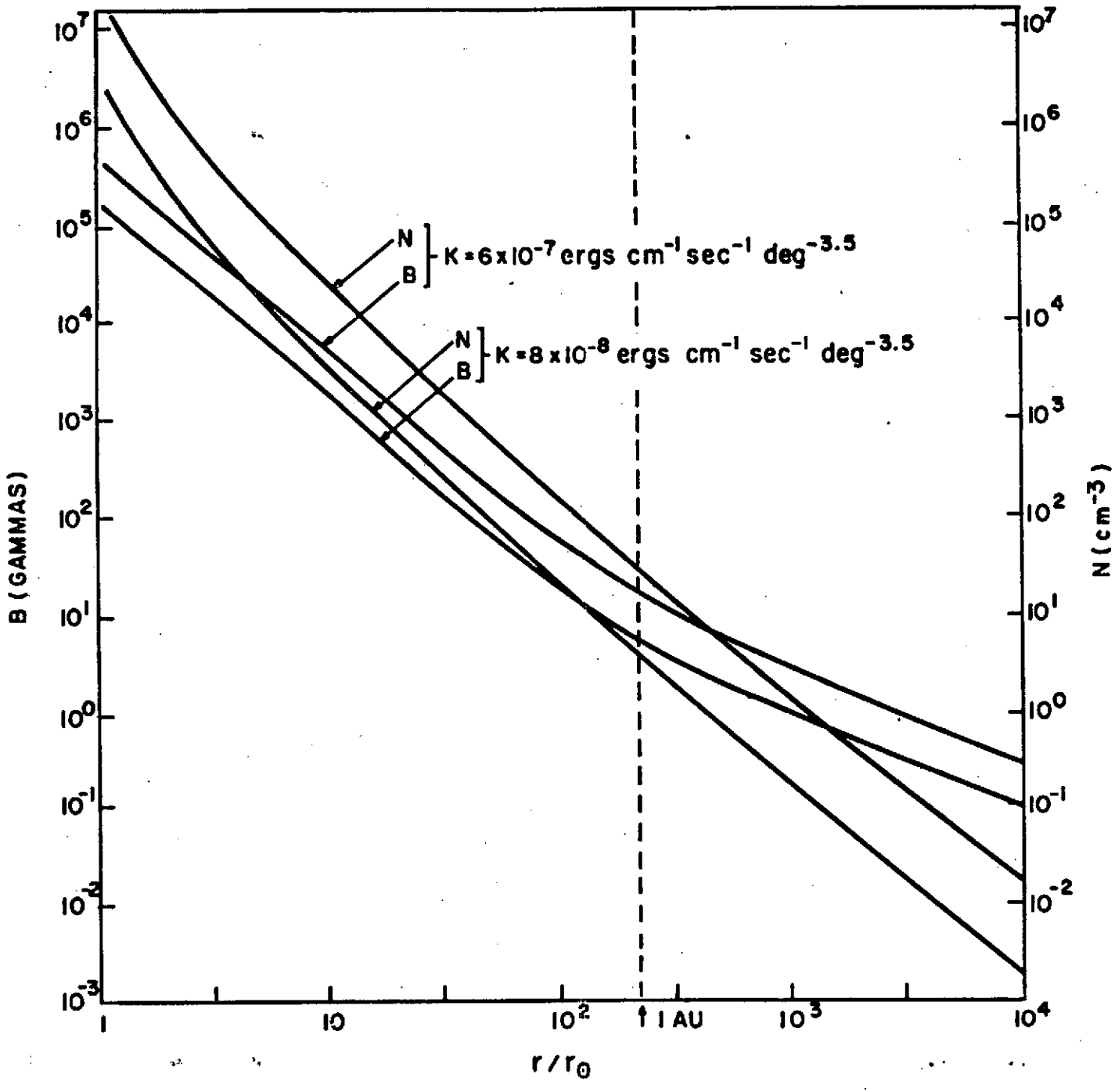
B (GAMMAS)
N (cm⁻³)
r / r₀
1 AU
N
B
K = 6 x 10⁻⁷ ergs cm⁻¹ sec⁻¹ deg⁻³·⁵
N
B
K = 8 x 10⁻⁸ ergs cm⁻¹ sec⁻¹ deg⁻³·⁵

Figure 11

The thermal energy flux Q, as a function of heliocentric distance for $K=8\times10^{-8}$ and 6×10^{-7} ergs $cm^{-1}sec^{-1}deg^{-3.5}$. Solution #2, one-fluid model.

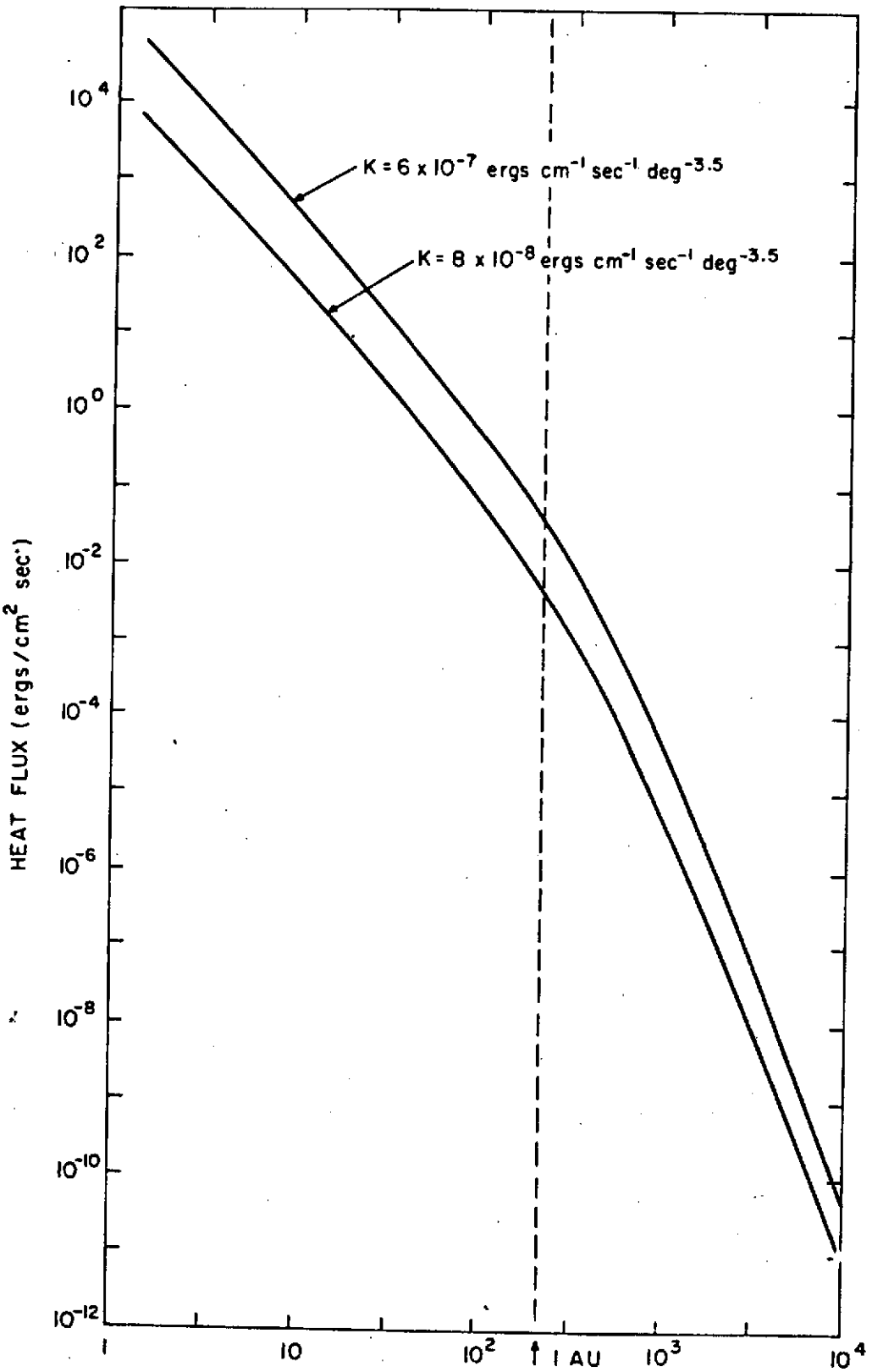
$K = 6 \times 10^{-7}$ ergs cm^{-1} sec^{-1} deg$^{-3.5}$
$K = 8 \times 10^{-8}$ ergs cm^{-1} sec^{-1} deg$^{-3.5}$
HEAT FLUX (ergs/cm^2 sec^{-1})
10^4
10^2
10^0
10^{-2}
10^{-4}
10^{-6}
10^{-8}
10^{-10}
10^{-12}
1
10
10^2
1 AU
10^3
10^4

TABLE V

TOTAL ENERGY FLUX, PARTICLE DENSITY, MAGNETIC FIELD INTENSITY AND HEAT FLUX PREDICTED BY SOLUTION #2 AT 1 A. U.

$K \times 10^{7}$ (ergs $cm^{-1}sec^{-1}deg^{-3.5}$)	$F \times 10^{-25}$ (ergs $sec^{-1}sterad^{-1}$)	F/r^2 (ergs $cm^{-2}sec^{-1}$)	n (cm^{-3})	B (gammas)	q (ergs $cm^{-2}sec^{-1}$)
6.00	33.0	1.487	35.4	17.8	4.62×10^{-2}
5.00	27.5	1.239	29.5	16.2	$3x84 \times 10^{-2}$
4.00	22.0	0.991	23.6	14.5	3.08×10^{-2}
3.00	16.5	0.743	17.7	12.6	2.30×10^{-2}
1.60	8.25	0.371	8.85	8.9	1.15×10^{-2}
1.40	7.70	0.347	8.26	8.6	1.07×10^{-2}
1.20	6.60	0.297	7.08	7.9	9.25×10^{-3}
1.00	5.50	0.247	5.90	7.2	7.71×10^{-3}
0.80	4.40	0.198	4.72	6.5	6.16×10^{-3}

Figure 12

The kinetic energy flux per steradian, $KEF=\frac{1}{2}\, mnu_r r^2(\underline{u}^2)$, as a function of heliocentric distance for $K=8\times10^{-8}$ ergs $cm^{-1}sec^{-1}deg^{-3.5}$. Solution #2, one-fluid model.

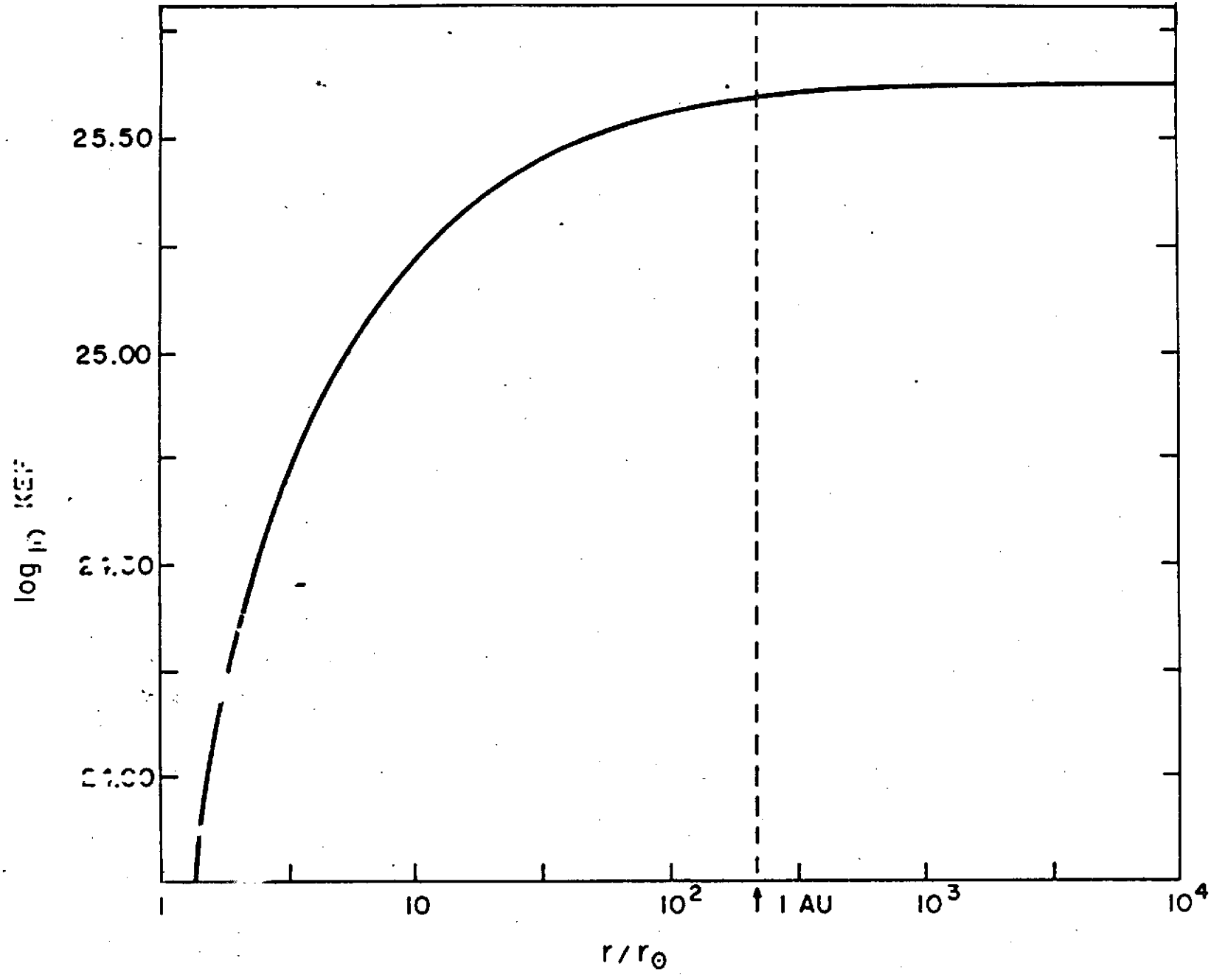
25.50
25.00
10
10^2
1 AU
10^3
10^4
$r/r_\odot$

Figure 13

The magnetic field energy flux per steradian,

$$MEF = \frac{r^2 B^2}{4\pi} (u_r \sin^2\phi - u_\omega \sin\phi \cos\phi)$$

as a function of heliocentric distance for $K=8\times10^{-8}$ ergs cm^{-1} sec^{-1} $deg^{-3.5}$. The amount of magnetic field energy converted into kinetic energy is a small fraction of the total energy flux.

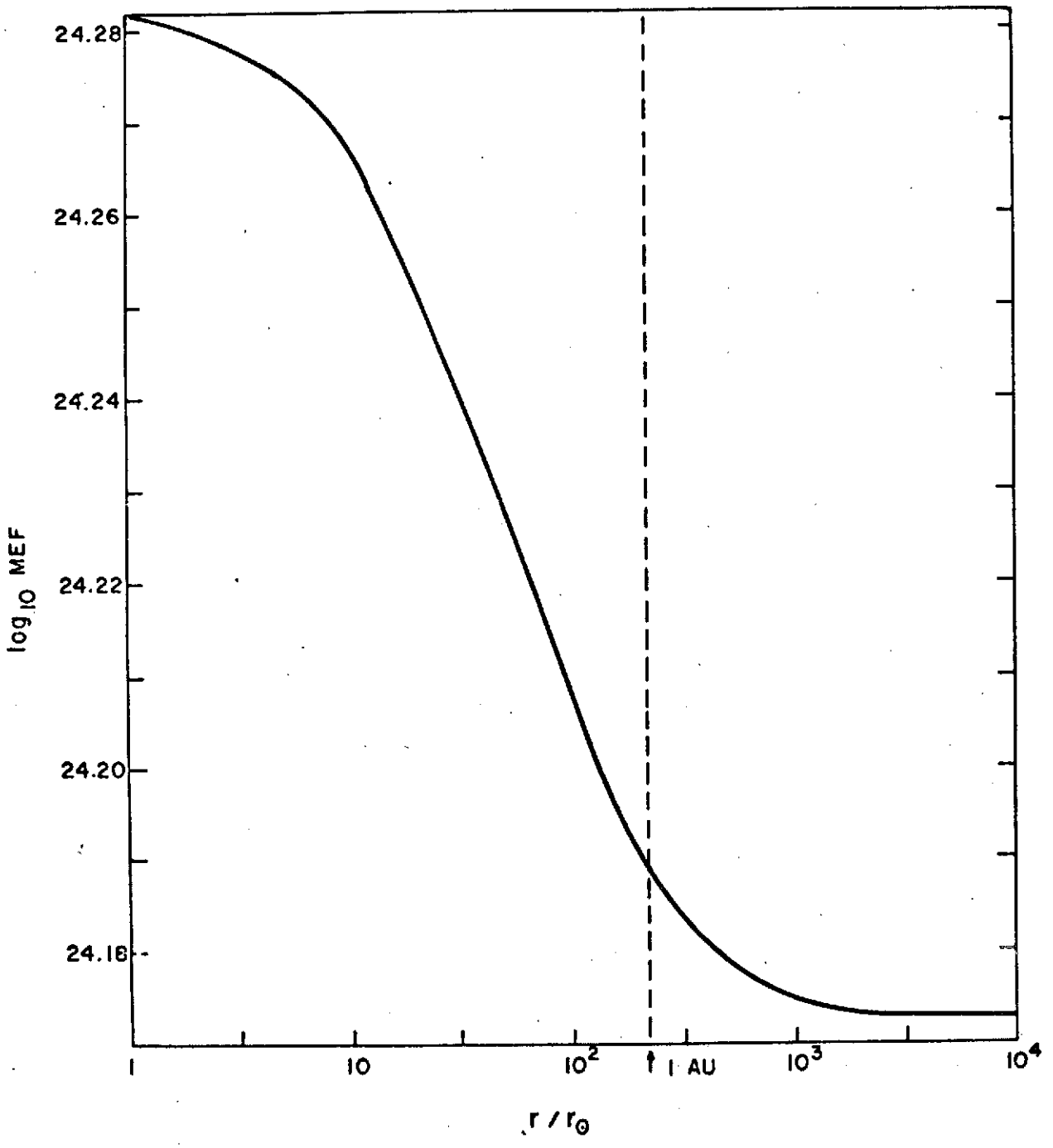
24.28
24.26
24.24
24.22
24.20
24.18
log10 MEF
1
10
10^2
1 AU
10^3
10^4
r / r⊙

coefficients in the plasma reducing the effective heat conductivity along the magnetic field lines and increasing the energy exchange rate between electrons and protons, (Hollweg, 1972; Hollweg and Jokipii, 1972; Perkins, 1973). Perkins has argued that Spitzer's conductivity is inapplicable in the region where the solar wind becomes collisionless and a reduced value should be used instead. The results obtained from the present model give support to these hypotheses since the choice of $K=6\times10^{-7}$ near the sun, corresponding approximately to Spitzer's value, leads to coronal densities in better agreement with observations (see Figure 10), while the reduced value $K=1\times10^{-7}$ gives agreement at 1 A.U. where the wind is essentially collisionless. These results imply the existence of two characteristic regions in the expansion process, with a transitional region in between. We shall consider these concepts in greater detail in the following chapter and develop a two-region, two-fluid model of the solar wind.

III. THE EFFECT OF THE PROTON THERMAL ANISOTROPY ON THE ANGULAR MOTION OF THE SOLAR WIND

III.1 Introduction to the Problem and Basic Assumptions

The particle velocity distribution function for a uniform, collisionless plasma in equilibrium in the presence of a magnetic field, possesses cylindrical symmetry around the field direction and is of the form

$$f(\underline{c}) = f(c_{\parallel}, c_{\perp}) \tag{III.1.1}$$

where $C_{\parallel}$ and $C_{\perp}$ denote the intrinsic velocity components parallel and perpendicular to the magnetic field. The second moments of (III.1.1) give the parallel and perpendicular pressures and are related to f by

$$p_{\parallel} = \int m c_{\parallel}^2 f \, d\underline{c} \tag{III.1.2}$$

and

$$p_{\perp} = \int \frac{m c_{\perp}^2}{2} f \, d\underline{c}$$

In addition, the parallel and perpendicular temperatures are defined by

$$nkT_{\parallel} = p_{\parallel} \quad ; \quad nkT_p = p_{\perp} \tag{III.1.3}$$

and the total plasma temperature is

$$T = (2T_{\perp} + T_{\parallel})/3 \tag{III.1.4}$$

The third moments of f give the conduction heat fluxes

$$q_{\parallel} = \int \frac{m}{2} c_{\parallel}^3 f \, d\underline{c} \tag{III.1.5}$$

and

$$q_{\perp} = \int \frac{m c_{\perp}^2}{2} c_{\parallel} f \, d\underline{c}$$

which are identically zero if f is Maxwellian in form. In a frame of reference with its $\underline{e}_1$ direction aligned with the magnetic field, the

pressure tensor $\underline{\underline{P}}$ will be given by

$$\underline{\underline{P}} = p_\perp \underline{\underline{I}} + (p_\parallel - p_\perp)\, \underline{e}_1 \underline{e}_1 \qquad \text{(III.1.6)}$$

where $\underline{\underline{I}}$ denotes the unit tensor. Solar wind observations indicate that in the vicinity of the Earth's orbit the proton pressure tensor is anisotropic with $P_\parallel > P_\perp$ and furthermore $q_\parallel \neq q_\perp \neq 0$ (Hundhausen, 1972), implying that f deviates from the Maxwellian form and the plasma is not in a state of thermal equilibrium. Figure 14 shows the contour map of a typical proton velocity distribution function reconstructed from observational data (Hundhausen, 1970).

The pressure tensor $\underline{\underline{P}}$ given by (III.1.6) may be used in the formulation of a more complete solar wind model if the rates of change of $P_\parallel$ and $P_\perp$ are known. Chew, Goldberger and Low (1956) obtained expressions for the second moments of the Vlasov equation under the assumptions described above which may be written as follows

$$\frac{D}{Dt}\left(\frac{B^2 T_\parallel}{n^2}\right) + \frac{2B^3}{n^3 k}\, \underline{e}_1 \cdot \nabla\left(\frac{q_\parallel}{B}\right) = 0$$

and (III.1.7)

$$\frac{D}{Dt}\left(\frac{T_\perp}{B}\right) + \frac{1}{nk}\, \underline{e}_1 \cdot \nabla\left(\frac{q_\perp}{B}\right) = 0$$

Since these expressions involve heat flux terms the general set of magnetohydrodynamic equations cannot be closed in terms of known moments of the velocity distribution function and thus two additional equations are required to determine $q_\parallel$ and $q_\perp$.

Whang (1971d) showed that the proton velocity distribution function in the solar wind could be approximated by

$$f = [1 + c_{11}\, h(c_1, c_\perp)]\, f^0 \qquad \text{(III.1.8)}$$

Figure 14

Contour map of the proton velocity distribution function at 1 A.U. as reconstructed from observational data, (Hundhausen, 1970). The Z-axis corresponds to the direction of the magnetic field and points away from the sun.

KM/SEC

0 50

VELA 3B

8-4-65

16.952 HRS.

HUNDHAUSEN (1970)

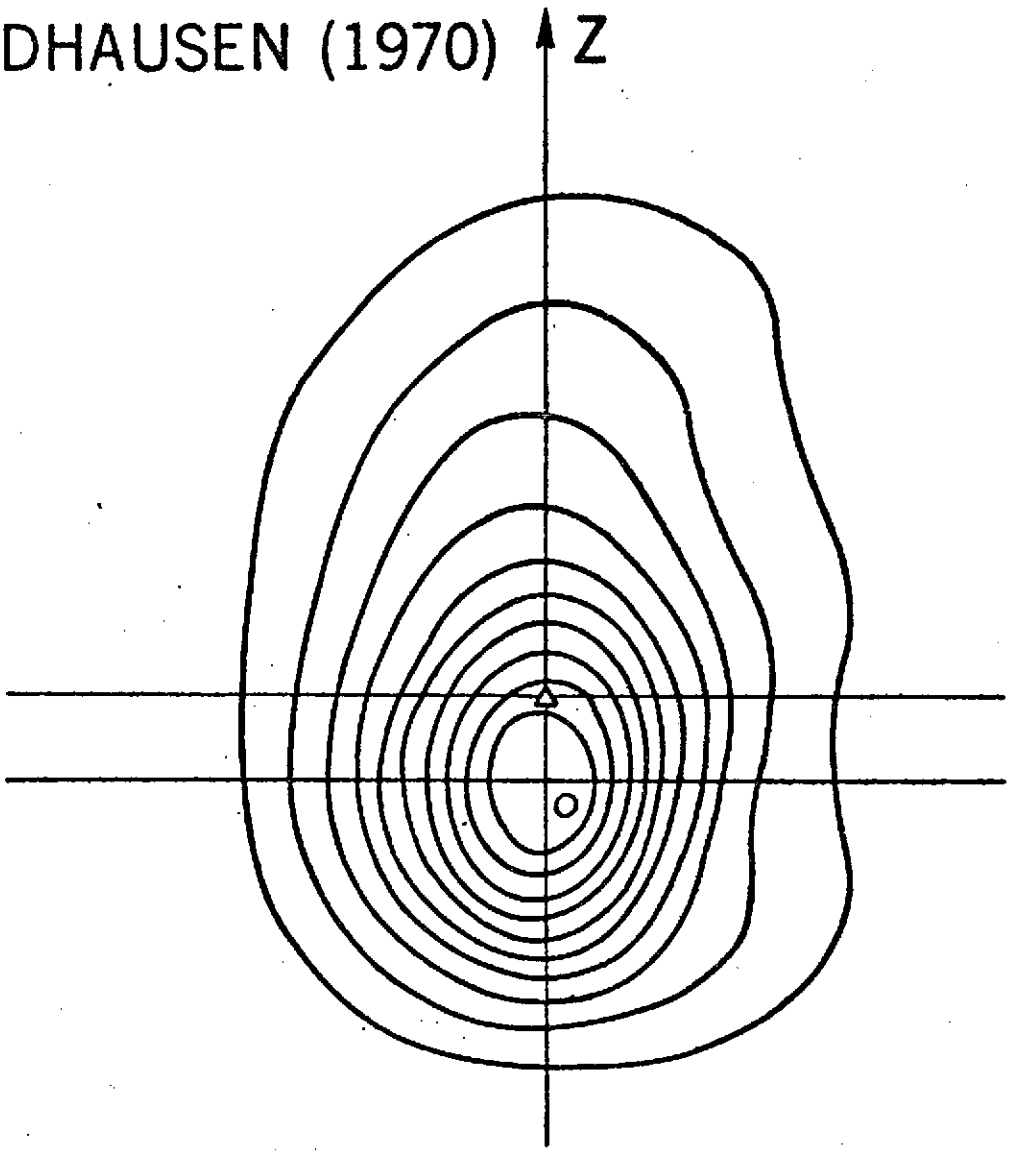

where f^o is the bi-Maxwellian distribution function

$$f^o = (n/\pi^{3/2} A_\perp^2 A_\parallel) \exp(-\xi_\parallel^2 - \xi_\perp^2) \qquad \text{(III.1.9)}$$

with

$$A_\parallel = (2kT_\parallel/m)^{1/2} \; ; \quad A_\perp = (2kT_\perp/m)^{1/2} \qquad \text{(III.1.10)}$$

and

$$\xi_\parallel = c_\parallel/A_\parallel \quad ; \quad \xi_\perp = c_\perp/A_\perp \qquad \text{(III.1.11)}$$

These are the dimensionless forms of the intrinsic velocity components; the dimensionless heat fluxes $\gamma_\parallel$ and $\gamma_\perp$ are defined by

$$\gamma_\parallel = q_\parallel/A_\parallel (nkT_\parallel/2) \; ; \quad \gamma_\perp = q_\perp/A_\parallel nkT_\perp \qquad \text{(III.1.12)}$$

The function h is an even function of $C_\parallel$ and $C_\perp$ and in this notation it takes the form

$$h(\xi_\parallel, \xi_\perp) = \gamma_\parallel \left(\frac{2}{3}\xi_\parallel^2 - 1\right) + 2\gamma_\perp \left(\xi_\perp^2 - 1\right) \qquad \text{(III.1.13)}$$

Using this form of the distribution function it is possible to compute the third and fourth moments of the Vlasov equation in terms of lower moments, closing the system of MHD equations. Whang has obtained the following expressions:

$$\frac{D}{Dt}\left(\frac{B^3 q_\parallel}{n^4}\right) = \frac{3k^2B^2}{2mn^3} \underline{e}_1 \cdot (T_\parallel T_\perp \nabla B - BT_\parallel \nabla T_\parallel) \qquad \text{(III.1.14)}$$

and

$$\frac{D}{Dt}\left(\frac{q_\perp}{n^2}\right) = \frac{k^2}{mnB} \underline{e}_1 \cdot (T_\perp^2 \nabla B - BT_\parallel \nabla T_\perp)$$

Equations (III.1.7) and (III.1.14) thus govern the variation of the proton temperatures $T_\parallel$ and $T_\perp$, and proton heat fluxes $q_\parallel$ and $q_\perp$ in a collisionless heat conducting plasma.

Near the sun, the energy exchange rate between electrons and protons is high and the solar wind behaves as a thermally isotropic one-fluid, that is, the electron temperature equals the proton temperature and the

anisotropy ratio is unity. As we proceed away from the sun the plasma density decreases and the interaction weakens causing the electron and proton temperatures to become different and anisotropic due to the presence of the magnetic field. Early models of the solar wind (Sturrock and Hartle, 1966; Hartle and Sturrock, 1968) which attempted to incorporate this effect by means of classical plasma theory based on binary Coulomb collisions failed to predict anisotropy and the observed solar wind conditions at 1 A.U. Due to the weak interaction with electrons, the protons cool off too rapidly leading to an adiabatic expansion at small heliocentric distances. As a consequence the predicted proton temperature at 1 A.U. is low while the electron temperature is high leading to values of the conduction heat flux much higher than observed.

Since then several mechanisms have been proposed to explain proton heating beyond the region in which classical collisions play a dominant role. They include collisionless heating by dissipation of hydromagnetic waves (Barnes, 1968, 1969; Barnes et al., 1971; Hung and Barnes, 1973), viscosity (Wolff et al., 1971), coronal Alfven waves (Belcher, 1971), MHD pulses (Papadopoulos, 1973) and electrostatic ion cyclotron waves (Toichi, 1971). Perkins (1973), on the basis of radio-star scintillation observations of the turbulent solar wind, has proposed that magnetoacoustic plasma instabilities are responsible for the increased energy exchange rate between electrons and protons. At this time the exact nature of the interaction is not known but we may consider an inner region in which the proton and electron temperatures are equal and isotropic, and an outer region in which the protons become collisionless and their temperature

anisotropic. In between there is a transition region in which the protons are neither collisionless nor isotropic or one-fluid. Figure 15 helps to illustrate these concepts; the dashed lines represent expected solar wind conditions as deduced from observations at 1 A.U., while the solid lines represent results obtained from the two-fluid models indicated.

The two-region concept has evolved from the theoretical work of Hollweg (1970, 1971), Burlaga (1971), Leer and Holzer (1972), Chen et al. (1972) and other authors. Whang (1972) has incorporated the two-region approach into a two-fluid model of the solar wind. This model, using the proton distribution function (III.1.7), provides macroscopic as well as microscopic information about solar wind protons; the results show good agreement with experimental observations.

The proton thermal anisotropy is of particular importance in the study of the solar wind angular momentum since the pressure tensor $\underline{\underline{P}}$ given by (III.1.6) will give rise to additional azimuthal forces not considered in Chapter II of this work. Weber and Davis (1970) have included these forces, as well as viscosity, in their analysis of the azimuthal motion, in an effort to explain the discrepancy between observed and predicted azimuthal velocities at 1 A.U. Nevertheless, the form of $(P_{\parallel}-P_{\perp})$ used in their calculations was a simple interpolation formula

$$P_{\parallel} - P_{\perp} = \varepsilon P_{\parallel} B_{\omega}^2/B^2 \qquad \text{(III.1.15)}$$

in which the parameter ε is varied between $\varepsilon = 1$ at 1 A.U. and $\varepsilon = 0$ near the sun and $P_{\parallel}$, $P_{\perp}$ represent the total thermal pressure (electron and proton) components parallel and perpendicular to the magnetic field. Solar wind observations (Montgomery, 1971) reveal that the electron

Figure 15

The two regions considered in the two-fluid model of the solar wind. The dashed lines represent expected solar wind conditions as deduced from observations at 1 A.U., while the solid lines represent results obtained from previous two-fluid models.

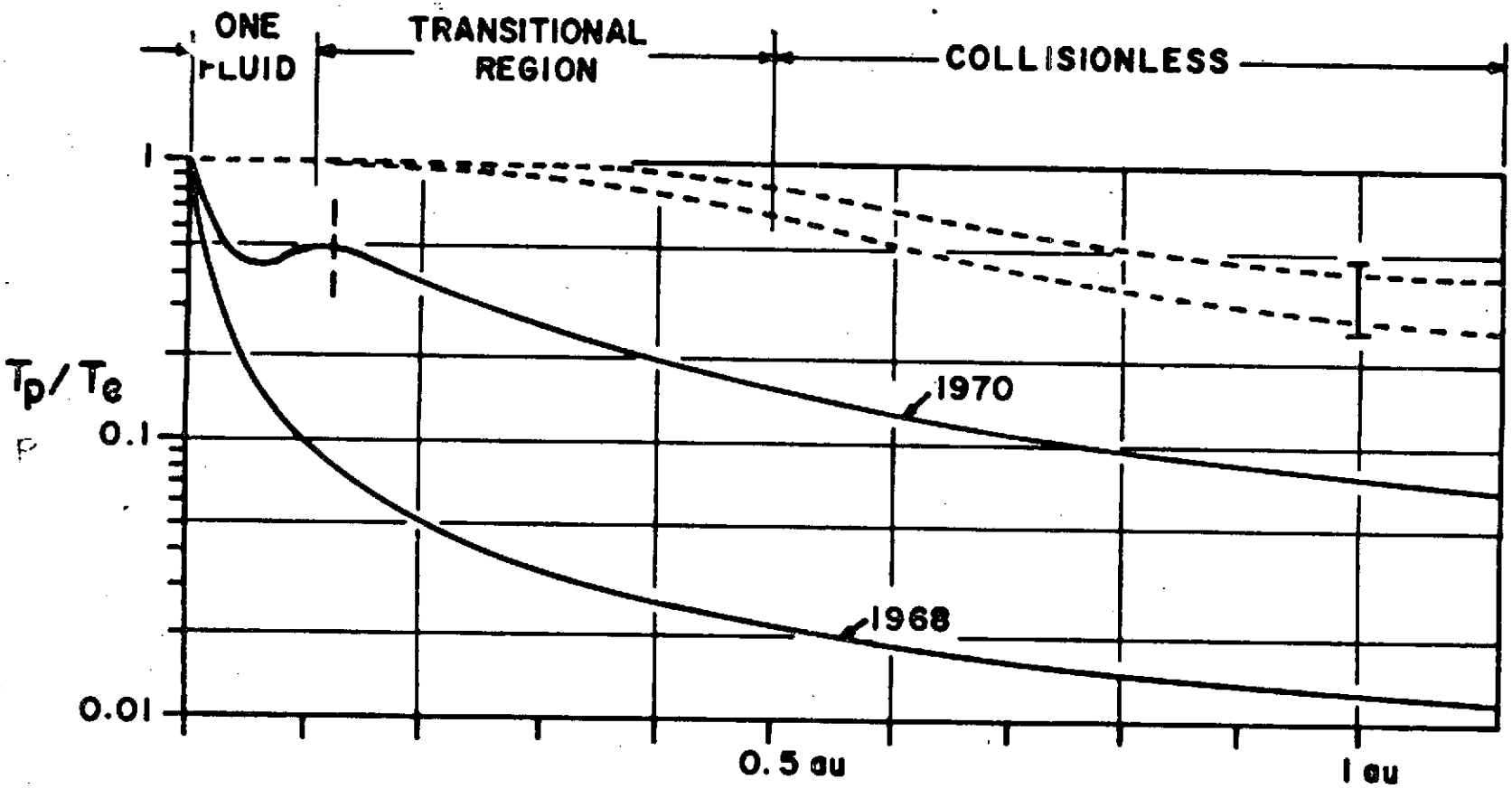

TWO-FLUID MODELS: 1968 HARTLE & STURROCK (COULOMB INTERACTION)
1970 HARTLE & BARNES (HEATING INSIDE .12 au)

thermal anisotropy at 1 A.U. is small, with $(P_{\parallel}/P_{\perp})\simeq 1$; consequently, the form (III.1.15)) is expected to overestimate electron thermal anisotropy effects and lead to larger azimuthal velocities at the earth's orbit.

In the following sections we shall expand the model developed in Chapter II to include the effects of the proton thermal anisotropy in the fashion described by Whang. The electrons will be considered isotropic throughout and treated in the same way as in Chapter II. In the inner region we will use the equations developed in Sections II.2 and II.3 to obtain a one-fluid solution for the model up to a transition point where the protons will be assumed to become collisionless. From this point out, we will use the equations developed below to obtain a two-fluid solution in which the proton temperature becomes anisotropic beyond the transition point and into the outer region. The general assumptions made in II.1 regarding the interplanetary magnetic field, steady state and fluid behavior of the solar wind, apply without modification to this case.

III.2 Governing Equations for the Outer Region

The equations of mass, momentum and energy conservation given in Chapter II have to be expanded to incorporate the anisotropic proton pressure tensor $\underline{\underline{P}}$ given by (III.1.6), the second moment equations of Chew-Goldberger-Low (III.1.7) and the third moment equations of Whang (III.1.14). The general forms (II.2.1), (II.2.2) and (II.2.3) are valid and we need only consider those terms involving pressure, temperature and heat flux.

The velocity $\underline{u}$ and magnetic field $\underline{B}$ will be expressed as in (II.2.11)

and (II.2.12) thus Maxwell's equations apply without modification. Equation (III.1.6) will represent the proton pressure tensor and may be written as

$$\underline{\underline{P}}_p = p_\perp \underline{\underline{I}} + \frac{\underline{B}\,\underline{B}}{B^2}(p_\parallel - p_\perp) \qquad \text{(III.2.1)}$$

Furthermore, the force component due to the proton pressure is given by (Appendix B)

$$\nabla \cdot \underline{\underline{P}}_p = \nabla p_\perp + \frac{(p_\parallel - p_\perp)}{B^2}(\underline{B}\cdot\nabla)\underline{B} + (\underline{B})\,\underline{B}\cdot\nabla\left(\frac{p_\parallel - p_\perp}{B^2}\right) \qquad \text{(III.2.2)}$$

The total thermal pressure tensor for our model is then

$$\underline{\underline{P}} = (nkT_e + p_\perp)\underline{\underline{I}} + \frac{\underline{B}\,\underline{B}}{B^2}(p_\parallel - p_\perp) \qquad \text{(III.2.3)}$$

where T_e denotes the isotropic electron temperature. The radial and azimuthal components of the pressure force are thus given by

$$(\nabla\cdot\underline{\underline{P}})_r = \frac{\partial}{\partial r}(nkT_e) + \sin^2\phi\,\frac{\partial}{\partial r}(nkT_\perp) + \cos^2\phi\,\frac{\partial}{\partial r}(nkT_\parallel) + \frac{nk(T_\parallel - T_\perp)}{r}(4\cos^4\phi - \cos^2\phi - 1) - \frac{2nk(T_\parallel - T_\perp)}{B^2}\cos^2\phi\, B_\omega \frac{\partial B_\omega}{\partial r} \qquad \text{(III.2.4)}$$

and

$$(\nabla\cdot\underline{\underline{P}})_\omega = \cos\phi\sin\phi\,\frac{\partial}{\partial r}[nk(T_\parallel - T_\perp)] + \frac{nk(T_\parallel - T_\perp)}{r}\cos\phi\sin\phi\,(1 + 4\cos^2\phi) + \frac{B_r}{B^2}\frac{\partial B_\omega}{\partial r}\,nk(T_\parallel - T_\perp)\cos 2\phi \qquad \text{(III.2.5)}$$

The corresponding components of the equation of motion are obtained by introducing (III.2.4) and (III.2.5) in (II.2.2) and making use of Maxwell's equations. The results are respectively

$$\frac{1}{u_r}\frac{\partial u_r}{\partial r}\left\{u_r^2 - \frac{k}{m}\left[T_\perp \sin^2\phi(1+2\cos^2\phi) + T_\parallel \cos^2\phi(1-2\sin^2\phi) + T_e\right] - \frac{B_\omega^2}{4\pi mn}\right\} =$$

$$\frac{1}{r}\left\{-\frac{kr}{m}\left(\frac{\partial T_e}{\partial r} + \sin^2\phi\,\frac{\partial T_\perp}{\partial r} + \cos^2\phi\,\frac{\partial T_\parallel}{\partial r}\right) + \frac{k}{m}\left[2(T_e + T_\perp) + (T_\parallel - T_\perp)\sin^2\phi(1+2\cos^2\phi)\right]\right.$$

$$-\frac{GM_\odot}{r}+\left(\frac{\partial u_\omega}{\partial r}-\frac{u_\omega}{r}\right)\left[\frac{2kr(T_{11}-T_\perp)}{m u_r}\cos^2\phi\sin\phi-\frac{rB_\omega B_r}{4\pi mn u_r}\right]+u_\omega^2\Bigg\} \tag{III.2.6}$$

and

$$\frac{1}{u_r}\frac{\partial u_\omega}{\partial r}\left[u_r^2+\frac{k}{m}(T_{11}-T_\perp)\cos 2\phi\cos^2\phi-\frac{B_r^2}{4\pi mn}\right.=$$

$$\frac{1}{u_r}\frac{\partial u_r}{\partial r}\left[\frac{k}{m}(T_{11}-T_\perp)\sin 2\phi\cos^2\phi-\frac{B_\omega B_r}{4\pi mn}\right]-\frac{k}{m}\cos\phi\sin\phi\frac{\partial}{\partial r}(T_{11}-T_\perp)$$

$$-\frac{k}{m}\frac{(T_{11}-T_\perp)}{r}\sin 2\phi\cos^2\phi-\frac{2u_\omega u_r}{r} \tag{III.2.7}$$

We observe in (III.2.7) that the anisotropic proton pressure introduces additional terms in the azimuthal part of the momentum equation and it cannot be integrated directly as in Chapter II. These terms will tend to increase the total angular momentum in the solar wind.

We must now find expressions for the terms in the energy equation that involve the new form of the pressure tensor, thus we calculate

$$\nabla\cdot(\underline{\underline{P}}\cdot\underline{u})=\frac{1}{r^2}\frac{\partial}{\partial r}r^2\Big\{u_r\left[nk(T_e+T_\perp)+\cos^2\phi\, nk(T_{11}-T_\perp)\right] \tag{III.2.8}$$

$$+\,u_\omega\cos\phi\sin\phi\, nk(T_{11}-T_\perp)\Big\}$$

For the heat flux term $\nabla\cdot\underline{Q}$, we have

$$\nabla\cdot\underline{Q}=\frac{1}{r^2}\frac{\partial}{\partial r}r^2 q_r \tag{III.2.9}$$

where q_r is now composed of three terms: the radial component of the electron heat flux and the radial components of the parallel and perpendicular proton heat fluxes. In a collisionless plasma in the presence of a magnetic field, the proton heat flux is

$$\underline{q}_p=\frac{\underline{B}}{B}(q_{11}+q_\perp)-\underline{\Omega}(q_{11}-q_\perp) \tag{III.2.10}$$

For the electrons we consider the inhibited conduction heat flux

$$(\underline{q}_e)_r = -\kappa_e \cos^2\phi \frac{\partial T_e}{\partial r} \qquad \text{(III.2.11)}$$

where ϕ is defined as in Figure 1b, and it follows that

$$q_r = \cos\phi\left(-\kappa_e \cos\phi \frac{\partial T_e}{\partial r} + q_{\parallel} + q_{\perp}\right) \qquad \text{(III.2.12)}$$

with

$$\kappa_e = K T_e^{5/2} \qquad \text{(III.2.13)}$$

Introducing these results in the energy equation, we obtain after one integration

$$n u_r r^2\left[\frac{k}{2}(5T_e + 4T_{\perp} + T_{\parallel}) + k\cos^2\phi(T_{\parallel} - T_{\perp}) + \frac{B_w^2}{4\pi n} + \frac{1}{2}mu^2 - \frac{mGM_{\odot}}{r}\right] + \qquad \text{(III.2.14)}$$

$$n u_w r^2\left[\cos\phi \sin\phi\, k(T_{\parallel} - T_{\perp}) - \frac{B_w B_r}{4\pi n}\right] = r^2\cos\phi\left(-\kappa_e \cos\phi \frac{\partial T_e}{\partial r} + q_{\parallel} + q_{\perp}\right) + F$$

where F is the total energy flux per steradian. We must now obtain expressions for $T_{\parallel}$, $T_{\perp}$, $q_{\parallel}$ and $q_{\perp}$ from the second moment equations of Chew-Goldberger-Low and third moment equations of Whang. Under the assumptions made for the model under study, these equations take the respective forms

$$u_r \frac{\partial}{\partial r}\left(\ln \frac{T_{\parallel} B^2}{n^2}\right) = -\frac{2B_r}{nkT_{\parallel}} \frac{\partial}{\partial r}\left(\frac{q_{\parallel}}{B}\right) \qquad \text{(III.2.15)}$$

$$u_r \frac{\partial}{\partial r}\left(\ln \frac{T_{\perp}}{B}\right) = -\frac{B_r}{nkT_{\perp}} \frac{\partial}{\partial r}\left(\frac{q_{\perp}}{B}\right) \qquad \text{(III.2.16)}$$

and

$$u_r \frac{\partial}{\partial r}\left(\frac{B^3 q_{\parallel}}{n^4}\right) = \frac{3k^2 B}{2mn^3} B_r\left(T_{\parallel} T_{\perp} \frac{\partial B}{\partial r} - B T_{\parallel} \frac{\partial T_{\parallel}}{\partial r}\right) \qquad \text{(III.2.17)}$$

$$u_r \frac{\partial}{\partial r}\left(\frac{q_{\perp}}{n^2}\right) = \frac{k^2 B_r}{mnB^2}\left(T_{\perp}^2 \frac{\partial B}{\partial r} - B T_{\parallel} \frac{\partial T_{\perp}}{\partial r}\right) \qquad \text{(III.2.18)}$$

wit[illegible]

$$\frac{1}{B}\frac{\partial B}{\partial r} = -\frac{2\cos^2\phi}{r} - \sin^2\phi\left(\frac{1}{u_r}\frac{\partial u_r}{\partial r} + \frac{1}{r}\right) + \frac{\sin\phi\cos\phi}{u_r}\left(\frac{\partial u_w}{\partial r} - \frac{u_w}{r}\right) \tag{III.2.19}$$

In Chapter II we have obtained from Maxwell's equations and conditions in the sun's vicinity

$$r(u_r B_w - u_w B_r) = \text{const.} = -\Omega r^2 B_r \tag{III.2.20}$$

hence

$$\tan\phi = \frac{r}{u_r}\left(\frac{u_w}{r} - \Omega\right) \tag{III.2.21}$$

These equations may now be expressed in dimensionless form by introducing the dimensionless variables and parameters defined in Chapter II, except for the dimensionless temperatures which in this case are given by

$$\theta_e = T_e/T_3 \;;\; \theta_{11} = T_{11}/T_3 \;;\; \theta_\perp = T_\perp/T_3 \tag{III.2.22}$$

and dimensionless heat fluxes

$$Q_{11} = q_{11}/n_3 k T_3 u_{r_3} \;;\; Q_\perp = q_\perp/n_3 k T_3 u_{r_3} \tag{III.2.23}$$

The parameter α is now given by

$$\alpha_e = 2n_3 u_{r_3} r_3 k/\kappa_{e_3}\cos^2\phi_3 \tag{III.2.24}$$

The system of dimensionless equations may be expressed in the compact form

$$a_{i1}\frac{dV}{dz} + a_{i2}\frac{d}{dz}\left(\frac{W}{z}\right) + a_{i3}\frac{d\theta_{11}}{dz} + a_{i4}\frac{d\theta_\perp}{dz} + a_{i5}\frac{dQ_{11}}{dz} + a_{i6}\frac{dQ_\perp}{dz} + a_{i7}\frac{d\theta_e}{dz} = a_{i8} \tag{III.2.25}$$

where the coefficients a_{ij} are given by the following expressions:

$$a_{11} = \xi V^2 - \frac{1}{2}\left[\theta_\perp\sin^2\phi(1+2\cos^2\phi) + \theta_{11}\cos^2\phi(1-2\sin^2\phi) + \theta_e\right] - \xi\mu V\tan^2\phi/z^2 \tag{III.2.26}$$

$$a_{12} = -\delta z\left[\frac{1}{2}(\theta_{11}-\theta_\perp)\sin 2\phi\cos^2\phi - \xi\mu V\tan\phi/z^2\right] \tag{III.2.27}$$

$$a_{13} = V\cos^2\phi/2 \;\;;\;\; a_{14} = V\sin^2\phi/2 \tag{III.2.28}$$

$$a_{15} = a_{16} = 0 \quad ; \quad a_{17} = V/2 \tag{III.2.29}$$

$$a_{18} = \frac{V}{2}\left[\theta_e + \theta_\perp + \frac{1}{2}(\theta_{11} - \theta_\perp)\sin^2\phi(1+2\cos^2\phi) - \frac{\gamma\xi}{2} + \xi\delta^2 W^2\right] \tag{III.2.30}$$

These coefficients a_{1j}, (j=1,8) correspond to the radial part of the equation of motion. The coefficients for the azimuthal part, a_{2j}, (j=1,8) are

$$a_{21} = \frac{1}{2}(\theta_{11} - \theta_\perp)\sin 2\phi \cos^2\phi - (\xi\mu V + \tan\phi)/z^2 \tag{III.2.31}$$

$$a_{22} = -\delta z\left[\xi V^2 + \frac{1}{2}(\theta_{11} - \theta_\perp)\cos 2\phi \cos^2\phi - \xi\mu V/z^2\right] \tag{III.2.32}$$

$$a_{23} = -(V\cos\phi \sin\phi)/2 \tag{III.2.33}$$

$$a_{24} = (V\cos\phi \sin\phi)/2 \quad ; \quad a_{25} = a_{26} = a_{27} = 0 \tag{III.2.34}$$

$$a_{28} = (V/2z)(\theta_{11} - \theta_\perp)\sin 2\phi \cos^2\phi + 2\delta\xi W V^2/z \tag{III.2.35}$$

The equations of Chew, Goldberger and Low may be combined with the third moment equations of Whang to reduce the number of coefficients to be calculated. The modified third moment equations coefficients are used in (III.2.25) and may be written as

$$a_{31} = (2\cos\phi/V)\left[\theta_{11}\cos\phi(1 - 3\theta_\perp \sin^2\phi/4\xi V^2) - 4z^2 Q_{11}\cos^2\phi\right] \tag{III.2.36}$$

$$a_{32} = (\delta z/V)\cos\phi \sin\phi\left[\theta_{11}(1 + 6\theta_\perp \cos^2\phi/4\xi V^2) - 8z^2 Q_1 \cos\phi\right] \tag{III.2.37}$$

$$a_{33} = 1 - 6\theta_{11}\cos^2\phi/4\xi v^2 \; ; \; a_{34} = a_{35} = a_{36} = a_{37} = 0 \qquad \text{(III.2.38)}$$

$$a_{38} = \left(\frac{2\theta_{11}}{z}\right)\left[\frac{3\theta_\perp \cos^2\phi(1+\cos^2\phi)}{4\xi v^2} - \sin^2\phi\right] + 8z\cos\phi\sin^2\phi Q_{11} \qquad \text{(III.3.39)}$$

$$a_{41} = \left(\frac{Q_\perp}{v}\right) z^2\cos\phi(1+\cos^2\phi) + \left(\frac{\theta_\perp}{v}\right)\sin^2\phi\left[(\theta_\perp\cos^2\phi/2\xi v^2) - 1\right] \qquad \text{(III.2.40)}$$

$$a_{42} = \left(\frac{\delta z}{v}\right)\cos\phi\sin\phi\left[Q_\perp z^2\cos\phi + \theta_\perp(1 - \theta_\perp\cos^2\phi/2\xi v^2)\right] \qquad \text{(III.2.41)}$$

$$a_{43} = 0 \; ; \; a_{44} = \left(\theta_{11}\cos^2\phi/2\xi v^2\right) - 1 \; ; \; a_{45} = a_{46} = a_{47} = 0 \qquad \text{(III.2.42)}$$

$$a_{48} = Q_\perp z\cos\phi(\cos^2\phi - 3) + \left(\frac{\theta_\perp}{z}\right)(1+\cos^2\phi)(1 - \theta_\perp\cos^2\phi/2\xi v^2) \qquad \text{(III.2.43)}$$

The coefficients corresponding to the Chew-Goldberger-Low equations are given by

$$a_{51} = (2c\cos\phi/v)(\cos\phi\,\theta_{11} + z^2 Q_{11}\sin^2\phi) \qquad \text{(III.2.44)}$$

$$a_{52} = \left(\frac{\delta z}{v}\right)\cos\phi\,\sin\phi\,(\theta_{11} - 2z^2\cos\phi Q_{11}) \qquad \text{(III.2.45)}$$

$$a_{53} = 1 \quad ; \quad a_{54} = 0 \qquad \text{(III.2.46)}$$

$$a_{55} = 2z^2\cos\phi$$

$$a_{56} = a_{57} = 0 \quad ;$$

$$a_{58} = -\left(\frac{2}{z}\right)\left[\sin^2\phi\,\theta_{11} + \cos\phi\,(1+\cos^2\phi)\,Q_{11}z^2\right] \qquad \text{(III.2.47)}$$

$$a_{61} = \left(\frac{\sin^2\phi}{V}\right)\left(\theta_\perp + z^2\cos\phi\,Q_\perp\right) \qquad \text{(III.2.48)}$$

$$a_{62} = -\left(\frac{\delta z}{V}\right)\sin\phi\cos\phi\left(\theta_\perp + z^2\cos\phi\,Q_\perp\right) \qquad \text{(III.2.49)}$$

$$a_{63} = 0 \quad ; \quad a_{64} = 1 \quad ; \quad a_{65} = 0 \quad ;$$

$$a_{66} = z^2\cos\phi \qquad \text{(III.2.50)}$$

$$a_{67} = 0$$

$$a_{68} = -\left(\frac{1}{z}\right)(1+\cos^2\phi)\left(\theta_\perp + z^2\cos\phi\,Q_\perp\right) \qquad \text{(III.2.51)}$$

e remaining coefficients a_{7j}, are associated with the energy equation
d are given by

$$_{71} = a_{72} = a_{73} = a_{74} = a_{75} = a_{76} = 0 \; ; \; a_{77} = z^2\theta_e^{5/2}\cos^2\phi \qquad \text{(III.2.52)}$$

$$_{18} = \alpha_e\cos^2\phi_3\left[\frac{\kappa}{2}\left(v^2+\delta^2w^2\right) + \frac{1}{4}\left(5\theta_e + 4\theta_\perp + \theta_\parallel\right) + \right.$$

$$\left. \cos^2\phi\,(\theta_{11}-\theta_\perp) + \frac{\delta w}{2v}\cos\phi\sin\phi\,(\theta_{11}-\theta_\perp) - \right.$$

$$\frac{\xi\mu\beta\tan\phi}{z} - \frac{\gamma\xi}{z} - H\xi + \frac{z^2\cos\phi}{2}(Q_{\parallel}+Q_{\perp}) \qquad \text{(III.2.53)}$$

The system of equations of (III.2.25) has to be solved in the outer region of the model to determine the unknown variables V, θ_e, $\theta_{\parallel}$, $\theta_{\perp}$, $Q_{\parallel}$ and $Q_{\perp}$. In the inner region $\theta_e=\theta_{\parallel}=\theta_{\perp}$ and the equations reduce to those obtained in Chapter II except for the CGL and third moment equations which were not considered. We shall find that the transition point from the inner to the outer regions must be chosen such that it lies beyond the three critical points previously discussed. Hence, we need not concern ourselves with singularities in the differential equations since they occur outside of the region for which the system (III.2.25) is assumed valid.

III.3 Numerical Solutions

We found in Chapter II that the solutions for V(Z) and θ(Z) depend upon five dimensionless parameters ϕ_3, β_3, γ, ζ and H. For a given set of values assigned to these parameters the solutions in the inner region are found in the same manner as in the one-fluid model up to the boundary point between the inner and outer regions ($Z=Z_4=r_4/r_3$), with $Z_4>1$. At the transition point all quantities are continuous and we must specify the value of $Q_{\parallel}$ and $Q_{\perp}$ in order to obtain a solution to the system (III.2.25) in the outer region.

We shall assume that the proton heat flux ($Q_{\parallel}+Q_{\perp}$) at the transition point is that flux available at this radius from magnetic field inhibited heat conduction by protons as given by the one-fluid solution for the inner region. Braginskii (1965) gives for the electron and proton heat conduction coefficients respectively

$$\kappa_{\parallel e} = 3.16\, n_e T_e \tau_e / m_e \qquad \text{(III.3.1)}$$

$$\kappa_{\parallel p} = 3.9\, n_p T_p \tau_p / m_p \qquad \text{(III.3.2)}$$

where it is assumed that $\omega_p \tau_p \gg 1$ and τ_e, τ_p are the collision times given by

$$\tau_e = 3.5\times 10^4 T_e^{3/2}/(\lambda/10) n_e \qquad \text{(III.3.3)}$$

$$\tau_p = 3.0\times 10^6 T_p^{3/2}/(\lambda/10) n_p \qquad \text{(III.3.4)}$$

and furthermore λ , the Coulomb logarithm is taken as 24. if $T_e = T_p$, it follows that for the one-fluid model

$$\kappa_3 = \kappa_{e3}(1 + 0.04074) \qquad \text{(III.3.5)}$$

and

$$\alpha = 1.040704\, \alpha_e \qquad \text{(III.3.6)}$$

From equation (III.1.12) we obtain for the dimensionless heat fluxes $Q_\parallel$ and $Q_\perp$

$$Q_\parallel = \frac{\gamma_\parallel \theta_\parallel}{2VZ^2}\sqrt{\frac{\theta_\parallel}{\xi}} \qquad \text{(III.3.7)}$$

$$Q_\perp = \frac{\gamma_\perp \theta_\perp}{VZ^2}\sqrt{\frac{\theta_\parallel}{\xi}} \qquad \text{(III.3.8)}$$

hence at the transition point $Z = Z_4$

$$\left(\frac{Q_\parallel}{Q_\perp}\right)_4 = \left(\gamma_\parallel / 2\gamma_\perp\right)_4 \qquad \text{(III.3.9)}$$

Introducing (III.3.5) into (II.2.67) and requiring that the total thermal energy flux be continuous across Z_4, we obtain

$$\left(Q_\parallel + Q_\perp\right)_4 = \frac{.07828\, \theta_4^{5/2}\cos\phi_4}{\alpha \cos^2\phi_3}\left(\frac{d\theta}{dz}\right)_4 \qquad \text{(III.3.10)}$$

and

$$\frac{1}{2}\gamma_{\parallel} + \gamma_{\perp} = \frac{.07828\, V_4 Z_4^2 \sqrt{\xi}\, \theta_4 \cos\phi_4}{\alpha \cos^2\phi_3}\left(\frac{d\theta}{dz}\right)_4 \qquad \text{(III.3.11)}$$

Thus, once a solution for the inner region is obtained we need only specify the ratio $\gamma_{\parallel}/\gamma_{\perp}$ at the boundary $Z=Z_4$ to obtain the solution in the outer region. It is convenient therefore to introduce an additional parameter defined by

$$\eta = \left(\gamma_{\parallel}/\gamma_{\perp}\right)_{z=z_4} \qquad \text{(III.3.12)}$$

and the solutions for V, θ_e, $\theta_{\parallel}$, $\theta_{\perp}$, $Q_{\parallel}$ and $Q_{\perp}$ take the general form

$$f = f(z, \beta_3, \phi_3, \zeta, \gamma, H, \eta) \qquad \text{(III.3.13)}$$

The requirement that the solutions extend from the sun's surface to large heliocentric distances with physically meaningful values, restricts our freedom to assign arbitrary values to the parameters in (III.3.13). As discussed in Chapter II. for any given values of H, β_3 and ϕ_3, ζ is adjusted to obtain a solution passing through the inner critical point while γ is determined from the condition that the thermal energy flux at infinity is assumed zero. Thus we may write (III.3.13) as

$$f = f(z, \beta_3, \phi_3, H, \eta) \qquad \text{(III.3.14)}$$

that is, the values obtained for the quantities in a given model depend upon four independent parameters rather than the six previously indicated.

From (III.3.11) and (III.3.12) it follows that

$$\gamma_{\perp} = \frac{.07828\, V_4 Z_4^2 \sqrt{\xi}\, \theta_4 \cos\phi_4}{(1+\eta/2)\,\alpha \cos^2\phi_3}\left(\frac{d\theta}{dz}\right)_4 \qquad \text{(III.3.15)}$$

The numerical integration procedure used to obtain solutions to the system (III.2.25) is the same as the one described in Chapter II. The system of seven simultaneous non-linear differential equations is written in terms of the independent variable $X=Z^{-1}$ and the results are given in Appendix C.

For large Z, asymptotic series solutions may be found by introducing the formal asymptotic expansions of Whang (1972) in the system (III.2.25). These forms are given by $(\varepsilon = Z^{-1/3})$

$$
\begin{aligned}
V &= V_\infty \left(1 + \varepsilon^3 \sum_0^\infty c_{1j} \varepsilon^j\right) \\
\Theta_e &= A_2 \varepsilon^4 \left(1 + \sum_1^\infty c_{2j} \varepsilon^j\right) \\
\Theta_{11} &= A_3 \varepsilon^6 \left(1 + \sum_1^\infty c_{3j} \varepsilon^j\right) \\
\Theta_\perp &= A_4 \varepsilon^3 \left(1 + \sum_1^\infty c_{4j} \varepsilon^j\right) \\
Q_{11} &= A_5 \varepsilon^{15} \left(1 + \sum_1^\infty c_{5j} \varepsilon^j\right) \\
Q_\perp &= A_6 \varepsilon^{12} \left(1 + \sum_1^\infty c_{6j} \varepsilon^j\right)
\end{aligned}
\qquad \text{(III.3.16)}
$$

In addition to the above we introduce

$$
W = A_7 \varepsilon^3 \left(1 + \sum_1^\infty c_{7j} \varepsilon^j\right) \qquad \text{(III.3.17)}
$$

as the asymptotic form for the azimuthal dimensionless velocity. For large Z we may approximate

$$
\tan\phi \simeq -\frac{\mathcal{P}}{V} \varepsilon^{-3} \qquad \text{(III.3.18)}
$$

When these forms and their derivatives are introduced in (III.2.25) and the coefficients of every power of ε are set equal to zero, we obtain

$$
V_\infty^2 + \frac{\mu \mathcal{P}^2}{V_\infty} - H = 0 \qquad \text{(III.3.19)}
$$

and the non-zero coefficients C_{ij} for j=1,8 are

$$C_{10} = (\gamma\xi - A_4)/\xi P \quad ; \quad C_{11} = -5A_2/4\xi P$$

$$C_{13} = (4A_4 C_{10} - A_3 - 5A_2 C_{22})/4\xi P$$

$$C_{14} = (4A_4 C_{11} - 5A_2 C_{23})/4\xi P \quad ; \quad C_{15} = -5A_2 C_{24}/4\xi P$$

$$C_{16} = (1/4\xi P)\left[-5A_2 C_{25} - 4A_4 C_{46} + (2V_\infty/\rho)(A_6 - A_4 V_\infty/\rho)\right]$$

$$C_{17} = (1/\xi P)\left(\frac{V_\infty^2 C_{10} A_4}{\rho^2} - A_4 C_{47} - \frac{5A_2 C_{26}}{4}\right)$$

$$C_{18} = (1/\xi P)\left(\frac{V_\infty^2 C_{11} A_4}{\rho^2} - A_4 C_{48} - \frac{5A_2 C_{27}}{4}\right) \qquad \text{(III.3.20a)}$$

$$C_{22} = (1/A_2)\, 2C_{10}(A_4 + \xi S C_{10} - \gamma\xi)$$

$$C_{23} = (11/42A_2)\left[C_{11}(6A_4 + 14\xi S C_{10} - 6\gamma\xi) - A_2 C_{10}\right]$$

$$C_{24} = C_{11}(1 + 4\xi S C_{11}/3A_2)$$

$$C_{25} = (1/5A_2)\left[2A_4 C_{46} + (2V_\infty/\rho)\left(\frac{V_\infty A_4}{\rho} - 3A_6\right) + 2C_{10}(6\xi S C_{13} + 3A_2 C_{22} - 2A_4 C_{10} + A_3) - 4\gamma\xi C_{13}\right]$$

$$C_{26} = (1/9A_2)\left[-7A_4C_{47} + 20C_{10}\left(\frac{V_\infty^2 A_4}{5^2} + \xi S C_{14} + \frac{A_2 C_{23}}{2}\right) + \right.$$

$$C_{11}(3A_3 + 20\xi S C_{13} - 5A_4C_{10} + 8A_2C_{22}) - C_{14}(6\gamma\xi + A_4) +$$

$$\left. 4A_2C_{13}\right]$$

$$C_{27} = (1/21A_2)\left[-16A_4C_{48} - 2C_{11}\left(\frac{22V_\infty^2 A_4}{5^2} + 22\xi S C_{14} - 6A_4C_{11} + \right.\right.$$

$$\left. 9A_2C_{23}\right) - C_{10}\left(44\xi S C_{15} + \frac{1650}{61}A_2C_{24}\right) - 4A_2C_{14} +$$

$$\left. 4C_{15}(A_4 + 3\gamma\xi)\right] \qquad \text{(III.3.20b)}$$

$$C_{36} = (V_\infty/5)\left(\frac{4A_5}{A_3} - \frac{V_\infty}{5}\right)$$

$$C_{43} = -C_{10} \quad ; \quad C_{44} = -C_{11}$$

$$C_{46} = C_{10}^2 - C_{13} + \frac{V_\infty}{5}\left(\frac{3}{2}\frac{A_6}{A_4} + \frac{V_\infty}{25}\right)$$

$$C_{47} = 2C_{10}C_{11} - C_{14}$$

$$C_{48} = C_{11}^2 - C_{15}$$

$$C_{53} = -C_{10} - 3A_3A_4/4\xi^2 V_\infty A_5$$

$$C_{54} = -C_{11}$$

$$C_{56} = \frac{3}{4}\frac{A_3^2}{\xi\zeta V_\infty A_5} - C_{13} + \frac{3}{2}\frac{V_\infty^2}{\zeta^2} - C_{10}(C_{10} + 2C_{53})$$

$$C_{57} = -C_{14} - 2C_{11}C_{53}$$

$$C_{58} = C_{11}^2 - C_{15} = C_{48}$$

$$C_{63} = -2C_{10} - A_4^2/2\xi\zeta V_\infty A_6$$

$$C_{64} = -2C_{11}$$

$$C_{66} = -2C_{10}(2C_{63} + C_{10}) - 2C_{13} + A_3A_4/4\xi\zeta V_\infty A_6$$

(III.3.20c)

$$C_{67} = (6C_{10}C_{11}/7) - 2C_{14} - (18C_{11}C_{63}/7)$$

$$C_{68} = -(3C_{11}C_{64}/2) - 2C_{15}$$

$$C_{73} = (1/\delta A_7)\left(\frac{\mu\zeta C_{10}}{V_\infty} - \frac{A_4}{2\xi\zeta}\right)$$

$$C_{74} = \mu\zeta C_{11}/\delta V_\infty A_7$$

$$C_{76} = (\mu\xi C_{13}/\delta V_\infty A_7) - C_{10}C_{73} + (\mu/V_\infty) +$$

$$A_3/2\delta\xi\xi A_7$$

$$C_{77} = (\mu\xi C_{14}/\delta V_\infty A_7) - (6C_{11}C_{73}/7) - (8C_{10}C_{74}/7) +$$

$$A_4/14\delta\xi\xi A_7 \qquad \text{(III.3.20d)}$$

$$C_{78} = (\mu\xi C_{15}/\delta V_\infty A_7) - C_{11}C_{74}$$

where as before

$$P = \frac{3}{2}V_\infty^2 - H$$

and (III.3.21)

$$S = \frac{3}{2}V_\infty^2 + H$$

The coefficients A_i are obtained by successive iterations such that the numerical and asymptotic solutions join smoothly together at a given value of Z.

We have obtained two solutions to the system of differential equations (III.2.25) in the outer region and the corresponding one-fluid solutions for the inner region. The parameter values used in each case are given in Table VI, while the computer programs developed for the two-region model are given in Appendix D. The one-fluid solutions are obtained by the same procedure described in Chapter II. The transition point from the one-fluid formulation to the two-fluid description is chosen at Z=3.3 (~0.4 A.U.) and the ratio of $\gamma_\parallel$ to $\gamma_\perp$ (η) as 4.62 in both cases. These values were

TABLE VI

Parameters	Solution #3	Solution #4
H	0.8	0.85
ϕ_3	169.8^{o}	169.8^{o}
ζ	.1948	.1953
β_3	.200	.200
γ	.10911	.097257
η	4.62	4.62
Related constants		
α	.4645	.31455
μ	.96529	.96529
ξ	10.035	10.035
δ	.01488	.01538
σ	.98384	.98388
u_{r_3}	263.38 Km/sec.	273.44 Km/sec.
u_{ω_3}	3.92 Km/sec.	4.20 Km/sec.
r_3	25.247 $r_\odot$	26.278 $r_\odot$
r_2	24.839 $r_\odot$	25.854 $r_\odot$
r_1	3.75 $r_\odot$	3.965 $r_\odot$
T_3	5.01×10^5	5.41×10^5
u_∞	326.95 Km/sec.	350.45 Km.sec.
$(\frac{d\theta}{dZ})_3$	-.58753	-.5184
$(\frac{dV}{dZ})_3$	.16748	.17314

TABLE VI (CONTINUED)

Parameters	Solution #3	Solution #4
Asymptotic Solution		
r_a	421	752
A_2	6.1625	12.035
A_3	17.346	20.067
A_4	.7702	.8056
A_5	3.6174	6.9959
A_6	.03617	.07407
A_7	2.6172	2.5661

selected to obtain reasonable agreement with experimental observations for the proton temperature and anisotropy ratio at 1 A.U.

III.4 Results and Physical Interpretations

The results obtained for the radial velocity u_r, azimuthal velocity u_ω, electron temperature T_e, and proton temperatures $T_{p\parallel}$ and $T_{p\perp}$ are shown in Figure 16 for Solution #3 and Figure 17 for Solution #4. The radial velocity solutions are essentially the same obtained previously for the one-fluid models since similar values of the parameters have been used in the calculations.

The azimuthal velocity solutions for the inner region are of the same general form as in the one-fluid models; in the outer region the effect of the proton thermal anisotropy is to increase the azimuthal speed as shown in the figures. The dashed curves represent the more likely physical situation rather than the abrupt transition predicted by the model. Since the fluid is assumed inviscid, the increase in azimuthal velocity is due solely to proton thermal anisotropy effects. The predicted azimuthal velocities at 1 A.U. are 1.44 Km/sec. for Solution #3 and 1.68 Km/sec. for Solution #4. These values should be compared with those obtained from the one-fluid models in Chapter II, 1.02 Km/sec. and 1.19 Km/sec. respectively. Thus the increase in azimuthal velocity at 1 A.U. is of the order of 0.5 Km/sec.

Weber and Davis (1970), in considering the effects of thermal anisotropy and viscosity in the solar wind, incorporated an ad-hoc relationship for $\underline{\underline{P}}$ which tends to overemphasize the effects of the electron

Figure 16

The radial and azimuthal velocities, the electron temperature and parallel and perpendicular proton temperatures obtained for Solution #3 of the two-fluid model, as a function of heliocentric distance. The dashed lines represent a possible physical situation for the azimuthal velocity in the transitional region.

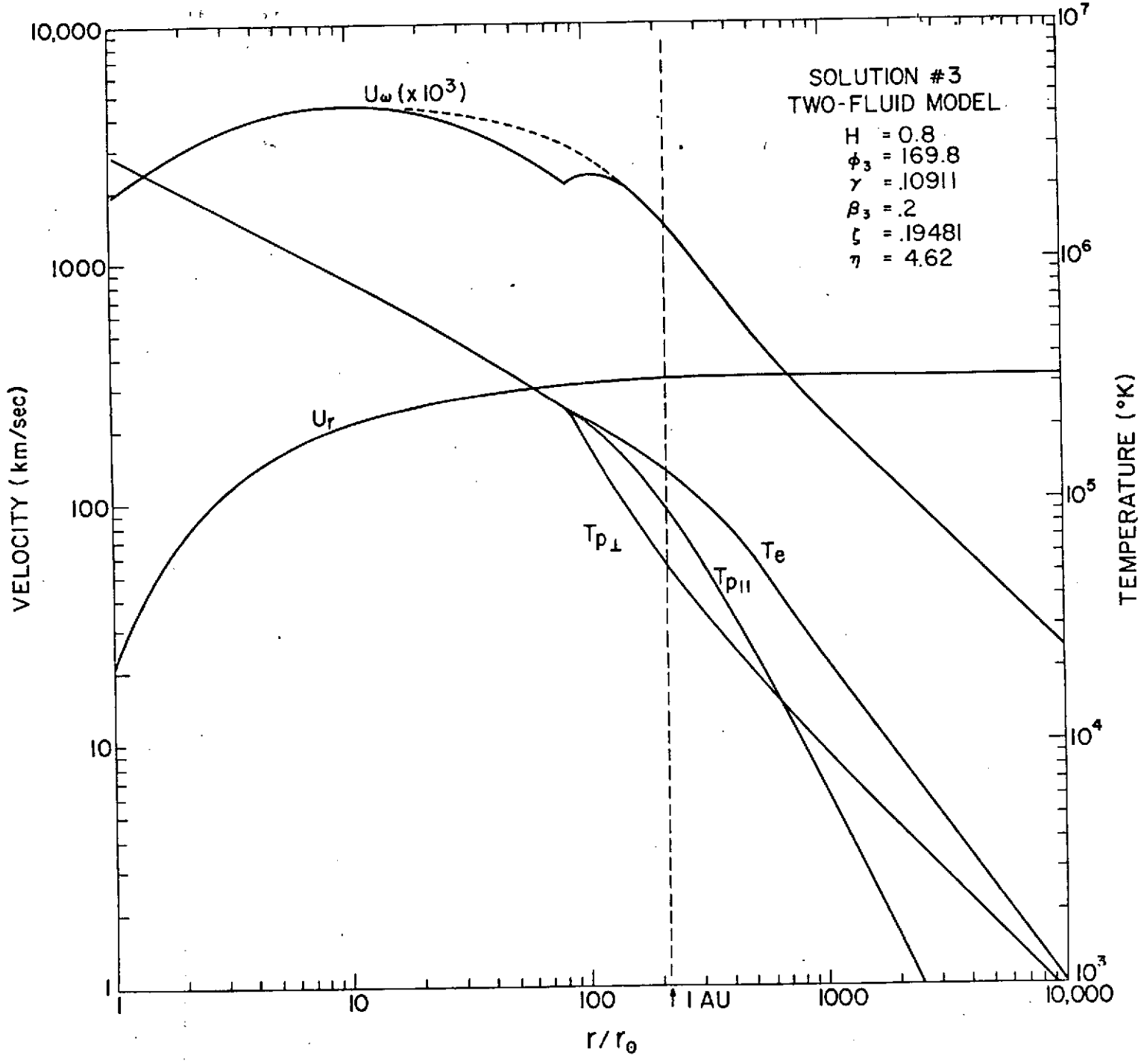
SOLUTION #3
TWO-FLUID MODEL
H = 0.8
ϕ_3 = 169.8
γ = .10911
β_3 = .2
ζ = .19481
η = 4.62
U_ω (x 10^3)
U_r
$T_{p\perp}$
$T_{p\parallel}$
T_e
VELOCITY (km/sec)
TEMPERATURE (°K)
r/r_0
1 AU
10,000
1000
100
10
1
10^7
10^6
10^5
10^4
10^3
10
100
1000
10,000

Figure 17

The radial and azimuthal velocities, the electron temperature and parallel and perpendicular proton temperatures obtained for Solution #4 of the two-fluid model, as a function of heliocentric distance. The dashed curve represents a possible physical situation for the azimuthal velocity in the transitional region.

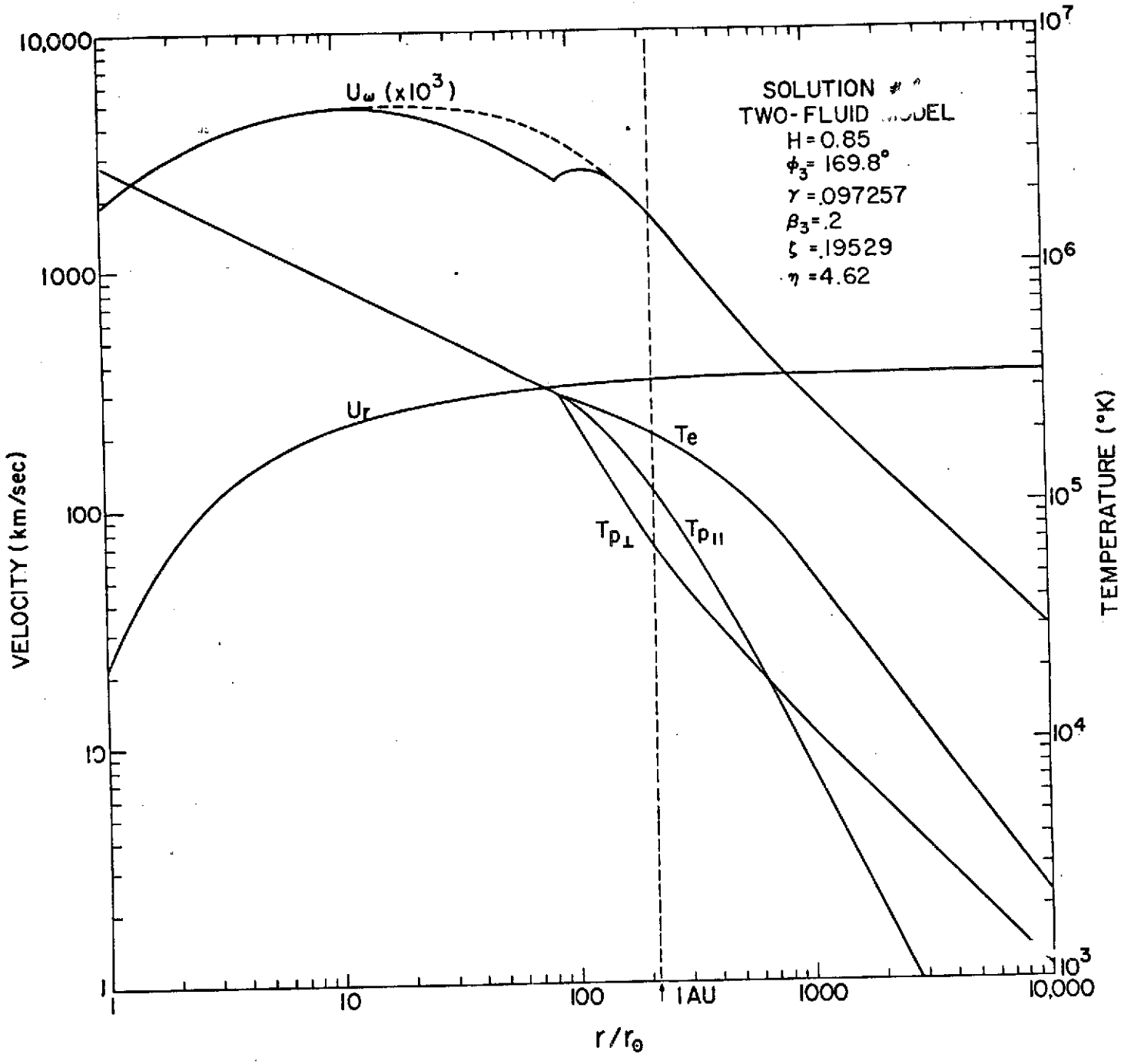
SOLUTION #
TWO-FLUID MODEL
H = 0.85
ϕ_3 = 169.8°
γ = .097257
β_3 = .2
ζ = .19529
η = 4.62
U_ω (x10^3)
U_r
T_e
$T_{p\perp}$
$T_{p\parallel}$
VELOCITY (km/sec)
TEMPERATURE (°K)
r/r$_\odot$
1 AU
10,000
1000
100
10
1
10
100
1000
10,000
10^7
10^6
10^5
10^4
10^3

anisotropy upon the angular motion. They obtained u_ω=6 Km/sec. at 1 A.U. although this was accomplished assuming a one-fluid model in which the viscous stress is greatly enhanced by the elevated proton temperature assumed.

More recently Urch (1972) has given a perturbation solution to the one-fluid, isotropic MHD equations, which predicts a mean azimuthal velocity of 1-2 Km/sec at 1 A.U., with excursions of $\sim \pm 10$ Km/sec. caused by the rotating sector structure of the magnetic field. Since ours is a steady state model, we cannot calculate time-dependent effects but the range of azimuthal velocities that can be considered at the reference radius for which physically meaningful solutions can be obtained, is considerably smaller than the excursions indicated by Urch.

We can conclude from the results obtained in this Chapter, that the effects of thermal anisotropies upon the angular motion of the solar wind are relatively small and cannot increase the predicted azimuthal speed at 1 A.U. to values in agreement with observations.

The temperature profiles obtained for the inner region are analogous to those calculated for the one-fluid models. In the outer region where the proton thermal anisotropy is allowed to develop, the ratio of $T_{p\parallel}$ to $T_{p\perp}$ increases rapidly with increasing heliocentric distance reaching a maximum value of ~1.7 at 200 solar radii for both solutions. This ratio then decreases monotonically and becomes less than one for large heliocentric distances, as shown in Figures 18 and 19. The total proton temperature is given by

$$T_p = (2T_{p\perp} + T_{p\parallel})/3 \qquad \text{(III.4.1)}$$

Figure 18

The proton thermal anisotropy ratio $T_{p\parallel}/T_{p\perp}$ and the proton to electron temperature ratio T_p/T_e as a function of heliocentric distance, predicted by Solution #3, two-fluid model.

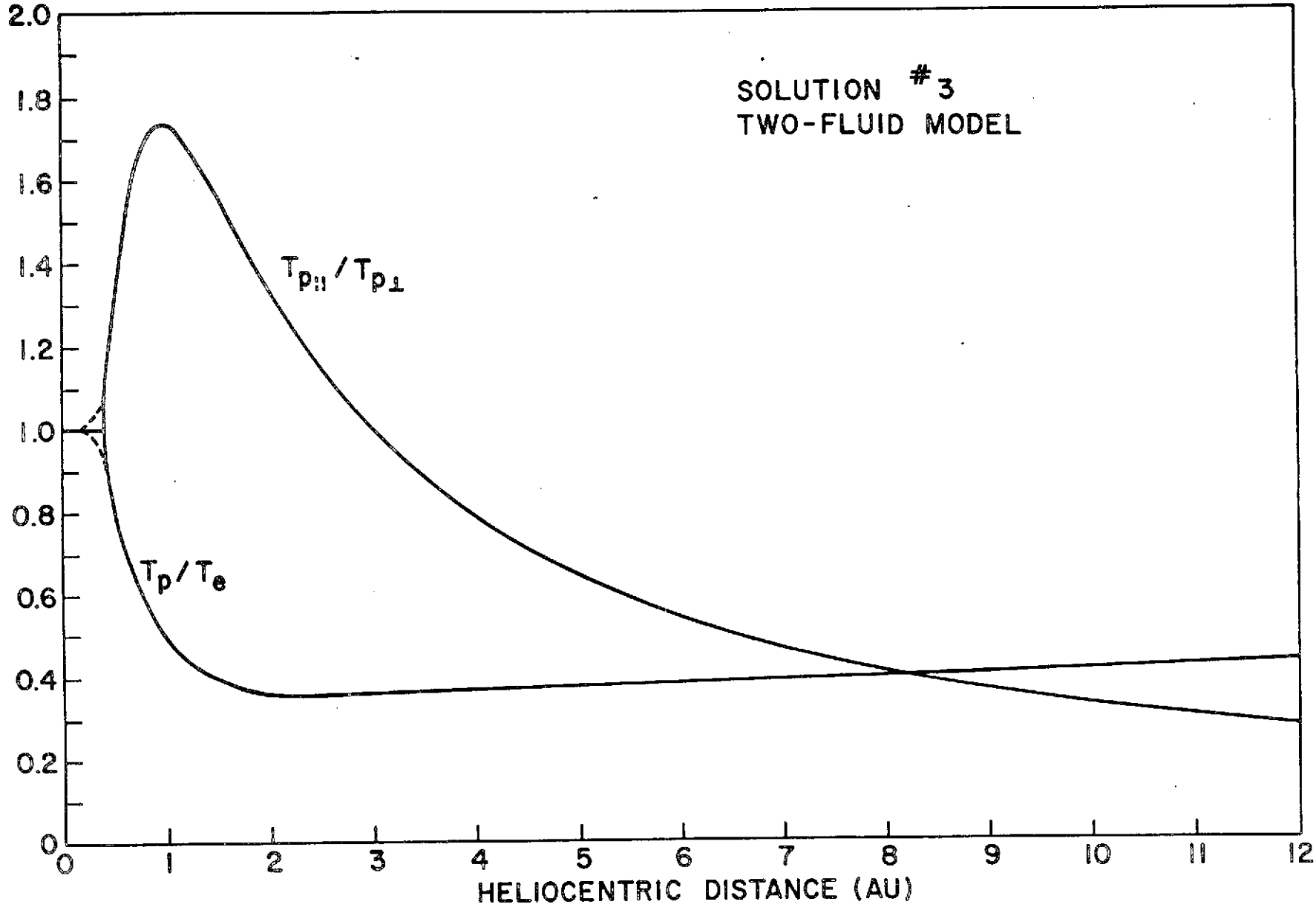
SOLUTION #3
TWO-FLUID MODEL
$T_{p\parallel}/T_{p\perp}$
T_p/T_e
2.0
1.8
1.6
1.4
1.2
1.0
0.8
0.6
0.4
0.2
0
0
1
2
3
4
5
6
7
8
9
10
11
12
HELIOCENTRIC DISTANCE (AU)

Figure 19

The proton thermal anisotropy ratio $T_{p\parallel}/T_{p\perp}$ and the proton to electron temperature ratio T_p/T_e as a function of heliocentric distance, predicted by Solution #4, two-fluid model.

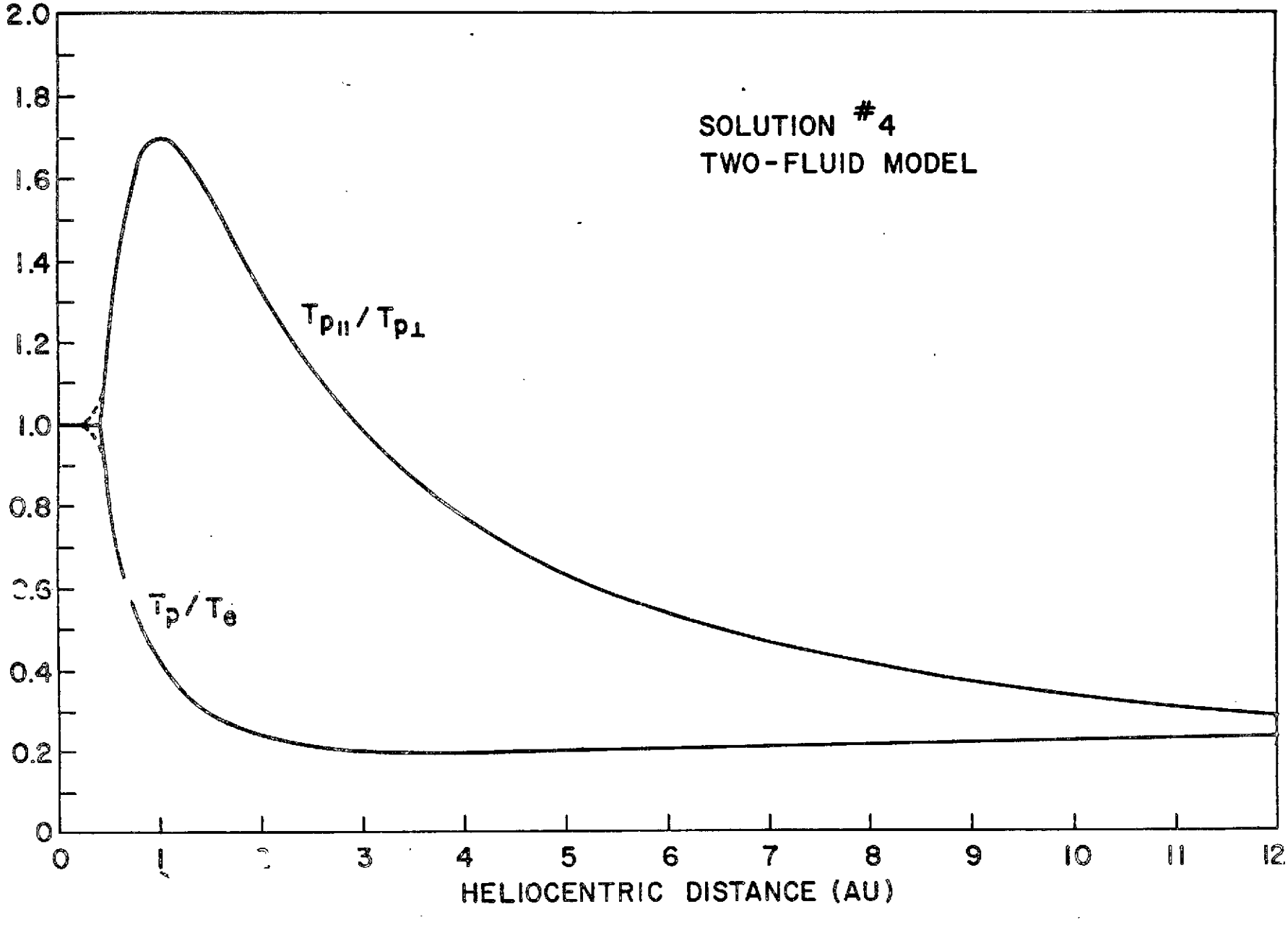
SOLUTION #4
TWO-FLUID MODEL
$T_{p\parallel} / T_{p\perp}$
T_p / T_e
2.0
1.8
1.6
1.4
1.2
1.0
0.8
0.6
0.4
0.2
0
0
1
2
3
4
5
6
7
8
9
10
11
12
HELIOCENTRIC DISTANCE (AU)

The dashed lines show the probable physical situation rather than the idealization assumed in the model.

It is of interest to consider the possibility that wave modes associated with plasma instabilities may be excited in the plasma due to the anisotropic proton pressure. Two particular types of instabilities warrant consideration: the firehose and mirror instabilities. These instabilities will occur if the following criteria are satisfied, (Clemmow and Dougherty, 1969; Krall and Trivelpiece, 1973)

$$\left(\frac{T_{p\parallel}}{T_{p\perp}} - 1\right) > \left(2/\beta_{p\perp}\right) \qquad \text{(firehose)} \qquad \text{(III.4.2)}$$

$$\left(\frac{T_{p\perp}}{T_{p\parallel}} - 1\right) > \left(1/\beta_{p\perp}\right) \qquad \text{(mirror)} \qquad \text{(III.4.3)}$$

where

$$\beta_{p\perp} = nkT_p/(B^2/8\pi) \qquad \text{(III.4.4)}$$

and we have neglected the effect of the electrons since they are assumed isotropic. When the instability criteria given by these equations are imposed on our solution we find that (III.4.2) and (III.4.3) are nowhere satisfied and hence no instabilities are expected to occur in the plasma; the magnetic field pressure is everywhere greater than the proton thermal pressure.

The plasma β and magnetic field angle ϕ are given in Figures 20 and 21, where

$$\beta = nk(T_e + T_p)/(B^2/8\pi) \qquad \text{(III.4.5)}$$

As in the case of $T_{p\parallel}$ and $T_{p\perp}$, the β curve shows an abrupt slope change at the boundary between the inner and outer regions caused by the idealizations assumed in the model.

Figure 20

The plasma β and magnetic field angle ϕ as a function of heliocentric distance. Solution #3, two-fluid model.

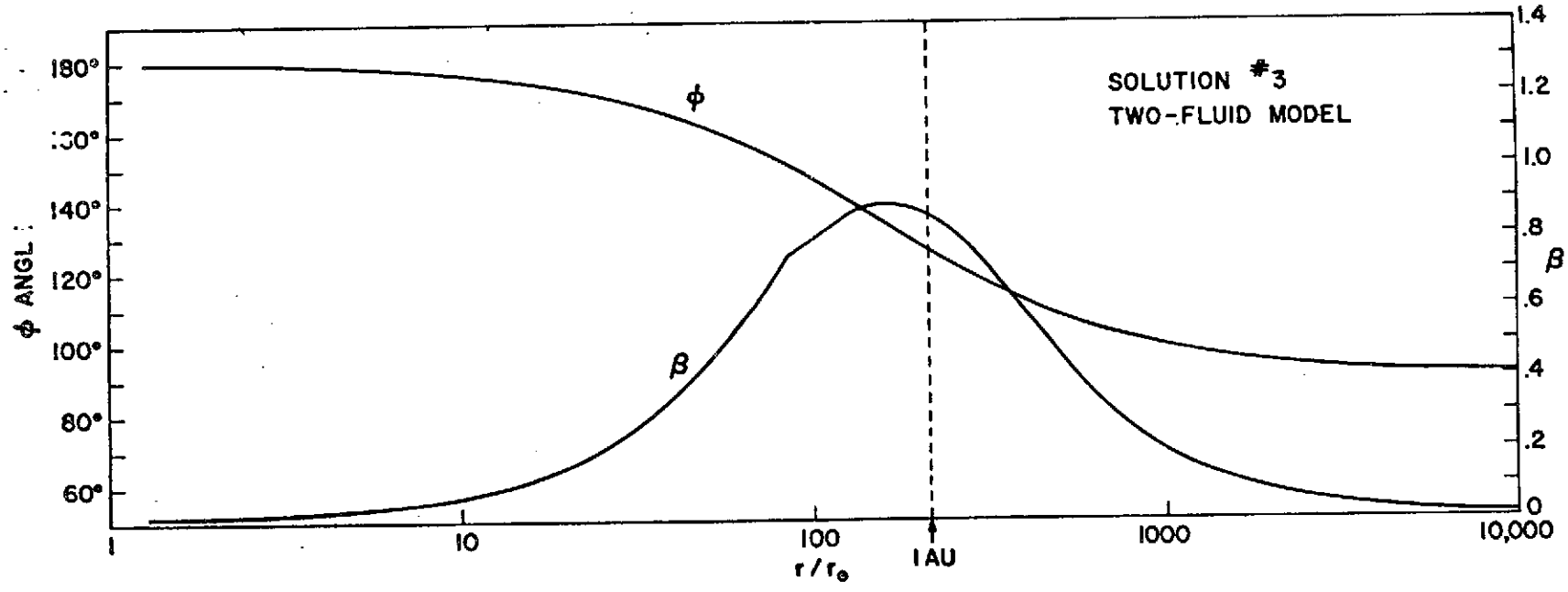
SOLUTION #3
TWO-FLUID MODEL
φ
β
φ ANGL
180°
130°
140°
120°
100°
80°
60°
1.4
1.2
1.0
.8
.6
.4
.2
0
1
10
100
1000
10,000
r / r₀
1 AU

Figure 21

The plasma β and magnetic field angle ϕ as a function of heliocentric distance. Solution #4, two-fluid model.

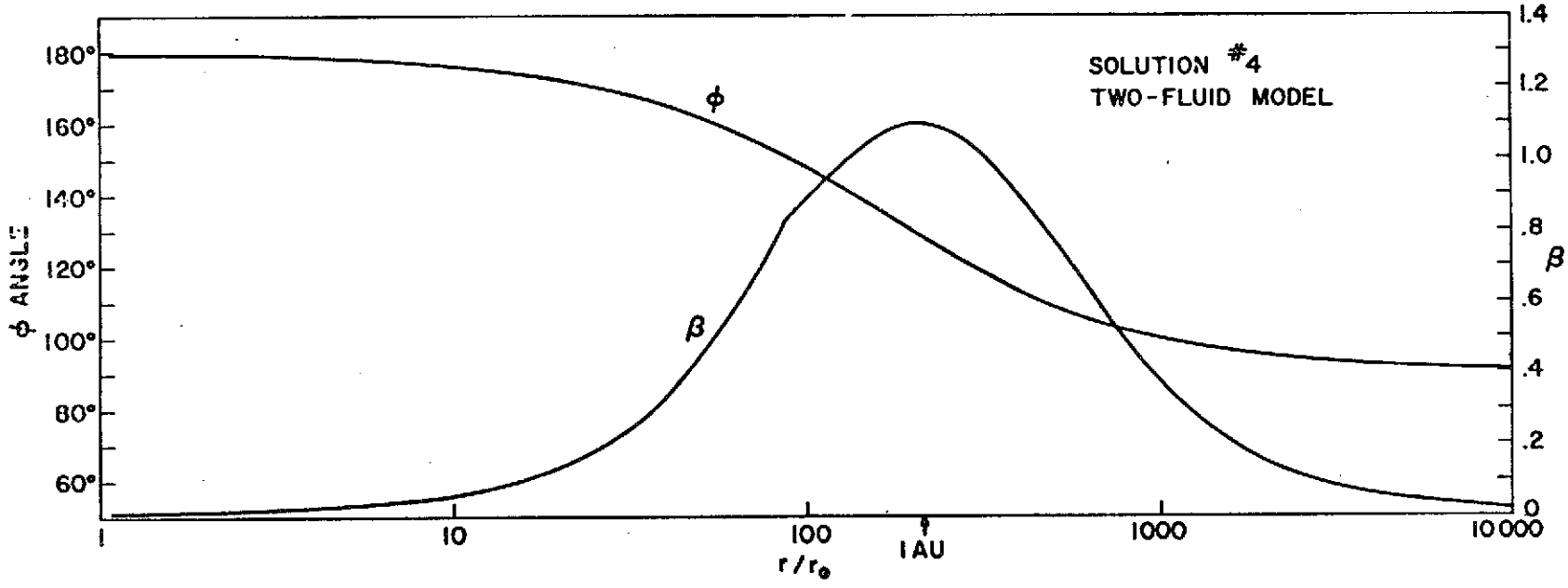
SOLUTION #4
TWO-FLUID MODEL
φ
β
φ ANGLE
180°
160°
140°
120°
100°
80°
60°
1.4
1.2
1.0
.8
.6
.4
.2
0
1
10
100
1000
10000
1 AU
r/r⊙

Flow conditions predicted by the two-region model at 1 A.U. are summarized in Table VII and compared with results obtained from previous two-fluid models. The quantities show generally good agreement with quiet-time solar wind observations. Tables VIII and IX give detailed numerical results for Solutions #3 and #4 in the inner and outer regions. These two solutions represent typical limits of observed electron temperature conditions at 1 A.U.

The quantities obtained and given in the tables, are independent of the value assigned to the thermal conductivity constant K, (see Chapter II). To compute the density, energy flow and magnetic field intensity we have chosen $K = 1.0 \times 10^{-7}$ for Solution #3 and $K = 1.0 \times 10^{-7}$ for Solution #4; these values of K give results that agree reasonably well with experimental observations at 1 A.U.

Figures 22 through 25 show the magnetic field intensity, density and heat fluxes predicted by the present model as a function of heliocentric distance. Table X summarizes the values predicted for these quantities at 1 A.U. For completeness, Figures 26 through 29 show the magnetic field and kinetic energy flows per steradian obtained in each case. As in Chapter II, we find that the amount of magnetic field energy converted into kinetic energy is small and has little effect upon the final expansion velocity.

The microscopic properties of the solution for the proton distribution function are determined by the values obtained for $\gamma_{\parallel}$, $\gamma_{\perp}$, $T_{p\parallel}$ and $T_{p\perp}$. From equations (III.3.7) and (III.3.8) it follows that

TABLE VII

PREDICTED FLOW CONDITIONS AT 1 A.U. - TWO FLUID MODELS

	Sol. #3	Sol #4	Whang (1972)	Wolff et al., (1971)	Hartle & Sturrock, (1968)
Radial Velocity (Km/sec.)	317.7	335.2	331	303	250
Azimuthal Velocity (Km/sec.)	1.44	1.68	-	1.8	-
Electron Temperature (^{o}K)	1.34×10^{5}	1.98×10^{5}	1.52×10^{5}	2.03×10^{5}	3.5×10^{5}
Parallel Proton Temperature, (^{o}K)	9.41×10^{4}	1.17×10^{5}	1.19×10^{5}	-	-
Perpendicular Proton Temperature, (^{o}K)	6.41×10^{4}	6.89×10^{4}	5.30×10^{4}	-	-
Total Proton Temperature (^{o}K)	6.75×10^{4}	8.5×10^{4}	7.5×10^{4}	4.0×10^{4}	4.4×10^{3}
Proton Thermal Anisotropy Ratio	1.73	1.70	2.23	-	-
Magnetic Field Angle	123.3^{o}	127.7^{o}	130.1^{o}	125^{o}	-
Plasma β	.860	1.09	1.09	-	-

TABLE VIII

NUMERICAL SOLUTION FOR THE INNER REGION

SOLUTION #3

$r/r_\odot$	u_r (Km/sec.)	u_ω (Km/sec.)	T (^oK)	$\frac{d\theta}{dZ}$	ϕ (deg.)	β
1.274	36.91	2.22	2.51×10^6	-52.72	179.4	.01879
1.843	66.29	2.80	2.06 "	-29.54	179.2	.01801
2.626	98.64	3.34	1.71 "	-17.15	178.8	.02040
3.733	129.5	3.88	1.42 "	-10.21	178.3	.02612
5.459	165.7	4.21	1.17 "	-5.699	177.6	.03573
8.240	198.2	4.47	9.39×10^5	-3.092	176.4	.05454
12.00	223.8	4.49	7.65 "	-1.772	174.9	.08318
19.08	250.0	4.22	5.90 "	-0.892	172.1	.1434
28.05	267.9	3.78	4.71 "	-0.500	168.7	.2265
37.68	279.3	3.35	3.94 "	-0.321	165.3	.3192
50.50	288.9	2.89	3.29 "	-0.205	160.9	.4412
69.18	297.6	2.40	2.70 "	-0.121	155.0	.6073
84.18	302.2	2.10	2.40 "	-0.079	150.7	.7301

TABLE VIII (CONTINUED)

NUMERICAL SOLUTION FOR THE OUTER REGION

SOLUTION #3

$r_\odot$	u_r (Km/sec)	u_ω (Km/sec)	$T_{p\parallel}$ (^oK)	$T_{p\perp}$ (^oK)	$Q_\parallel$	$Q_\perp$	T_e (^oK)	$\frac{d\theta e}{dZ}$	ϕ (deg)	β
5.61	302.6	2.13	2.37×10^{5}	2.33×10^{5}	1.29×10^{-3}	5.41×10^{-4}	2.38×10^{5}	-7.63×10^{-2}	150.4	.736
17.4	309.1	2.25	1.87 "	1.34 "	5.51×10^{-4}	1.31 "	1.99 "	-4.91 "	142.5	.840
52.9	314.3	1.88	1.33 "	7.89×10^{4}	1.75 "	2.89×10^{-5}	1.62 "	-3.23 "	133.6	.891
29.7	318.4	1.32	8.46×10^{4}	4.89 "	4.38×10^{-5}	6.13×10^{-6}	1.27 "	-2.12 "	124.3	.843
15.9	321.2	0.89	5.13 "	3.25 "	1.06 "	1.54 "	9.61×10^{4}	-1.41 "	116.6	.715
63.6	323.3	0.538	2.64 "	2.07 "	1.66×10^{-6}	3.15×10^{-7}	6.33 "	-9.71×10^{-3}	108.9	.512
17.0	324.6	0.379	1.57 "	1.51 "	3.65×10^{-7}	9.96×10^{-8}	4.24 "	-4.78 "	104.5	.362
12.3	325.4	0.278	9.10×10^{3}	1.12 "	8.32×10^{-8}	3.18 "	2.86 "	-2.39 "	101.0	.252
093	325.9	0.208	5.21 "	8.33×10^{3}	1.93 "	1.02 "	1.94 "	-1.20 "	98.34	.175
455	326.2	0.157	2.96 "	6.22 "	4.57×10^{-9}	3.29×10^{-9}	1.32 "	-6.14×10^{-4}	96.29	.121
936	326.5	0.119	1.68 "	4.66 "	1.08 "	1.05 "	9.00×10^{3}	-3.13 "	94.74	.084
577	326.6	0.090	9.53×10^{2}	3.49 "	2.59×10^{-10}	3.39×10^{-10}	6.14 "	-1.60 "	93.56	.059
431	326.7	0.068	5.38 "	2.62 "	6.20×10^{-11}	1.08 "	4.19 "	-8.20×10^{-5}	92.68	.041
566	326.8	0.052	1.96 "	1.48 "	1.48 "	3.48×10^{-11}	2.86 "	-4.2 "	92.01	.029
078	326.8	0.039	1.71 "	1.47 "	3.55×10^{-12}	1.11 "	1.95 "	-2.15 "	91.51	.020

TABLE IX

NUMERICAL SOLUTION FOR THE INNER REGION

SOLUTION #4

$r/r_\odot$	u_r (Km/sec)	u_ω (Km/sec)	T (^oK)	$\frac{d\theta}{dZ}$	ϕ (deg.)	β
1.206	31.88	2.16	2.5410^6	-52.95	179.5	0.0176
1.665	56.61	2.68	2.15 "	-31.81	179.3	0.1600
2.301	86.32	3.20	1.83 "	-19.25	179.0	0.0171
3.179	117.8	3.68	1.56 "	-11.70	178.6	0.0204
4.409	147.3	4.17	1.32 "	- 7.30	178.1	0.0266
6.100	177.0	4.49	1.13 "	- 4.50	177.4	0.0360
8.462	203.6	4.71	9.61×10^5	- 2.78	176.5	0.0511
11.92	228.2	4.77	8.08 "	- 1.69	175.1	0.0759
16.92	250.0	4.63	6.76 "	- 1.01	173.2	0.1161
24.98	270.6	4.31	5.53 "	-0.577	170.2	0.1880
32.24	282.6	3.92	4.86 "	-0.380	167.7	0.2580
43.44	294.6	3.46	4.16 "	-0.240	163.9	0.3720
58.40	304.8	2.97	3.57 "	-0.149	159.2	0.5280
79.65	313.9	2.46	3.07 "	-0.085	153.0	0.7470
87.62	316.4	2.32	2.95 "	-0.069	150.9	0.8278

TABLE IX (CONTINUED)

NUMERICAL SOLUTION FOR THE OUTER REGION

SOLUTION #4

$r/r_\odot$	u_r (Km/sec)	u_ϕ (Km/sec)	$T_{p\parallel}$ (^oK)	$T_{p\perp}$ (^oK)	$Q_\parallel$	$Q_\perp$	T_e (^oK)	$\frac{d\theta_e}{dZ}$	ϕ (deg)	β
89.10	316.9	2.35	2.92×10^{5}	2.86×10^{5}	2.28×10^{-3}	9.57×10^{-4}	2.93×10^{5}	-6.61×10^{-2}	150.5	.835
122.2	325.0	2.52	2.26 "	1.63 "	9.22×10^{-4}	2.38 "	2.56 "	-4.28 "	142.8	.975
169.6	331.5	2.10	1.58 "	9.66×10^{4}	2.92 "	5.50×10^{-5}	2.22 "	-2.85 "	134.0	1.07
239.1	336.8	1.48	9.96×10^{4}	5.88 "	7.40×10^{-5}	1.23 "	1.87 "	-1.95 "	124.8	1.08
328.8	340.5	1.01	6.00 "	3.89 "	1.83 "	3.20×10^{-6}	1.55 "	-1.41 "	117.0	.997
526.6	344.4	.559	2.60 "	2.24 "	2.03×10^{-6}	4.64×10^{-7}	1.07 "	-8.42×10^{-3}	107.8	.749
752.9	346.6	.376	1.32 "	1.52 "	3.62×10^{-7}	1.09 "	7.42×10^{4}	-5.89 "	102.7	.535
1002	347.8	.280	7.60×10^{3}	1.12 "	8.34×10^{-8}	3.49×10^{-8}	5.01 "	-3.31 "	99.69	.372
1333	348.7	.211	4.33 "	8.38×10^{3}	1.95 "	1.11 "	3.40 "	-1.67 "	97.33	.257
1775	349.2	.160	2.46 "	6.26 "	4.62×10^{-9}	3.55×10^{-9}	2.31 "	-8.51×10^{-4}	95.52	.178
2363	349.6	.121	1.39 "	4.69 "	1.10 "	1.13 "	1.57 "	-4.34 "	94.16	.123
3145	349.9	.092	7.88×10^{2}	3.51 "	2.62×10^{-10}	3.62×10^{-10}	1.07 "	-2.21 "	93.13	.085
4186	350.0	.070	4.45 "	2.64 "	6.27×10^{-11}	1.15 "	7.32×10^{3}	-1.13 "	92.35	.059
5572	350.2	.053	2.51 "	1.98 "	1.50 "	3.69×10^{-11}	4.99 "	-5.81×10^{-5}	91.77	.040
7416	350.3	.040	1.42 "	1.48 "	3.59×10^{-12}	1.17 "	3.41 "	-2.98 "	91.33	.028

Figure 22

The particle number density and magnetic field intensity as a function of heliocentric distance, for $K=1.0\times10^{-7}$ ergs $cm^{-1}sec^{-1}deg^{-3.5}$. Solution #3, two-fluid model.

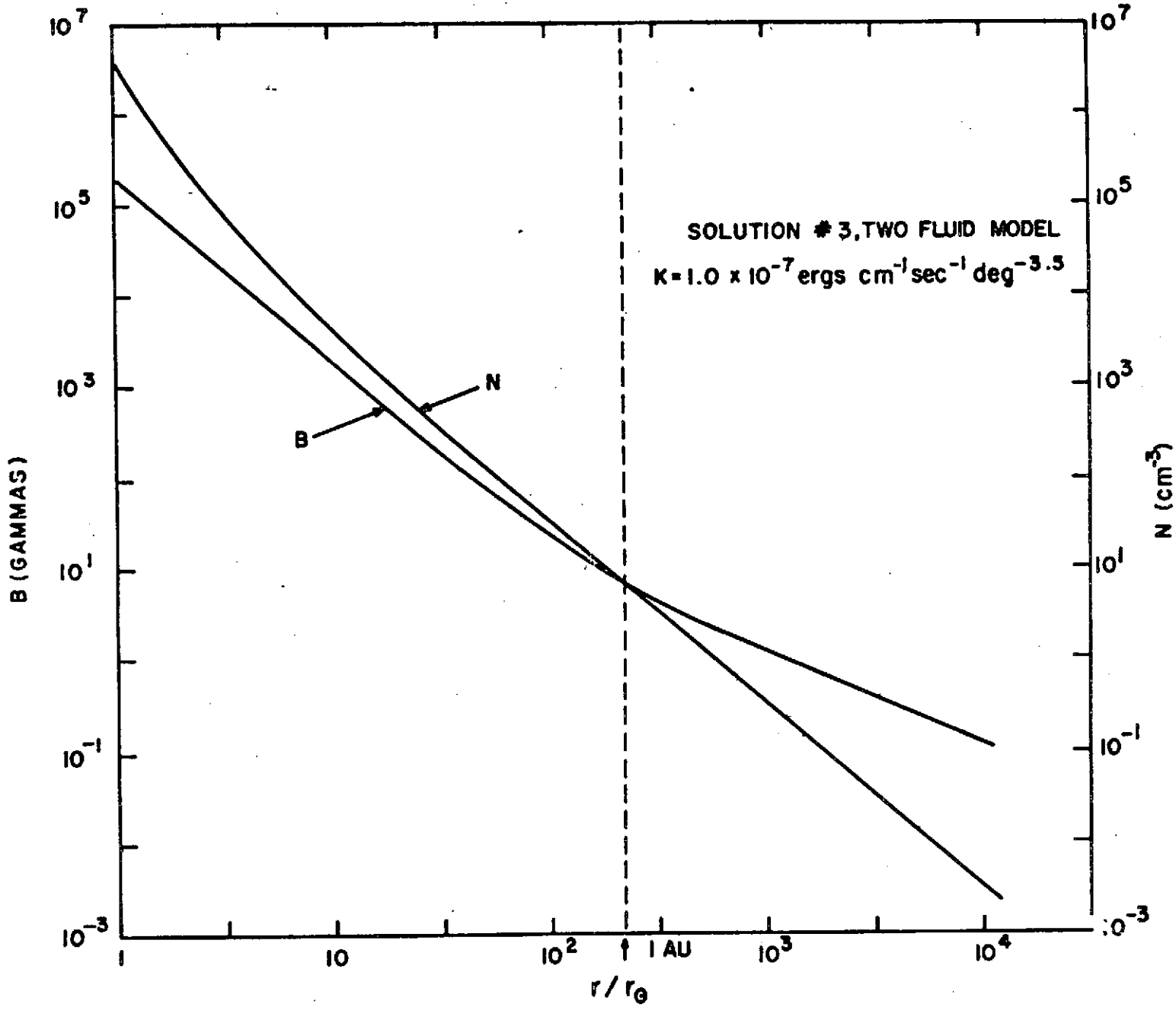
SOLUTION # 3, TWO FLUID MODEL
K = 1.0 x 10^-7 ergs cm^-1 sec^-1 deg^-3.5
N
B
B (GAMMAS)
N (cm^-3)
r / r_0
1 AU
10^7
10^5
10^3
10^1
10^-1
10^-3
1
10
10^2
10^3
10^4

Figure 23

The electron conduction heat flux Q_e and proton heat fluxes $Q_\parallel$ and $Q_\perp$ as a function of heliocentric distance, for $K=1.0\times10^{-7}$ ergs cm^{-1} $sec^{-1}deg^{-3.5}$. Solution #3, two-fluid model.

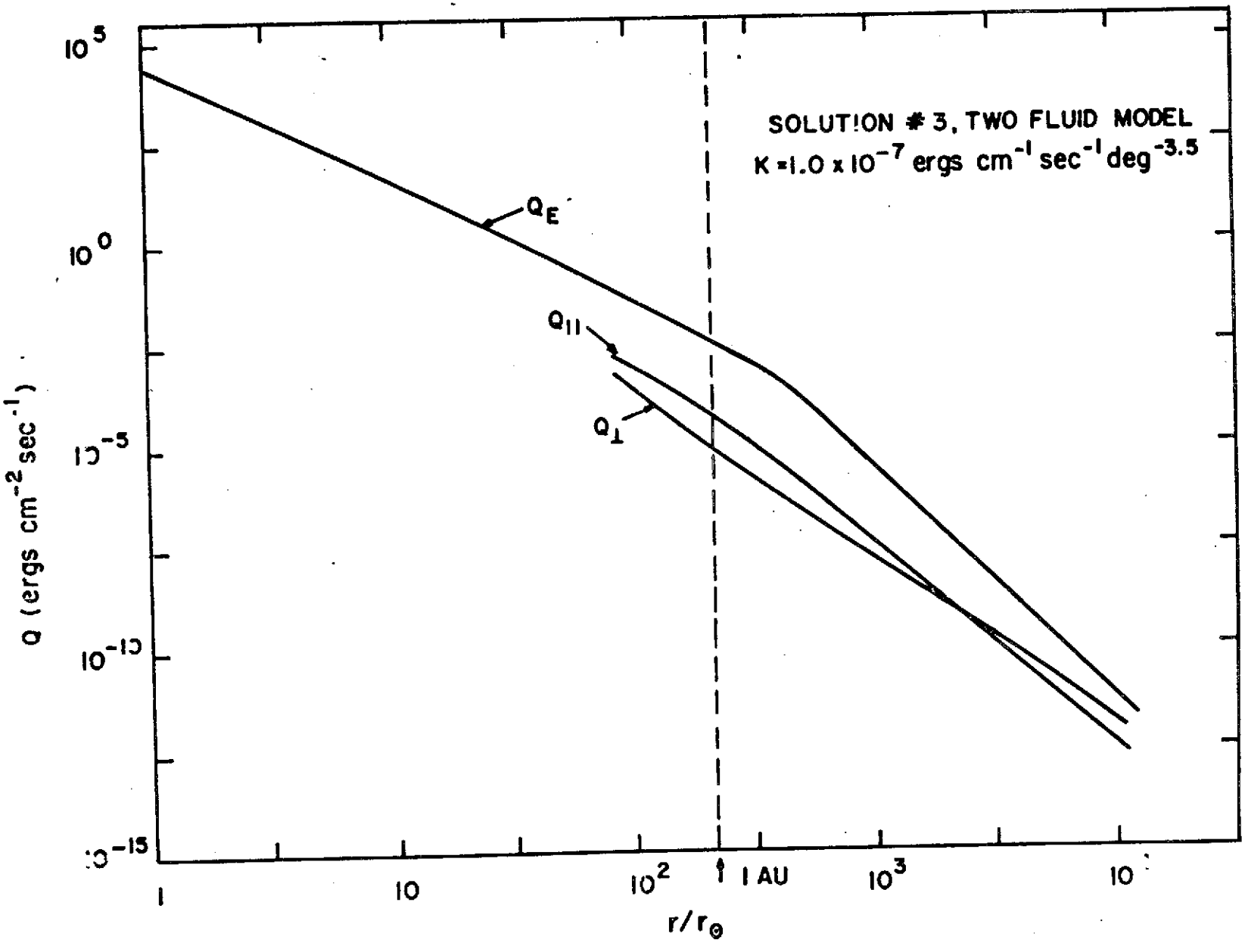
SOLUTION # 3, TWO FLUID MODEL
K = 1.0 x 10^-7 ergs cm^-1 sec^-1 deg^-3.5
Q_E
Q_II
Q_⊥
Q (ergs cm^-2 sec^-1)
10^5
10^0
10^-5
10^-10
10^-15
1
10
10^2
1 AU
10^3
r/r_⊙

Figure 24

The particle number density and magnetic field intensity as a function of heliocentric distance, for $K=1.0\times10^{-7}$ ergs $cm^{-1}sec^{-1}deg^{-3.5}$. Solution #4, two-fluid model.

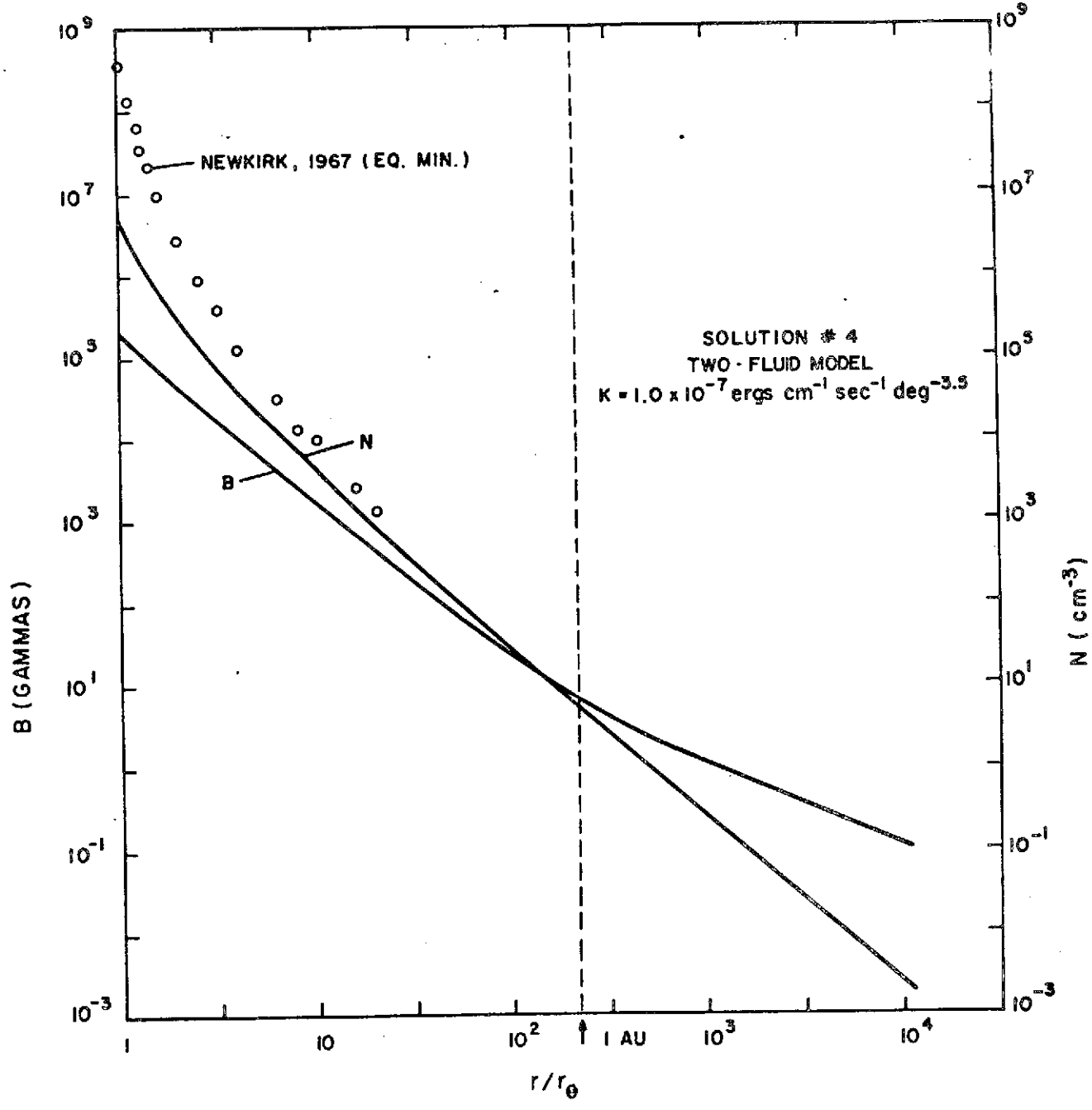
NEWKIRK, 1967 (EQ. MIN.)
SOLUTION # 4
TWO - FLUID MODEL
K = 1.0 x 10^-7 ergs cm^-1 sec^-1 deg^-3.5
N
B
B (GAMMAS)
N (cm^-3)
r/r_θ
1 AU
10^9
10^7
10^5
10^3
10^1
10^-1
10^-3
1
10
10^2
10^3
10^4

Figure 25

The electron conduction heat flux Q_e and proton heat fluxes $Q_{\parallel}$ and $Q_{\perp}$ as a function of heliocentric distance, for $K=1.0\times10^{-7}$ ergs cm^{-1} $sec^{-1}deg^{-3.5}$. Solution #4, two-fluid model.

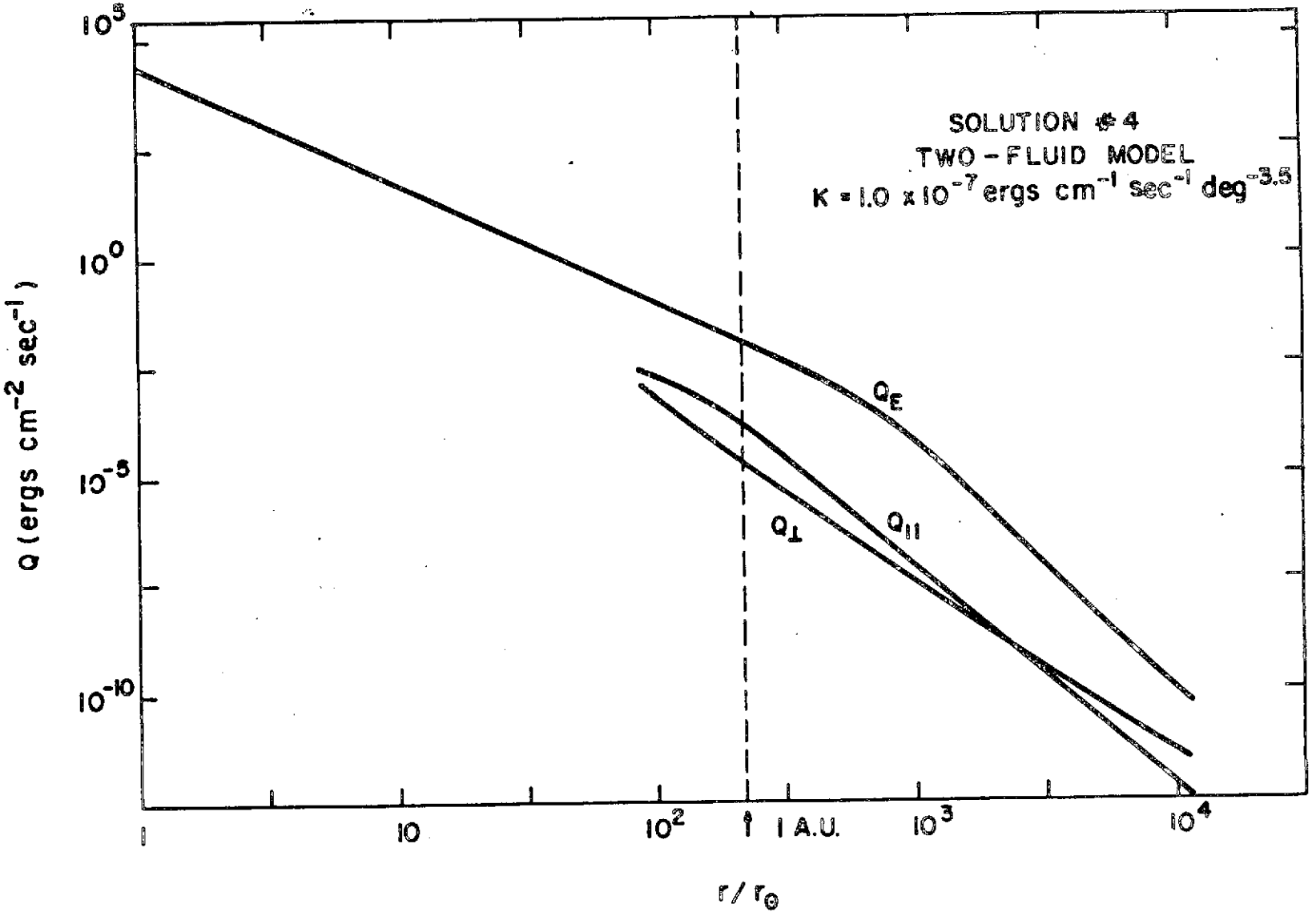
SOLUTION #4
TWO-FLUID MODEL
K = 1.0 x 10^-7 ergs cm^-1 sec^-1 deg^-3.5
Q_E
Q_II
Q_⊥
Q (ergs cm^-2 sec^-1)
10^0
10^-5
10^-10
1
10
10^2
1 A.U.
10^3
10^4
r / r_⊙

TABLE X

TOTAL ENERGY FLUX, PARTICLE NUMBER DENSITY, MAGNETIC FIELD INTENSITY AND HEAT FLUXES PREDICTED BY THE SOLUTIONS AT 1 A.U. FOR $K = 1 \times 10^{-7}$ (ergs-cm^{-1}-sec^{-1}-$deg^{-3.5}$).

	Solution #3	Solution #4
$F \times 10^{-25}$ (ergs-sec^{-1}-$sterad^{-1}$)	5.68	5.54
F / r^2 (ergs-cm^{-2}-sec^{-1})	0.256	0.249
n (cm^{-3})	7.31	5.85
B (gammas)	7.69	7.24
q_e (ergs-cm^{-2}-sec^{-1})	4.26×10^{-3}	1.10×10^{-2}
$q_{\parallel}$ (ergs-cm^{-2}-sec^{-1})	7.00×10^{-5}	1.15×10^{-4}
$q_{\perp}$ (ergs-cm^{-2}-sec^{-1})	1.00×10^{-5}	1.94×10^{-5}

Figure 26

The kinetic energy flux per steradian, $KEF = \frac{1}{2}$ mnu $r^2(\underline{u}^2)$ as a function of heliocentric distance, for $K=1.0\times10^{-7}$ ergs $cm^{-1}sec^{-1}deg^{-3.5}$. Solution #3, two-fluid model.

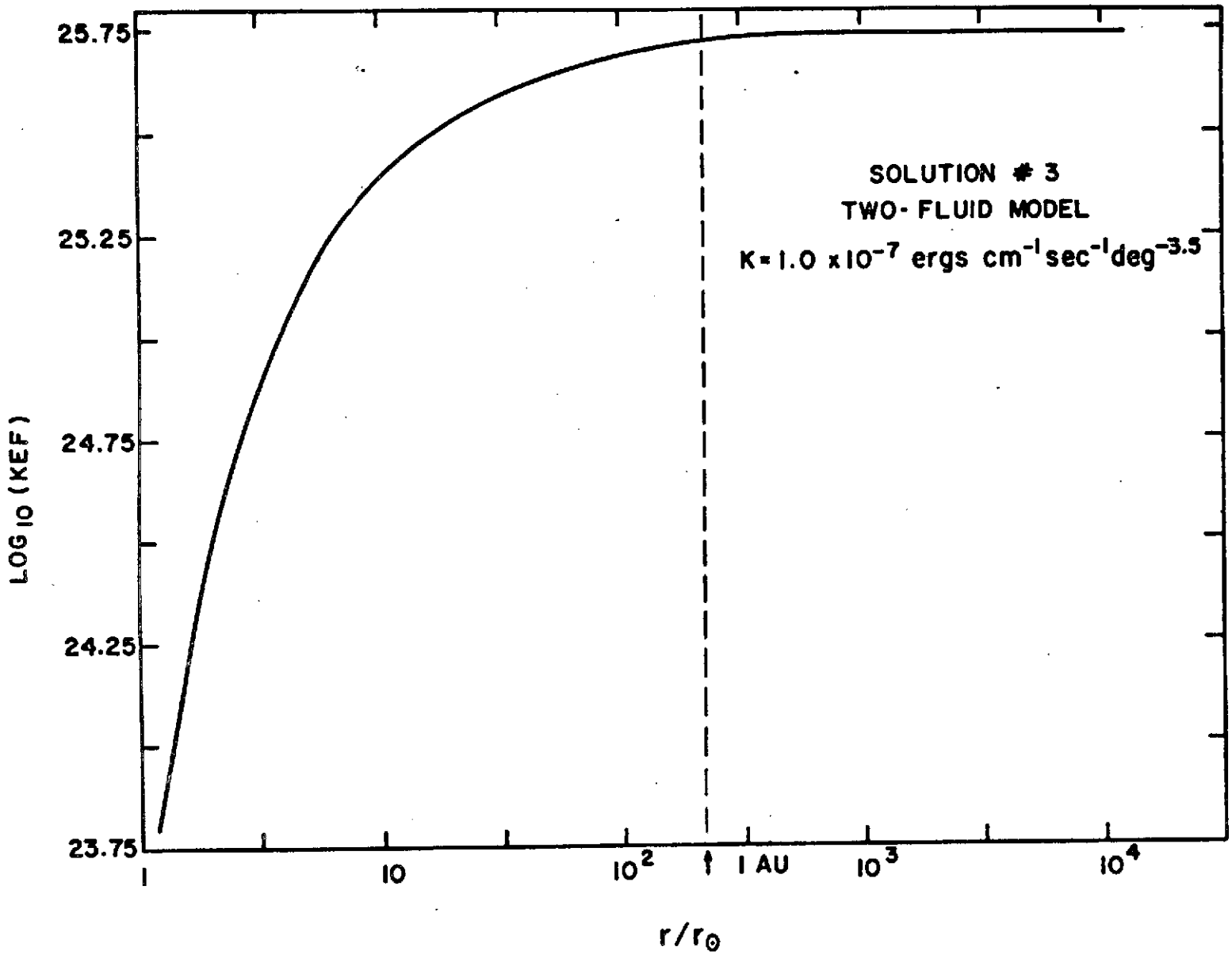
25.75
25.25
24.75
24.25
23.75
LOG 10 (KEF)
SOLUTION # 3
TWO- FLUID MODEL
K = 1.0 x 10^-7 ergs cm^-1 sec^-1 deg^-3.5
1
10
10^2
1 AU
10^3
10^4
r/r⊙

Figure 27

The magnetic field energy flux per steradian,

$$MEF = \frac{r^2 B^2}{4\pi} \left(u_r \sin^2\phi - u_\omega \sin\phi \cos\phi \right)$$

as a function of heliocentric distance, for $K=1.0\times10^{-7}$ ergs $cm^{-1}sec^{-1}deg^{-3.5}$.

Solution #3, two-fluid model.

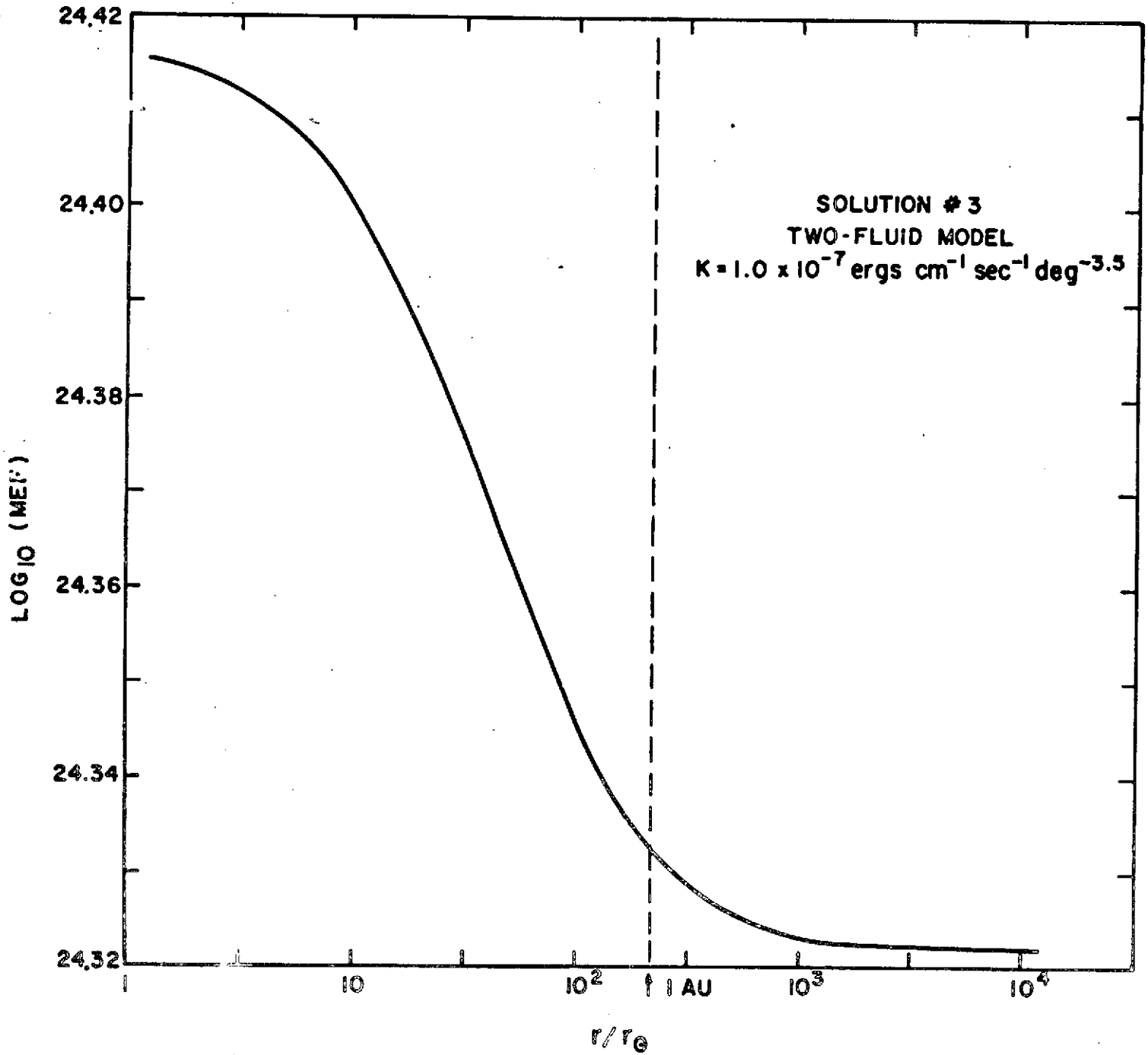
24.42
24.40
24.38
24.36
24.34
24.32
LOG10 (ME')
SOLUTION # 3
TWO-FLUID MODEL
K = 1.0 x 10^-7 ergs cm^-1 sec^-1 deg^-3.5
1
10
10^2
1 AU
10^3
10^4
r/r_e

Figure 28

The kinetic energy flux per steradian as a function of heliocentric distance for $K=1.0\times10^{07}$ ergs $cm^{-1}sec^{-1}deg^{-3.5}$. Solution #4, two-fluid model.

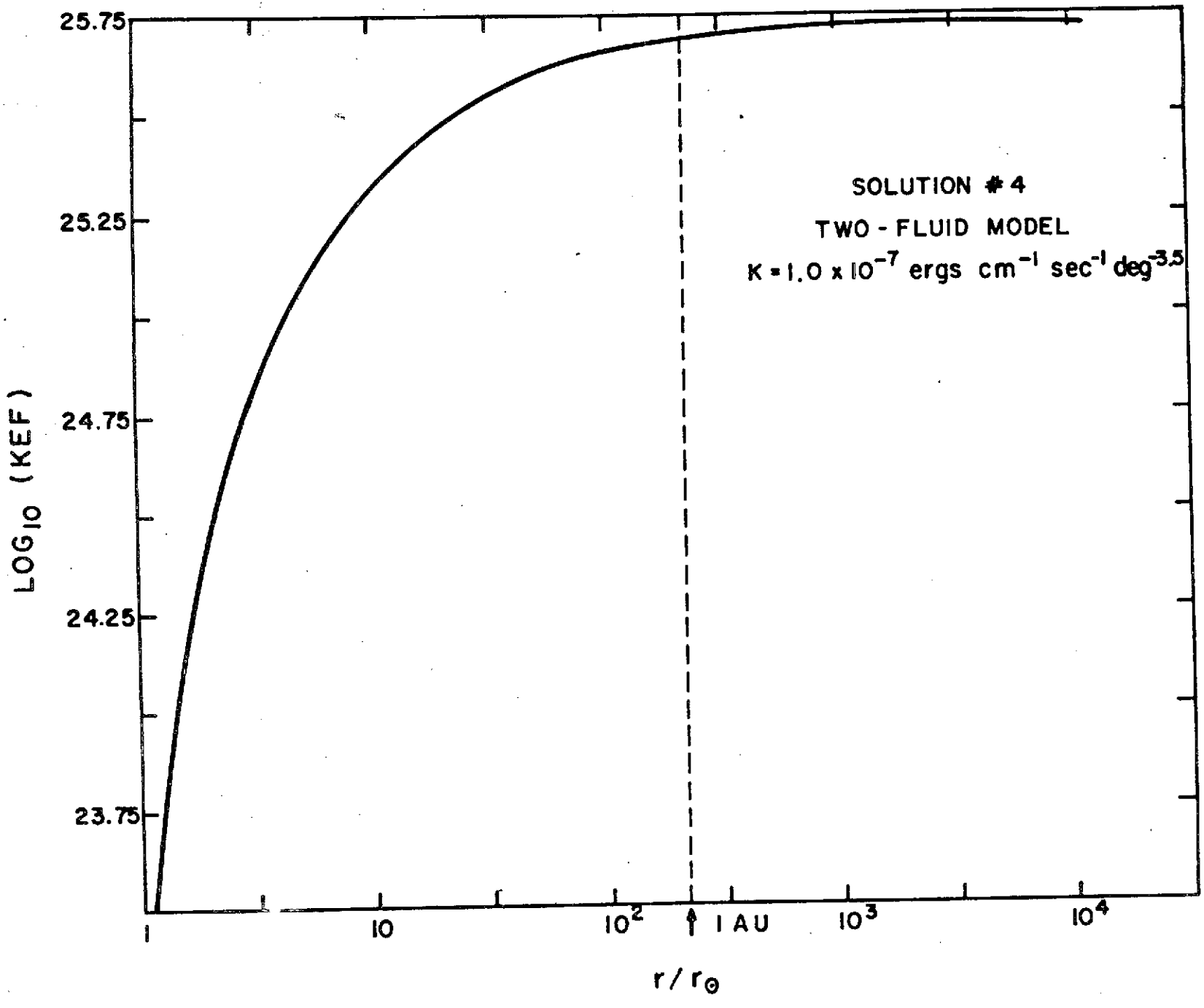
25.75
25.25
24.75
24.25
23.75
LOG10 (KEF)
SOLUTION # 4
TWO - FLUID MODEL
K = 1.0 x 10^-7 ergs cm^-1 sec^-1 deg^-3.5
1
10
10^2
1 AU
10^3
10^4
r / r⊙

Figure 29

The magnetic field energy flux per steradian as a function of heliocentric distance for $K=1.0\times10^{-7}$ ergs $cm^{-1}sec^{-1}deg^{-3.5}$. Solution #4, two-fluid model.

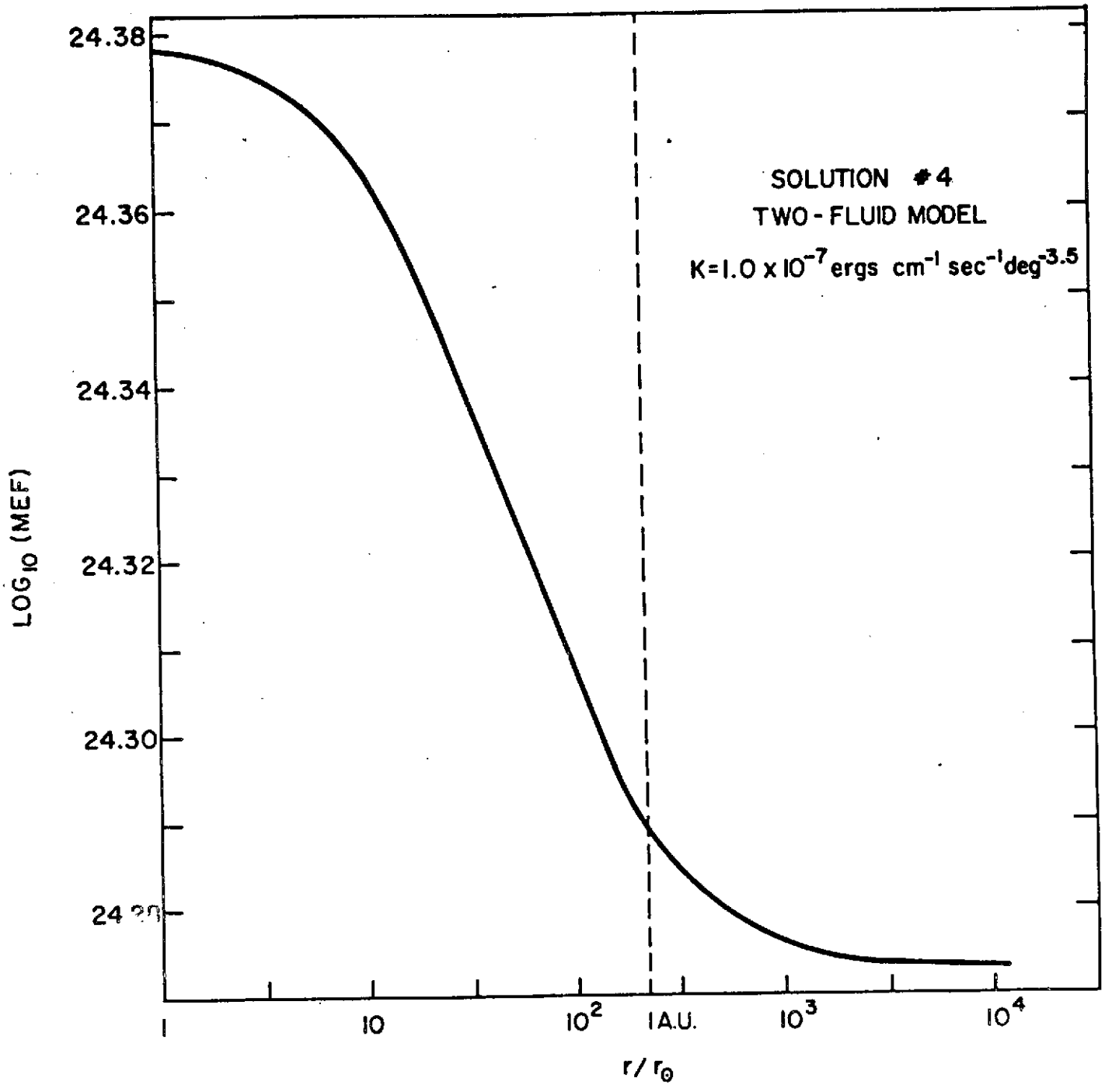
24.38
24.36
24.34
24.32
24.30
LOG10 (MEF)
SOLUTION #4
TWO-FLUID MODEL
K=1.0 x 10^-7 ergs cm^-1 sec^-1 deg^-3.5
1
10
10^2
1 A.U.
10^3
10^4
r/r0

$$\gamma_{\parallel} = \frac{2Q_{\parallel}}{\theta_{\parallel}}\left(Vz^2\sqrt{\xi/\theta_{\parallel}}\right) \qquad \text{(III.4.6)}$$

$$\gamma_{\perp} = \frac{Q_{\perp}}{\theta_{\perp}}\left(Vz^2\sqrt{\xi/\theta_{\parallel}}\right) \qquad \text{(III.4.7)}$$

The values of $\gamma_{\parallel}$, $\gamma_{\perp}$, $T_{p\parallel}$ and $T_{p\perp}$ obtained for various selected heliocentric distances are given in Table XI and Figures 30 through 43 show plots of constant contour maps of the proton distribution function for the parameter values given in the table. The velocity scale for each map has been normalized to the local characteristic thermal velocity as determined by the perpendicular temperature. The axis OZ is parallel to the magnetic field direction, facing outwards from the sun.

The maximum value of the distribution function is attained at point O and the triangle denotes the point in velocity space where the proton intrinsic velocity is zero. A comparison of the contour maps obtained at 1 A.U. with that given in Figure 14 shows that the form of the distribution function used in the analysis can adequately represent observed solar wind properties.

Whang has given several scale times obtained from the purely radial model such as deflection time, equipartition time and expansion time. Since the general features of the solution affecting the calculation of these times are not very different from those obtained by Whang, we shall not repeat the computation here. The equipartition time between electrons and protons is much larger than the expansion scale time implying that thermal equilibrium between the two fluids cannot be maintained by Coulomb interactions alone. We must resort to the physical phenomena mentioned previously to explain the increased proton heating within the solar envelope.

TABLE XI

PARAMETER VALUES WHICH DETERMINE THE PROTON DISTRIBUTION FUNCTION AT SELECTED HELIOCENTRIC DISTANCES

$r/r_\odot$	$\gamma_\parallel$	$\gamma_\perp$	$T_{p\parallel}$	$T_{p\perp}$	$T_{p\parallel}/T_{p\perp}$	$\gamma_\parallel$	$\gamma_\perp$	$T_{p\parallel}$	$T_{p\perp}$	$T_{p\parallel}/T_{p\perp}$
	SOLUTION #3					SOLUTION #4				
107 (.5 A.U.)	.378	.067	2.02×10^5	1.57×10^5	1.28	.532	.102	2.54×10^5	2.06×10^5	1.23
214 (1 A.U.)	.403	.0498	9.40×10^4	5.42×10^4	1.73	.601	.0867	1.17×10^5	6.89×10^4	1.70
428 (2 A.U.)	.384	.0437	3.05×10^4	2.28×10^4	1.33	.616	.0819	3.83×10^4	2.86×10^4	1.33
1112 (5.2 A.U.), Jupiter	.269	.0444	5.21×10^3	8.33×10^3	.625	.578	.0831	6.2×10^3	1.01×10^4	.613
2033 (9.5 A.U.), Saturn	.258	.0455	1.54×10^3	4.46×10^3	.345	.553	.0842	1.89×10^3	5.48×10^3	.345
4066 (19 A.U.), Uranus	.256	.0463	$3\times85\times10^2$	2.22×10^3	.173	.546	.085	4.75×10^2	2.73×10^3	.174
6420 (30 A.U.), Neptune	.256	.0466	1.55×10^2	1.4×10^3	.110	.546	.0853	1.90×10^2	1.73×10^3	.110

Figures 30 through 36

The proton velocity distribution function predicted by Solution #3 for selected heliocentric distances. The velocity scale has been normalized to the local characteristic thermal velocity determined by the perpendicular temperature.

T ANISOTROPY=1.3 GAMMA PAR=0.38 GAMMA PER=0.07

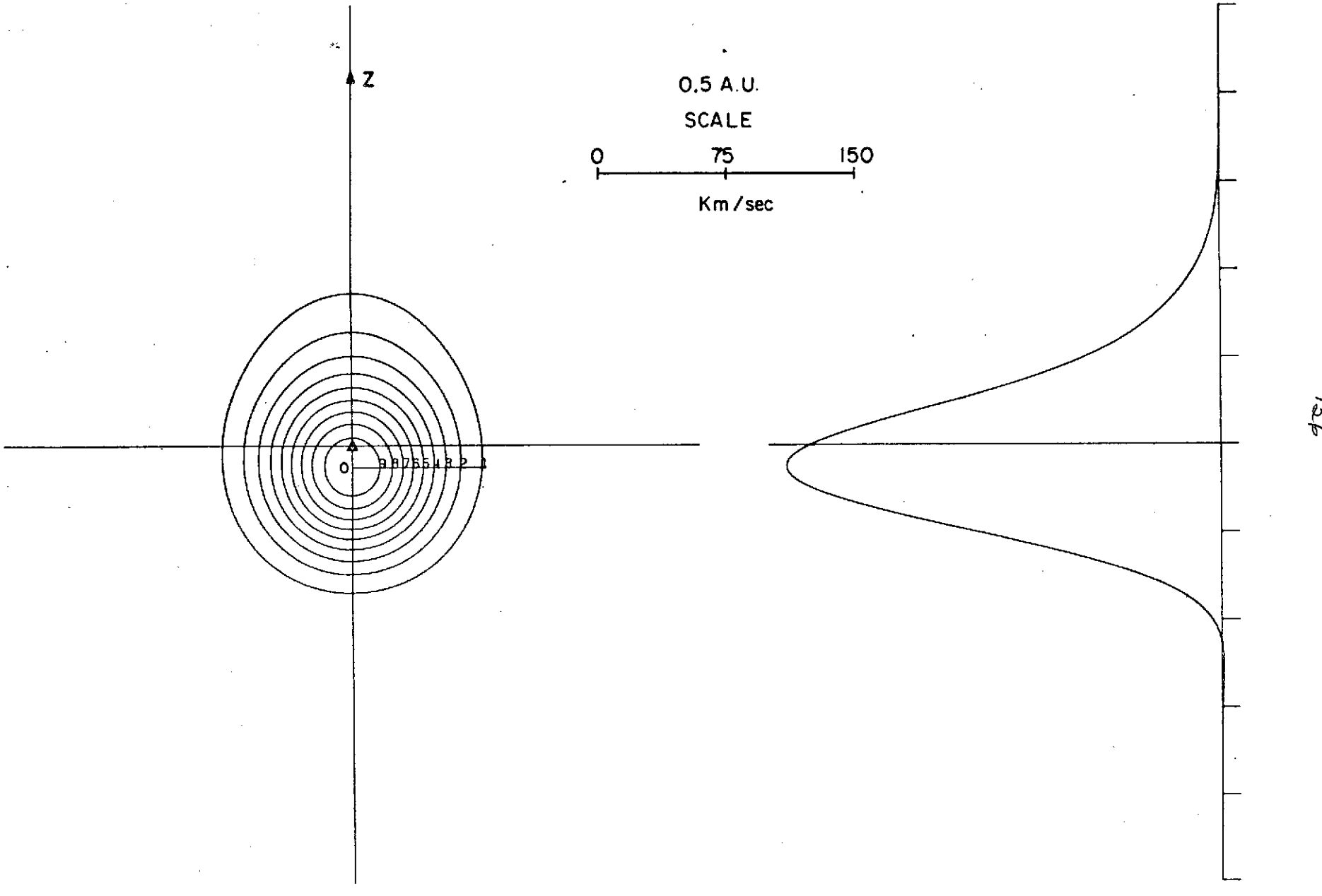

T ANISOTROPY=1.7 GAMMA PAR=0.40 GAMMA PER=0.05

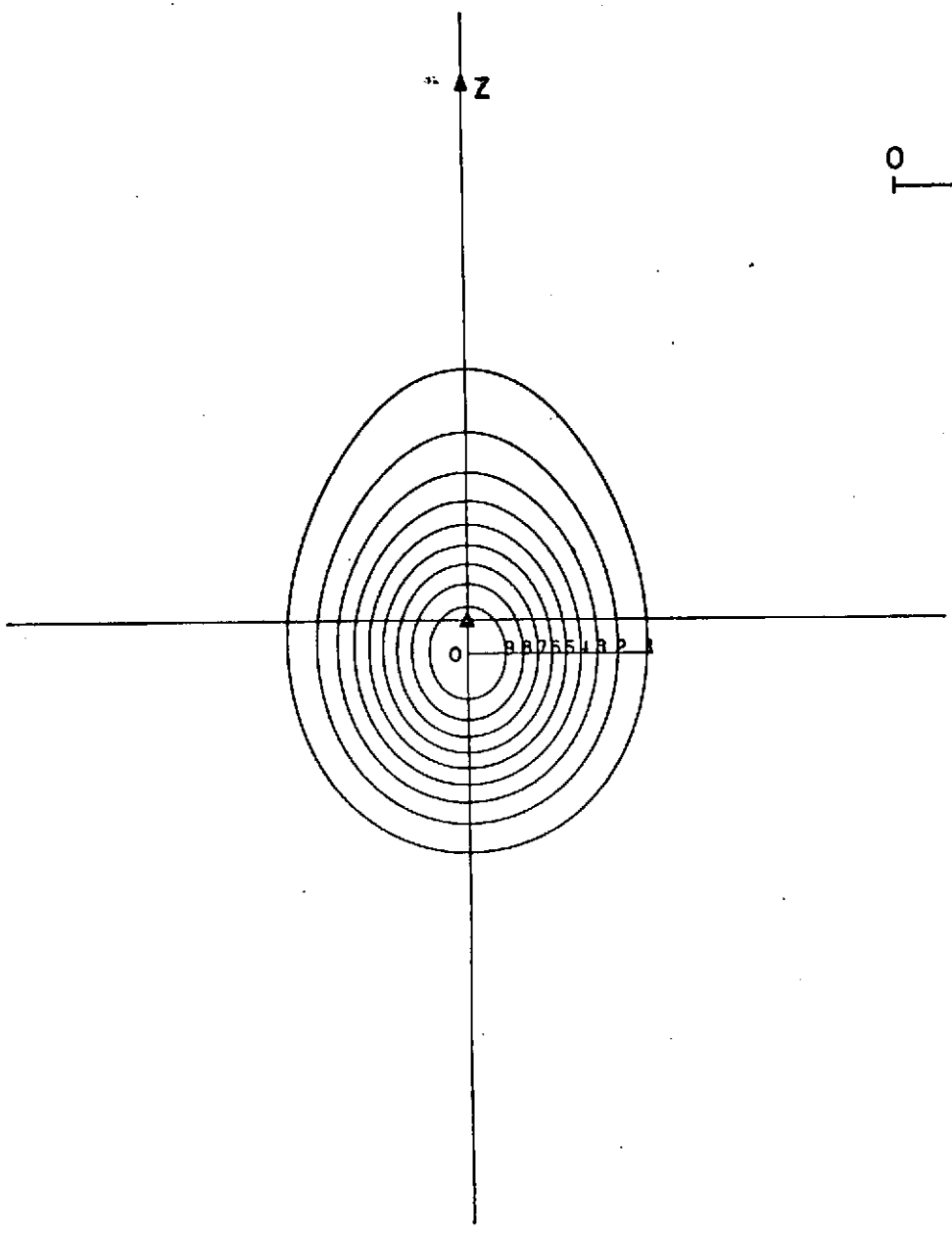

1 A.U.
SCALE
0 50 100
Km/sec

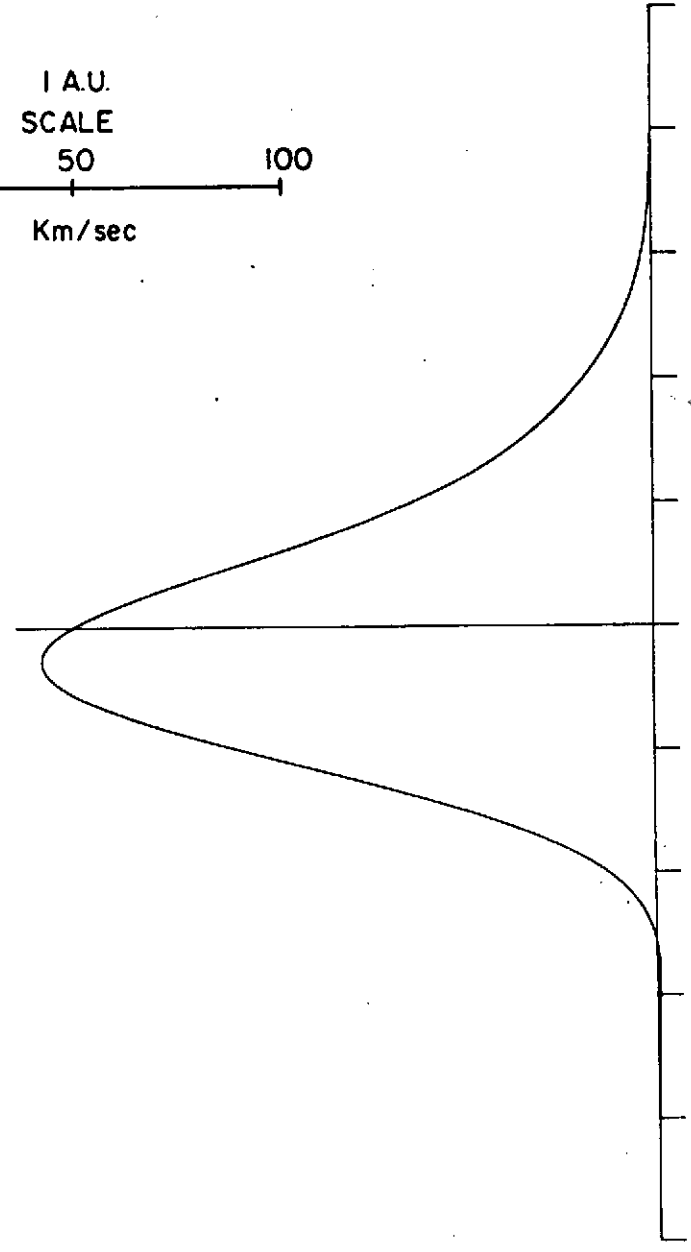

T ANISOTROPY=1.3 GAMMA PAR=0.38 GAMMA PER=0.04

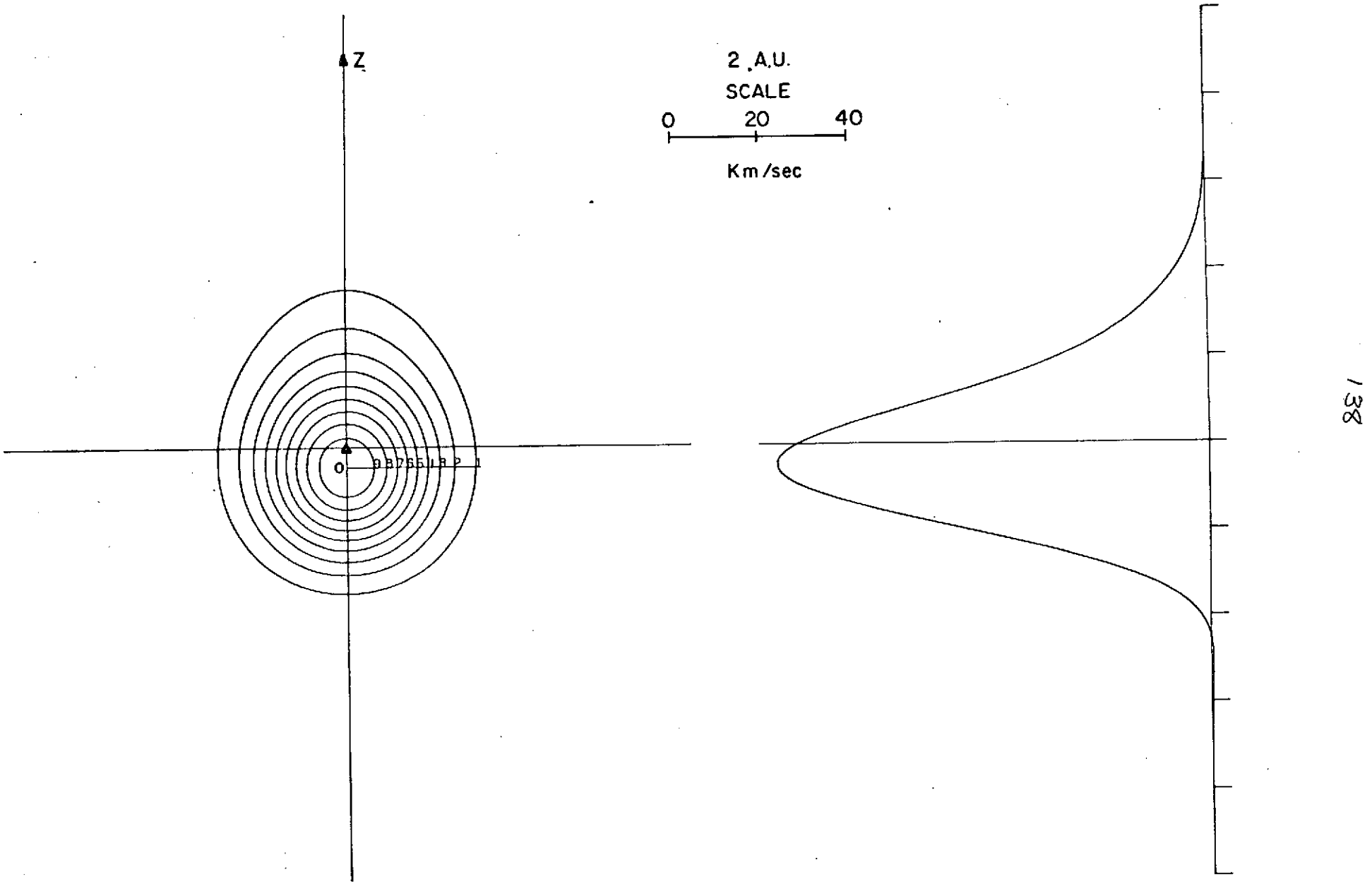

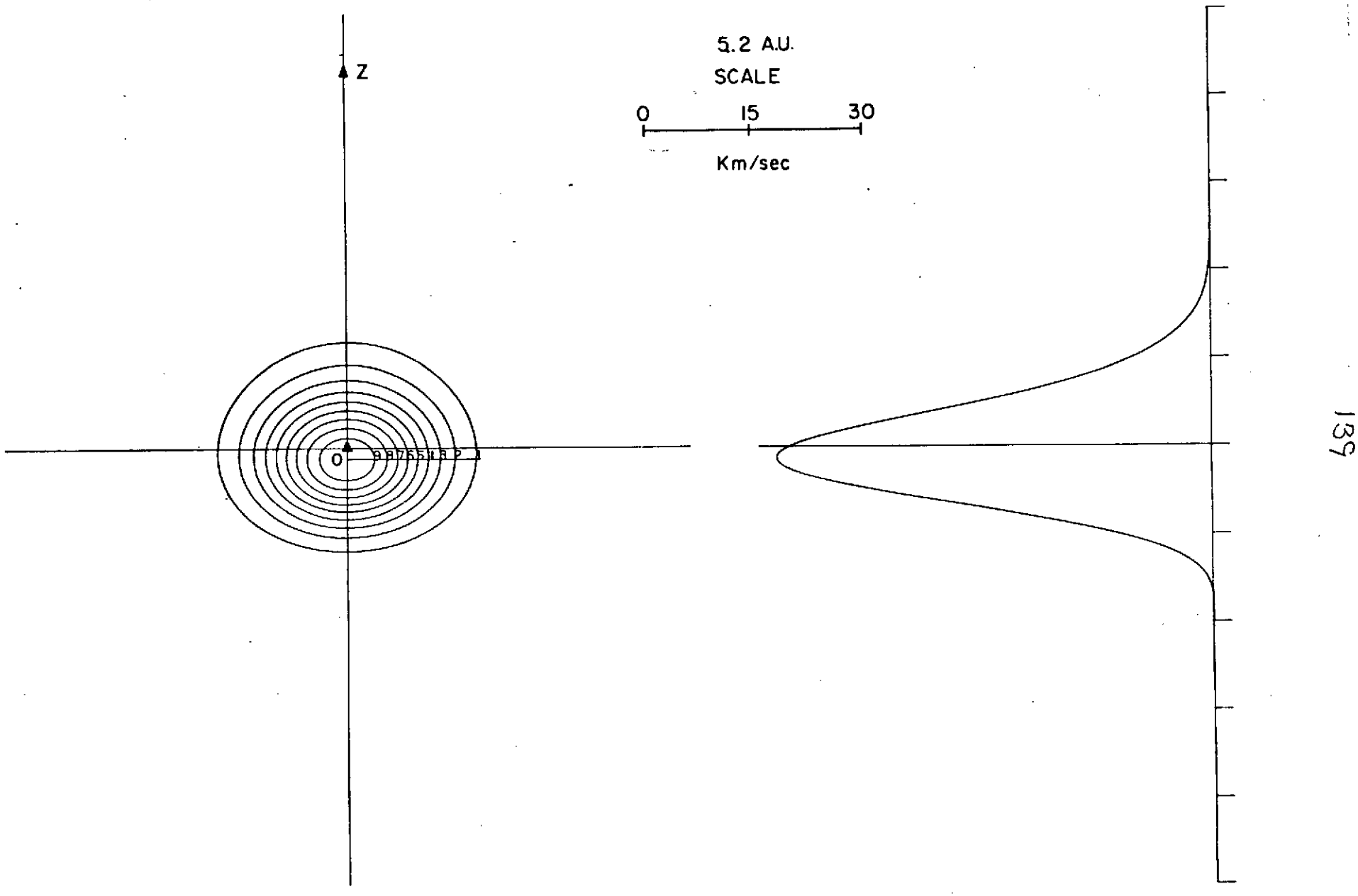
T ANISOTROPY=0.6 GAMMA PAR=0.27 GAMMA PER=0.04
Z
0
5.2 A.U.
SCALE
0
15
30
Km/sec

T ANISOTROPY=0.3 GAMMA PAR=0.26 GAMMA PER=0.05

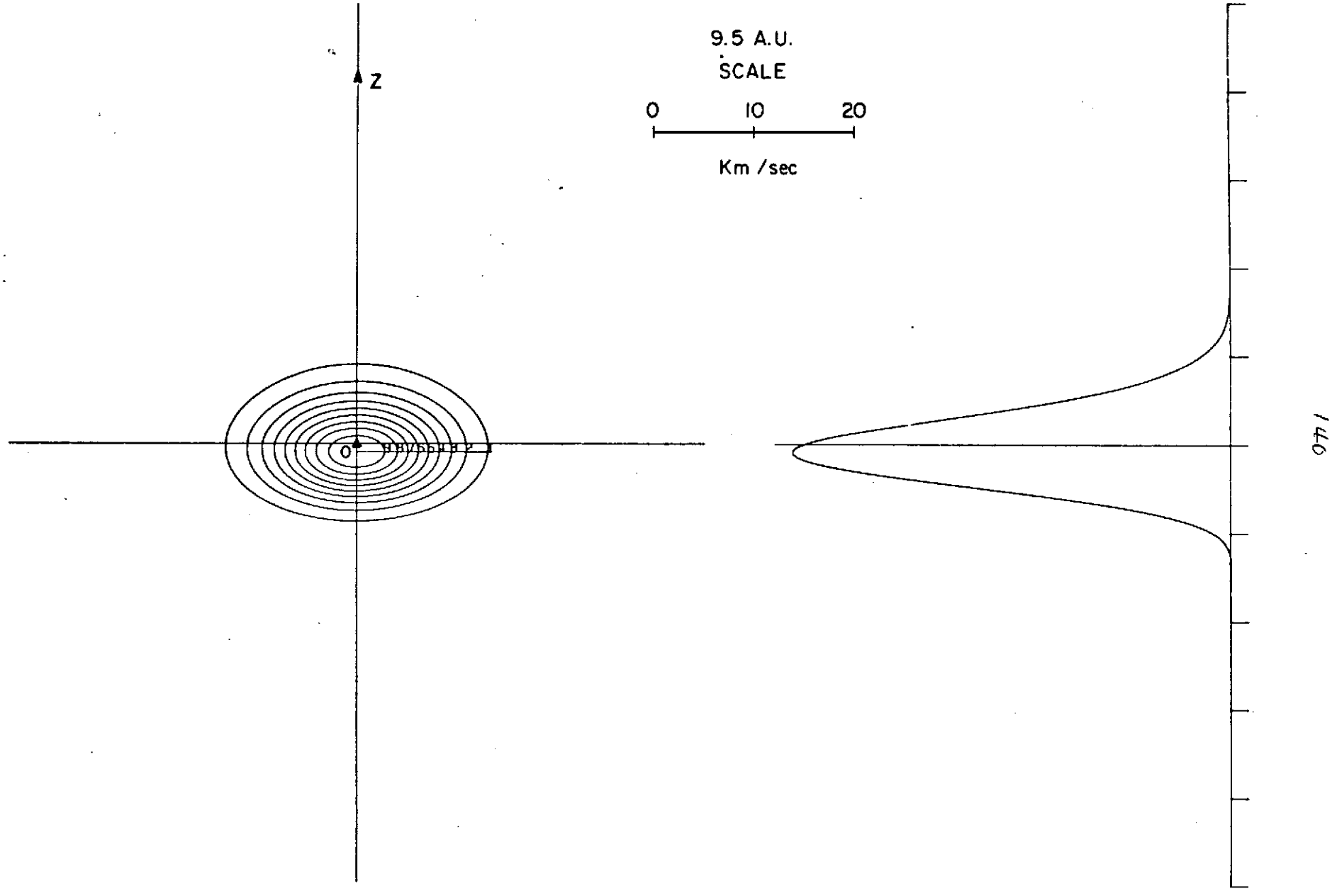

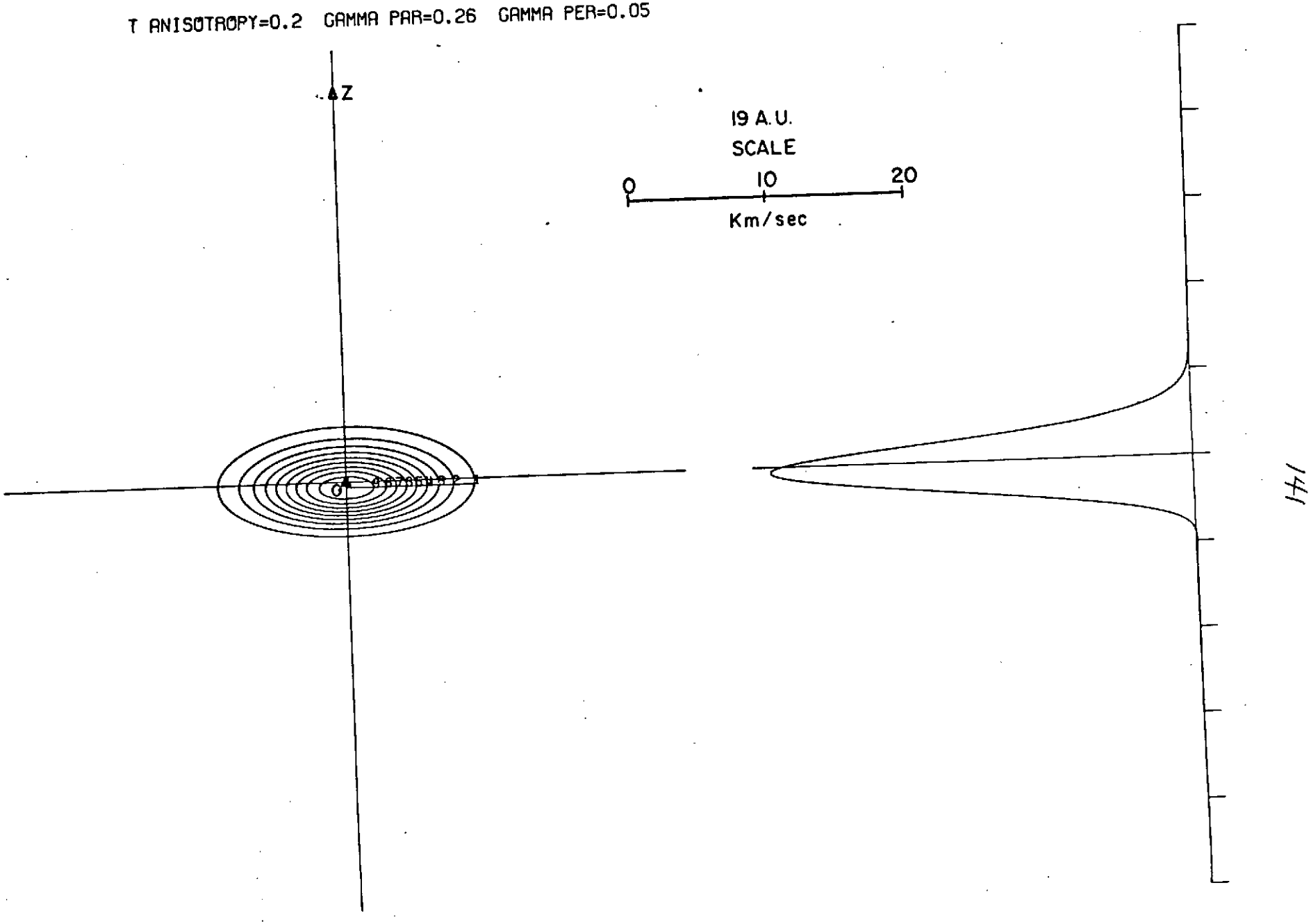
T ANISOTROPY=0.2 GAMMA PAR=0.26 GAMMA PER=0.05
Z
19 A.U.
SCALE
0
10
20
Km/sec

T ANISOTROPY=0.1 GAMMA PAR=0.26 GAMMA PER=0.05

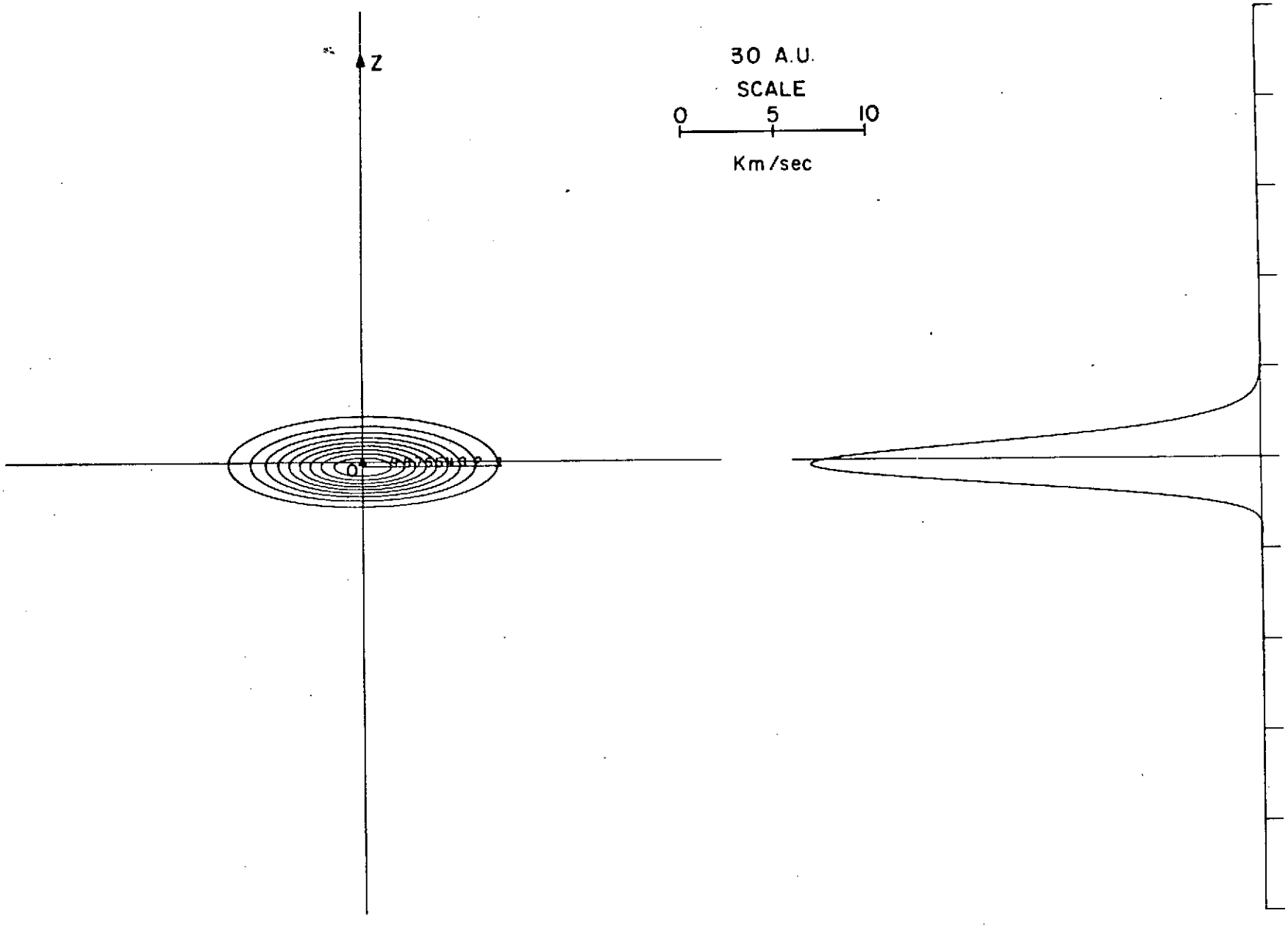

Figures 37 through 43

The proton velocity distribution function predicted by Solution #4 for selected heliocentric distances. The velocity scale has been normalized to the local characteristic thermal velocity determined by the perpendicular temperature.

T ANISOTROPY=1.2 GAMMA PAR=0.53 GAMMA PER=0.10

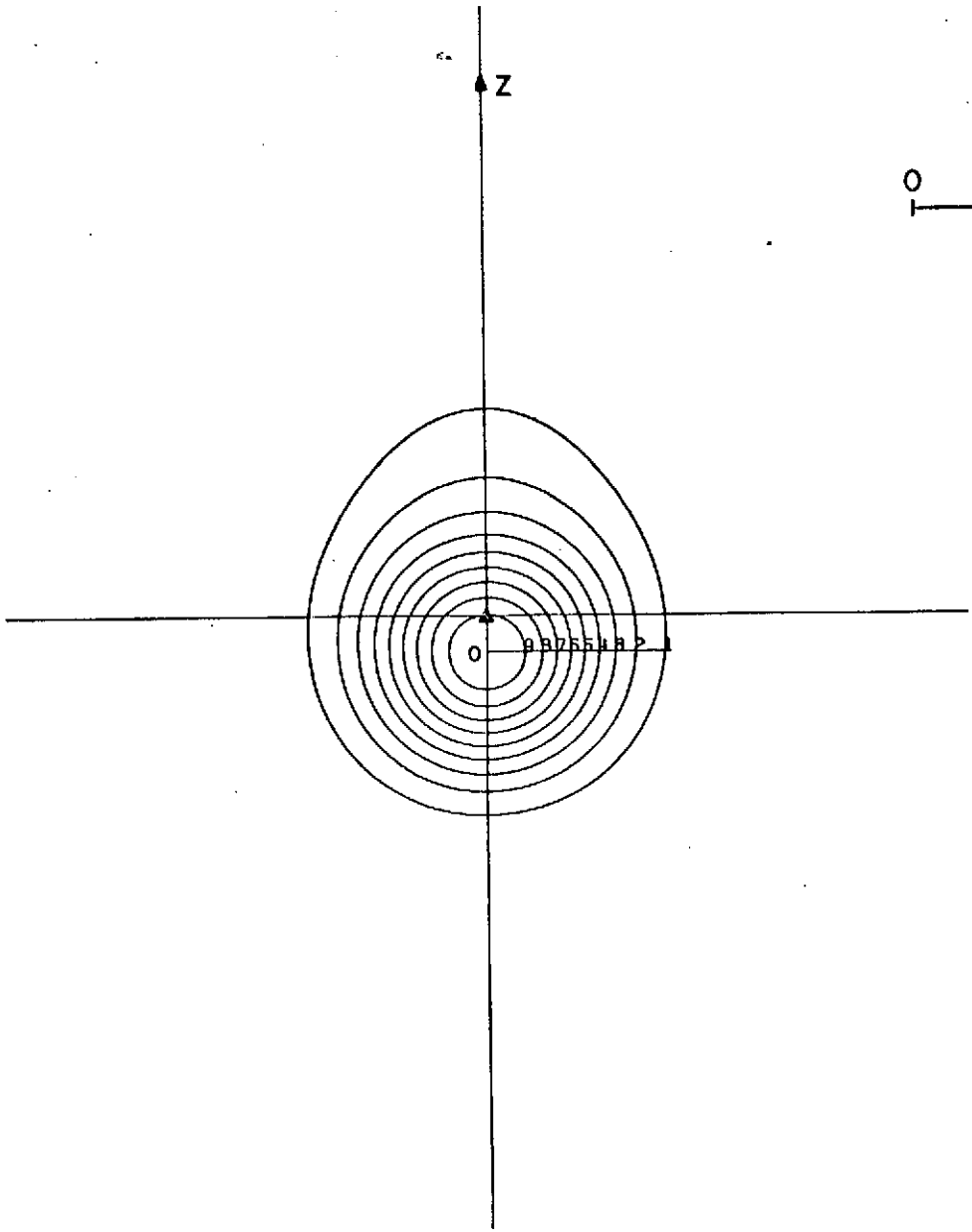

0.5 A.U.
SCALE
0 75 150
Km/sec

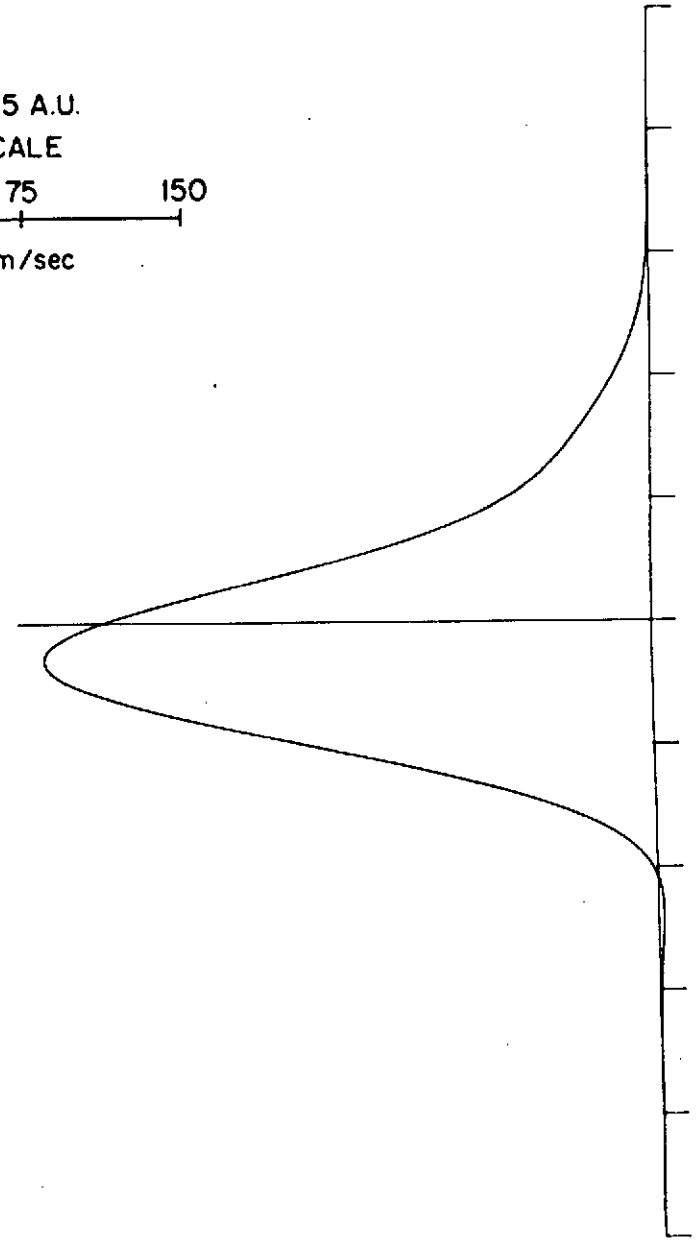

hhl

T ANISOTROPY=1.7 GAMMA PAR=0.60 GAMMA PER=0.09

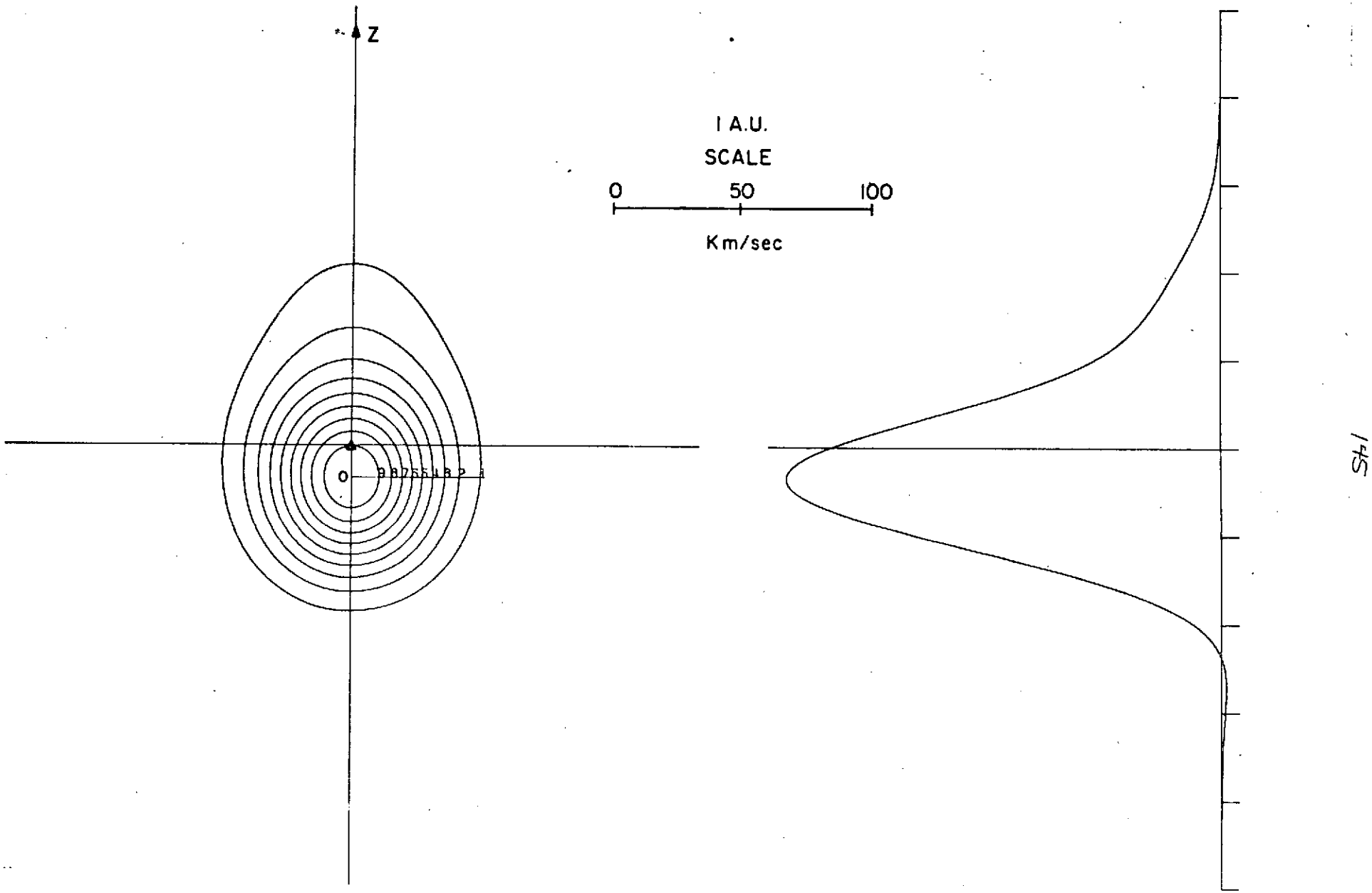

SH1

T ANISOTROPY=1.3 GAMMA PAR=0.62 GAMMA PER=0.08

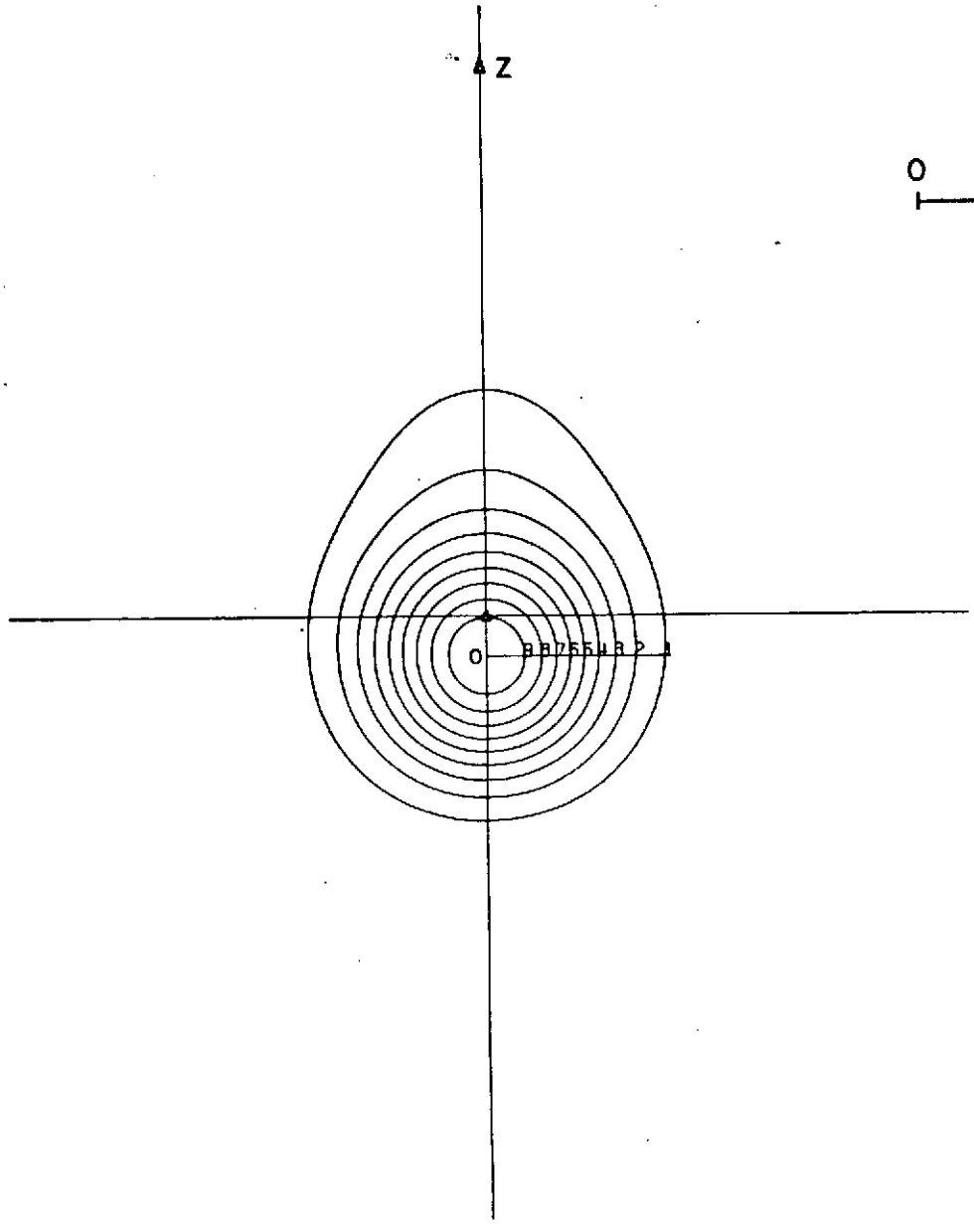

2 A.U.
SCALE
0 25 50
Km/sec

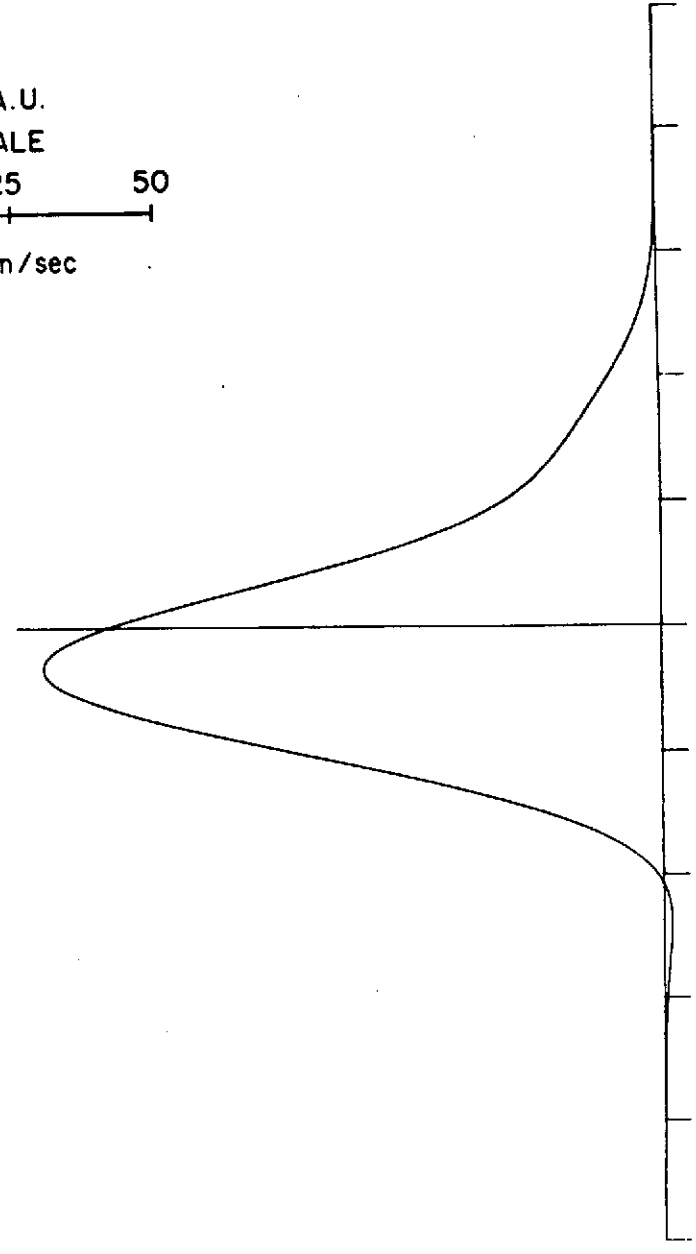

T ANISOTROPY=0.6 GAMMA PAR=0.58 GAMMA PER=0.08

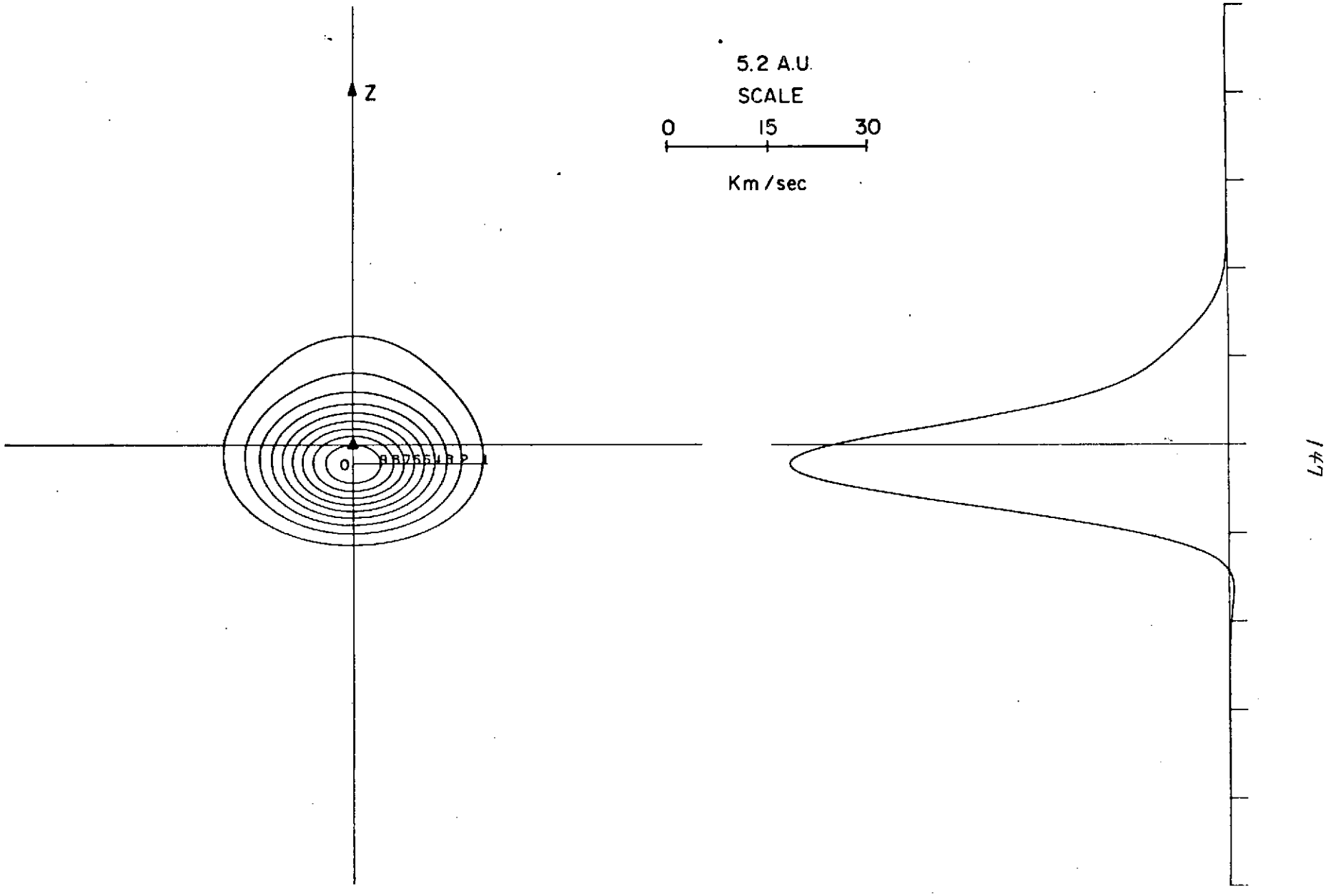

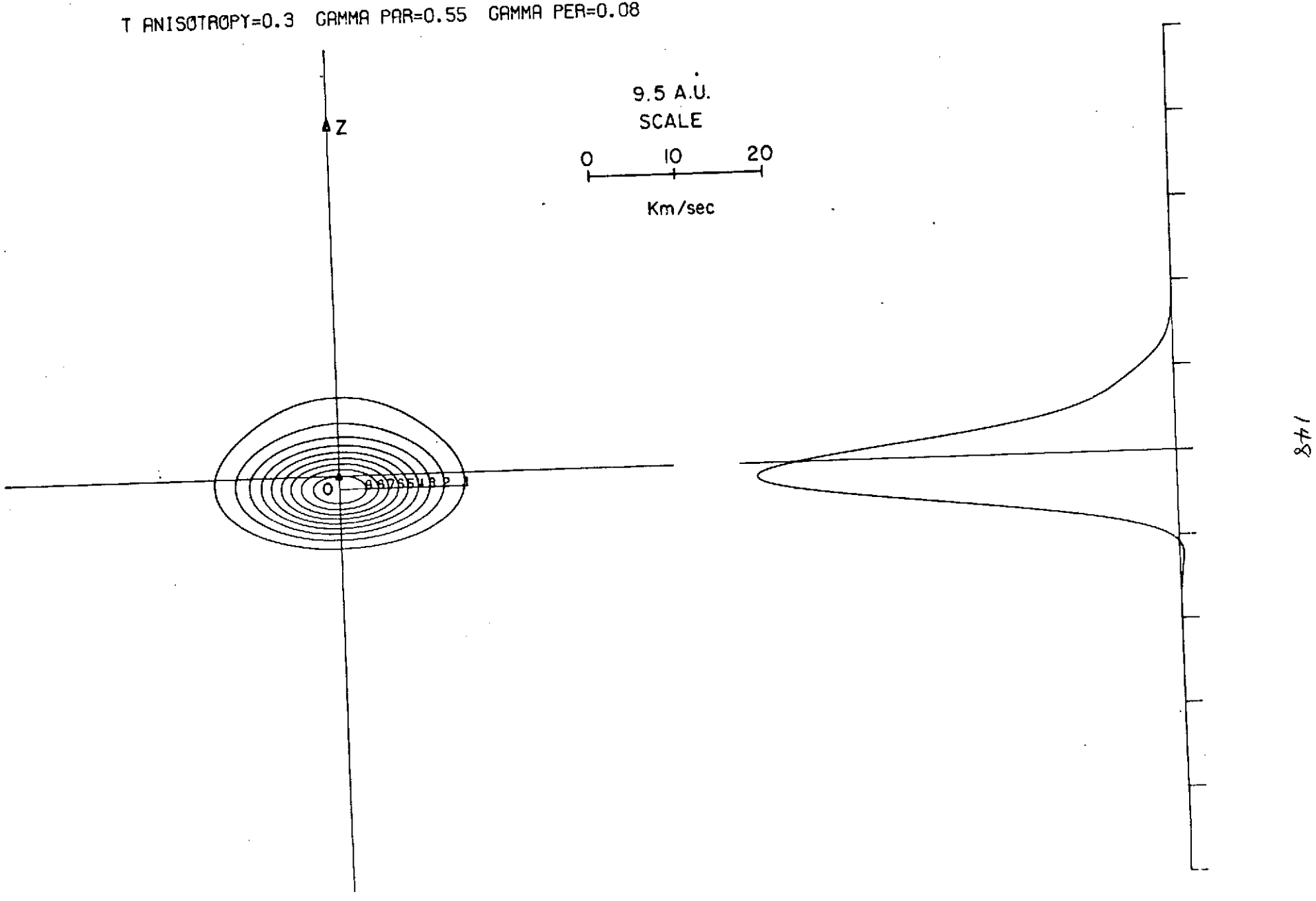
T ANISOTROPY=0.3 GAMMA PAR=0.55 GAMMA PER=0.08
Z
9.5 A.U.
SCALE
0
10
20
Km/sec
O

841

T ANISOTROPY=0.2 GAMMA PAR=0.55 GAMMA PER=0.08

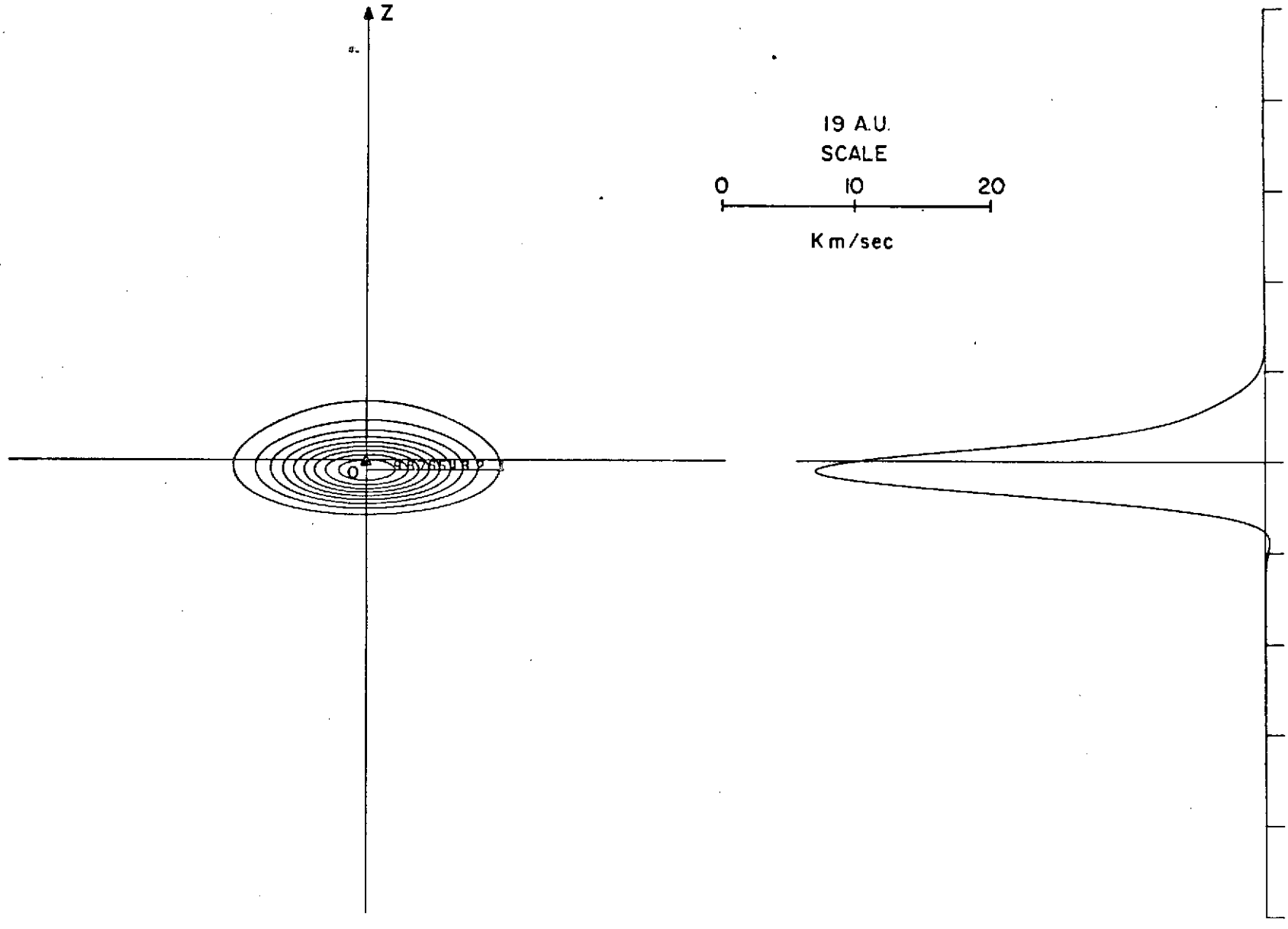

T ANISOTROPY=0.1 GAMMA PAR=0.54 GAMMA PER=0.09

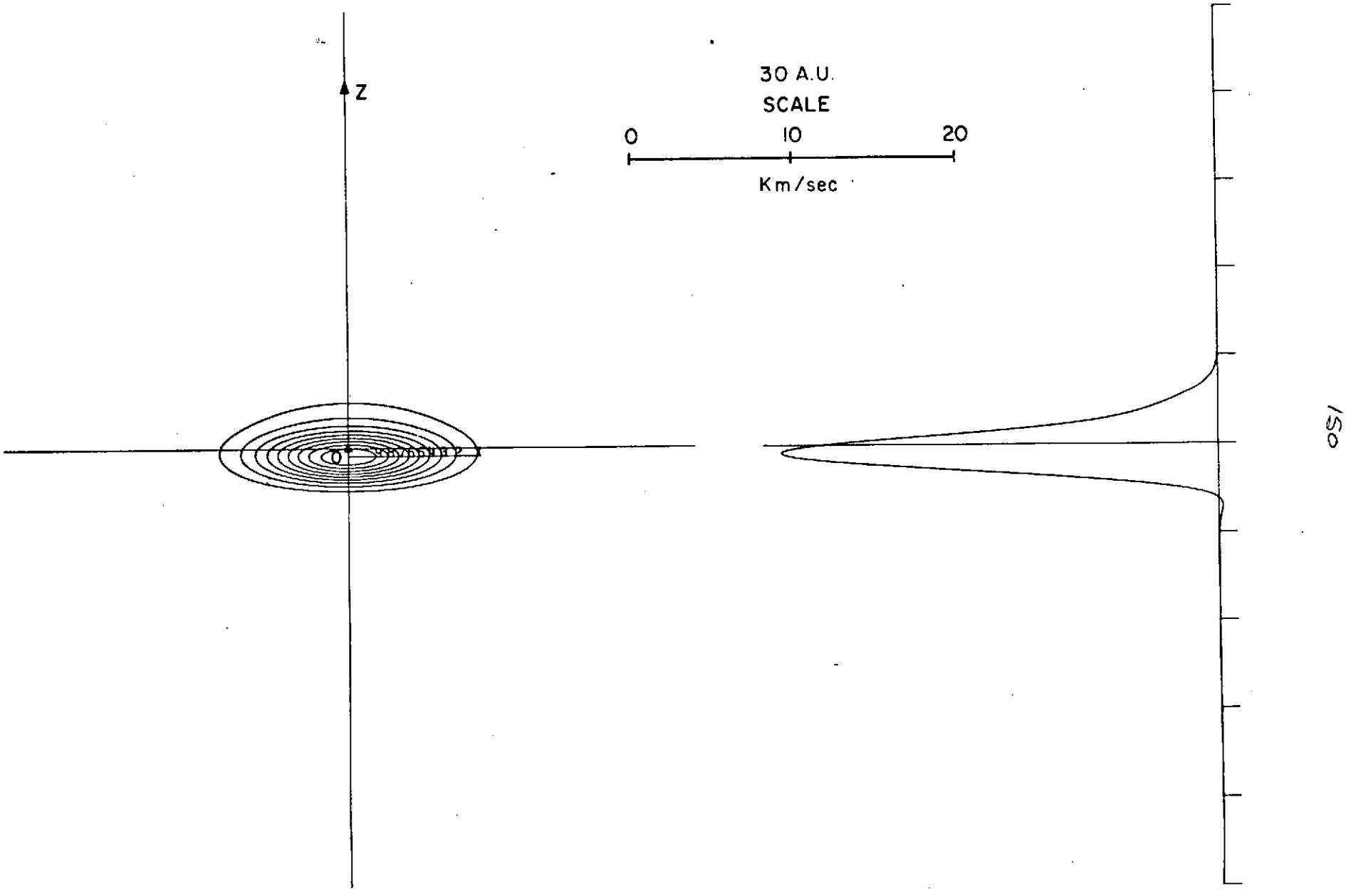

IV. SUMMARY AND CONCLUSIONS

This dissertation has considered the solution of the steady state magnetohydrodynamic equations governing the supersonic expansion of the solar corona into interplanetary space under various assumptions regarding the form in which proton thermal energy is carried away from the sun.

The fluid has been assumed to be inviscid and the flow axially symmetric about the sun's rotation axis.

In Chapter II we have obtained detailed numerical solutions to the one-fluid formulation of the MHD equations under the assumption that thermal energy is carried away by heat conduction from a thin shell heat source located at the base of the corona. The effects of the angular motion of the solar wind are included in the model as well as a complete description of the magnetic field, leading to the existence of three critical points through which the solution must pass in order to extend from the sun's surface to large heliocentric distances. The magnetic field is further assumed to inhibit the flux of thermal energy perpendicular to the field lines, leading to an adiabatic expansion at large r with $T \sim r^{-4/3}$.

The values predicted for the flow quantities at 1 A.U. are in good agreement with quiet-time solar wind observations except for the azimuthal component of the expansion velocity which is approximately a factor of five smaller than indicated by reported observations. This discrepancy may be due in part to the large degree of uncertainty associated with the experimental values and further work in this area seems to be necessary.

A two-fluid formulation of the MHD equations was obtained in Chapter

III in which the protons are assumed to become collisionless and anisotropic beyond an arbitrarily selected radius; the evolution of the proton temperature and heat flux can then be described by the Chew-Goldberger-Low theory and third moment equations of Whang, leading to a closed set of differential equations which admits numerical and asymptotic solutions. These equations were then applied to a solar wind model consisting of two regions: a) An inner region in which the energy exchange rate between protons and electrons is sufficiently high such that their temperatures are essentially equal and isotropic; under these conditions the model is adequately described by the one-fluid formulation of the MHD equations, and b) An outer region in which the protons are assumed to become collisionless and anisotropic beyond a given radius. The electrons are assumed everywhere isotropic and the associated heat flux due to conduction alone. The two-fluid formulation of the MHD equations is utilized in the outer region to obtain numerical and asymptotic solutions for the flow quantities throughout interplanetary space. In addition, the formulation of the CGL-Whang moment equations allows us to obtain microscopic information about the proton distribution function for various heliocentric distances.

The results obtained from the two-region model are in good agreement with experimental observations. In particular, it is shown that the effect of the proton thermal anisotropy upon the angular motion is small and does not significantly increase the predicted values for the azimuthal velocity at 1 A.U.

From the solutions obtained for the models described above, we find

that the amount of magnetic field energy converted into kinetic energy in the solar wind is small and has little effect upon the expansion velocity. The most important effects of the magnetic field are the retarding torque exerted upon the outer layers of the sun's atmosphere and the inhibition of the flow of thermal energy across the field lines, making possible a more complete conversion of this type of energy into kinetic energy in the acceleration region.

Finally, we find that in order to obtain reasonable values for the particle density, magnetic field intensity and energy fluxes at 1 A.U., it is necessary to use a reduced value of the thermal conductivity coefficient.

This value is approximately 1/6 of the classical Spitzer's value and leads to coronal densities which are almost two orders of magnitude lower than observed. These results give support to recent theoretical work indicating that the magnetic field and plasma instabilities play an important role in modifying the plasma transport coefficients.

APPENDIX A

The computer programs developed to obtain solutions to the one-fluid model equations are written in APL/360 language and listed below. The outward integration program is "MAIN" with subprograms "PARAM", "START", "SOLWIND2" and "DER".

The corresponding program for the inward integration process is "IMAIN" with subprograms, "PARAM1", "PARAM", "START", "SOLWIND2" and "DER". The asymptotic solution is obtained by the program "ASOL" with subprograms "PARAM1" and "PARAM".

The density, heat flux, magnetic field intensity and kinetic and magnetic field energy flows in all regions, are computed by the program "DBQ".

```
      ∇MAIN[□]∇
    ∇ MAIN;IC;FG;XM;KM;KL
[1]    'ENTER BETASTAR'
[2]    BSTR←□
[3]    KL←KM←0
[4]    'ENTER ZETA'
[5]    ZETA←□
[6]    'ENTER PHISTR IN DEGREES'
[7]    PHISTR←□×(○2÷360)
[8]    'ENTER GAMMA'
[9]    GAM←□
[10]   'ENTER H'
[11]   H←□
[12]   'ENTER STEP SIZE, MAX. Z   AND  PRINTOUT INTERVA
       L '
[13]   IC←□
[14]   'ENTER DGAM AND NO. OF EXECUTIONS'
[15]   AL←□
[16]   IJ←1
[17]   XM←1
[18] M11:PARAM
[19]   START
[20] M12:SOLWIND2
[21]   FG←(7,(⍴ZF))⍴(ZF×RST÷69600000000),(VF×UST),(WF×
       DEL×UST),(THETAF×TST),DODZF,(PHIF×360÷○
       2),BETAF
[22]   TSOL←ZF[⍴ZF],VF[⍴VF],THETAF[⍴THETAF]
[23]   MAT← 2 1 ⍴FG
[24]   →(MA=2)/0
[25]   →(MA=1)/M13
[26]   KM←1
[27]   →M14
[28] M13:KL←1
[29] M14:→((KL=1)×(KM=1))/M15
[30]   →M16
[31] M15:AL[1]←AL[1]÷2
[32] M16:→(MA=1)/M17
[33]   GAM←GAM-AL[1]
[34]   →M18
[35] M17:GAM←GAM+AL[1]
[36] M18:IJ←IJ+1
[37]   →(IJ=AL[2])/M19
[38]   →M11
[39] M19:'PROGRAM EXECUTED      ';IJ;'   TIMES;WISH TO
       SAVE?'
[40]   →M11
     ∇
```

```
      ∇PARAM[□]∇
    ∇ PARAM;A;B;OME;GMSN;XP;BP
[1]   OME←2.92E¯6
[2]   GMSN←1.33E26
[3]   XI←((÷2)+÷BSTR)+((((÷2)+÷BSTR)*2)-(2×(2○PHISTR)*
      2)÷BSTR)*0.5
[4]   UST←(GMSN×OME÷GAM×ZETA)*÷3
[5]   RST←((GMSN×ZETA*2)÷GAM×OME*2)*÷3
[6]   PSI←3○PHISTR
[7]   DEL←PSI+ZETA
[8]   MU←(1-XI)÷(1-(XI÷((2○PHISTR)*2)))
[9]   SIG←(1+(PSI×1-MU)÷ZETA)*0.5
[10]  A←2+(XI×DEL*2)+(2×DEL×XI×MU×PSI÷1-MU)-GAM×XI
[11]  B←XI×(0.5×1+DEL*2)+(MU×PSI*2)+(5÷2×XI)-H+GAM+DEL
      ×MU×PSI
[12]  ALPH←A÷B
[13]. MASS←(1836×9.1066E¯28)+(0.05×
      6.6442E¯24)
[14]  BC←1.38E¯16
[15]  TST←(MASS×UST*2)÷(2×BC×XI)
[16]  XP←0,(-2×H),(2×MU×ZETA*2)
[17]  VINF←(CUBIC XP)[1]
[18]  'GAMMA:    ';GAM;'  RSTAR:     ';(RST÷
      69600000000);'  BETASTAR:    ';BSTR
[19]  ' PHISTAR:     ';PHISTR×(360÷○2);'  XI:    ';XI
[20]  ' H:    ';H;' USTAR:     ';UST
[21]  'ZETA:     ';ZETA;'      PSI:     ';PSI
[22]  'DELTA:    ';DEL;'      MU:    ';MU
[23]  'SIGMA:     ';SIG
[24]  ' ALPHA:     ';ALPH;'   TSTAR:      ';TST;'       U
      INF:      ';(VINF×UST)
    ∇
```

```
      ∇START[□]∇
    ∇ START;A1;A2;B1;B2;C1;C2;C3;C4;C5;D1;D2;P;E1;Q;F1
      ;F2;R;S;T
[1]   DODZST←2+(XI×DEL*2)+(2×DEL×XI×MU×PSI÷1-MU)-GAM×
      XI
[2]   A1←((3×MU)-1+(1+MU)×SIG*2)÷(1-MU)×(¯1+SIG*
      2)
[3]   A2←-÷(1-MU)
[4]   B1←ZETA+A1×PSI
[5]   B2←PSI×1+A2
[6]   C1←1+MU×PSI*2
[7]   C2←(DEL*2)-DEL×MU×PSI
[8]   C3←(2×MU×PSI)-DEL×MU
[9]   C4←5÷2×XI
[10]  C5←(2×DEL×MU×PSI)+GAM-2×MU×PSI*2
[11]  D1←(ALPH×XI×C1)+(B2×C2×ALPH×XI÷DEL)+A2×(P←(ALPH×
      XI×C3×PSI)+DODZST×2×(1○PHISTR)*2)
[12]  D2←(ALPH×XI×C2×B1÷DEL)+(A1×P)+(((ALPH×XI×C4)-
      2)×DODZST)+(ALPH×XI×C5)-2.5×DODZST*2
[13]  E1←((Q←2×DEL×XI×MU×PSI÷(1-MU)*2)×((1-MU)×(A2+B2÷
      DEL))-MU)+(2×DEL×XI×B2)-D1
[14]  E2←(Q×((1-MU)×(A1+B1÷DEL))-2)+DODZST+(GAM×XI)+(
      2×DEL×XI×B1)-D2
[15]  F1←(2×XI)-(R←(XI×MU×PSI*2)÷(1-MU)*2)×(2×A2-(MU×
      A2)+MU)+1
[16]  F2←-DODZST+2×R×(A1×1-MU)-1
[17]  S←(E1-F2)÷2×F1
[18]  T←((S*2)+E2÷F1)*0.5
[19]  DVDZST1←S+T
[20]  DVDZST2←S-T
[21]  'DVDZST1     ';DVDZST1
[22]  'DVDZST2     ';DVDZST2
[23]  'DODZST      ';DODZST
[24]  VS←1+DVDZST1×0.0001
[25]  THETAS←1+DODZST×0.0001
[26]  ZS←1+0.0001
[27]  XS←÷ZS
[28]  TP←GAM,BSTR,ZETA,H,PHISTR
[29]  TN←MU,XI,DEL,SIG,ALPH,UST,TST,RST
    ∇
```

```
     ∇SOLWIND2[□]∇
   ∇ SOLWIND2;X;Y;K;D;I;J;FV1;L;R1;R2;R3;R4;R5;R6
1]   IV1←XS,VS,THETAS
2]   ZF←VF←WF←THETAF←DODZF←PHIF←BETAF←⍳0
3]   X←IV1[1],IC[1],(÷IC[2])
4]   Y←IV1[3],IV1[2]
5]   I←ZS
6]   R1←ALPH×XI×(2○PHISTR)*2
7]   R2←XI×ZETA*2
8]   R3←ZETA*2
9]   R4←GAM×XI
10] CDP:K←(4,⍴,Y)⍴L←X[J←1] DER M←Y
11]  →((L[1]=0)×(L[2]=0))/CJP
12]  →(L[1]<0)/CHP
13] CEP:→(J<3+⍴⍴⍴K[J;]←JL←(X[1]+D) DER M←Y+K[
     ¯1+J←J+1;]×D←X[2]÷ 2 2 1[J])/CEP
14]  FV1←(X[1]←+/X[⍳2]),Y←Y+(X[2]÷6)×+/[1] K[
     1 2 2 3 3 4 ;]
15] CKP:→((÷FV1[1])≥I)/CFP
16] COP:→((X[2]×X[3]-X[1])>0)/CDP
17]  MA←2
18]  →CGP
19] CFP:ZF←ZF,(÷FV1[1])
20]  I←ZF[⍴,ZF]×1+IC[3]
21]  VF←VF,FV1[3]
22]  THETAF←THETAF,FV1[2]
23]  DODZF←DODZF,(-L[1]×FV1[1]*2)
24]  →((⍴DODZF)=1)/MHA
25]  →((|DODZF[⍴DODZF])>(|DODZF[(⍴DODZF)-1]))/CJP
26] MHA:→COP
27] CHP:'DODZ POS.'
28]  MA←1
29]  →CGP
30] CJP:'TEMP.<0 OR DODZ INCREASING'
31]  MA←0
32]  →CGP
33] CGP:PHIF←(¯3○((ZETA×(SIG*2)-ZF*2)÷(VF×ZF)-MU÷ZF))
     +○1
34]  WF←((VF×3○PHIF)+ZETA×ZF)÷DEL
35]  BETAF←((BSTR×(1+PSI*2)×ZF*2)÷VF×(1+(3○PHIF)*
     2))×THETAF
   ∇
```

```
      ∇DER[□]∇
    ∇ Z←X DER M;M1;M2;Y1;Y2;T;P;A;B;C
[1]   →(M[1]<0)/D1
[2]   P←-(ZETA÷M[2]×X)×(A←1-X×X×SIG*2)×B←÷1-MU×X×X÷M[
      2]
[3]   M1←-(R1×1+P×P)÷M[1]*2.5
[4]   M2←(0.5×(M[2]-VINF)×M[2]+VINF)+(
      2.5×M[1]÷XI)-(GAM×X)-C←0.5×R3×X×X×B×B×((SIG*
      2)-MU÷M[2])*2
[5]   M2←M2+MU×R3×(A×B÷M[2])-÷VINF
[6]   Y1←(2×C×XI)+((2×MU×R2÷M[2])×(A×A×B*3)-A×B×B)+(X×
      M1×M2)+(2×M[1])-X×R4
[7]   Y2←(XI×M[2]×M[2])-M[1]+R2×MU×A×A×(B*3)÷M[
      2]
[8]   Z←(M1×M2),(-Y1×M[2]÷X×Y2)
[9]   →0
[10] D1:Z← 0 0
    ∇


      ∇DBQ[□]∇
    ∇ DBQ
[1]   'ENTER K'
[2]   K←□
[3]   NST←(ALPH×K×(TST*2.5)×(2○PHISTR)*2)÷2×UST×RST×BC
[4]   NF←NST÷VF×ZF*2
[5]   BF←((MU×○4×MASS×NST×UST*2)*
      0.5)÷(ZF*2)×(2○PHIF)
[6]   QF←-K×((THETAF×TST)*2.5)×DODZF×TST÷RST
[7]   PRF←(((ZF×RST×BF)*2)×(UST×VF×(1○PHIF)*2)-DEL×UST
      ×WF×(1○PHIF)×(2○PHIF))÷○4
[8]   KEF←(MASS×NF×VF×UST×(ZF×RST)*2)×
      0.5×((VF×UST)+WF×DEL×UST)*2
[9]   F←H×NST×UST×(RST*2)×MASS×UST*2
[10]  'TOTAL ENERGY FLUX';F
[11]  NBQO← 2 1 ⍉(6,(⍴ZF))⍴(ZF×RST÷
      69600000000),NF,BF,QF,PRF,KEF
    ∇
```

```
      ∇IMAIN[□]∇
    ∇ IMAIN;FG
[1]   'ENTER STEP SIZE, MAX. Z AND PRINTOUT INTERVAL'
[2]   IC←□
[3]   PARAM1
[4]   PARAM
[5]   START
[6]   SOLWIND2
[7]   FG←(7,(ρZF))ρ(ZF×RST÷69600000000),(VF×UST),(WF×
      DEL×UST),(THETAF×TST),DODZF,(PHIF×360÷○
      2),BETAF
[8]   MAT← 2 1 ⍉FG
[9]   MAT
[10]  →(MA=2)/0
    ∇

      ∇PARAM1[□]∇
    ∇ PARAM1
[1]   GAM←TP[1]
[2]   BSTR←TP[2]
[3]   ZETA←TP[3]
[4]   H←TP[4]
[5]   PHISTR←TP[5]
    ∇

      ∇PARAM[□]∇
    ∇ PARAM;A;B;OME;GMSN;XP;BP
[1]   OME←2.92E¯6
[2]   GMSN←1.33E26
[3]   XI←((÷2)+÷BSTR)+((((÷2)+÷BSTR)*2)-(2×(2○PHISTR)*
      2)÷BSTR)*0.5
[4]   UST←(GMSN×OME÷GAM×ZETA)*÷3
[5]   RST←((GMSN×ZETA*2)÷GAM×OME*2)*÷3
[6]   PSI←3○PHISTR
[7]   DEL←PSI+ZETA
[8]   MU←(1-XI)÷(1-(XI÷((2○PHISTR)*2)))
[9]   SIG←(1+(PSI×1-MU)÷ZETA)*0.5
[10]  A←2+(XI×DEL×2)+(2×DEL×XI×MU×PSI÷1-MU)-GAM×XI
[11]  B←XI×(0.5×1+DEL*2)+(MU×PSI*2)+(5÷2×XI)-H+GAM+DEL
      ×MU×PSI
[12]  ALPH←A÷B
[13]  MASS←(1836×9.1066E¯28)+(0.05×
      6.6442E¯24)
[14]  BC←1.38E¯16
[15]  TST←(MASS×UST*2)÷(2×BC×XI)
[16]  XP←0,(-2×H),(2×MU×ZETA*2)
[17]  VINF←(CUBIC XP)[1]
    ∇
```

```
      ∇START[□]∇
    ∇ START;A1;A2;B1;B2;C1;C2;C3;C4;C5;D1;D2;P;E1;Q;F1
      ;F2;R;S;T
[1]   DODZST←2+(XI×DEL*2)+(2×DEL×XI×MU×PSI÷1-MU)-GAM×
      XI
[2]   A1←((3×MU)-1+(1+MU)×SIG*2)÷(1-MU)×(¯1+SIG*
      2)
[3]   A2←-÷(1-MU)
[4]   B1←ZETA+A1×PSI
[5]   B2←PSI×1+A2
[6]   C1←1+MU×PSI*2
[7]   C2←(DEL*2)-DEL×MU×PSI
[8]   C3←(2×MU×PSI)-DEL×MU
[9]   C4←5÷2×XI
[10]  C5←(2×DEL×MU×PSI)+GAM-2×MU×PSI*2
[11]  D1←(ALPH×XI×C1)+(B2×C2×ALPH×XI÷DEL)+A2×(P←(ALPH×
      XI×C3×PSI)+DODZST×2×(10PHISTR)*2)
[12]  D2←(ALPH×XI×C2×B1÷DEL)+(A1×P)+(((ALPH×XI×C4)-
      2)×DODZST)+(ALPH×XI×C5)-2.5×DODZST*2
[13]  E1←((Q←2×DEL×XI×MU×PSI÷(1-MU)*2)×((1-MU)×(A2+B2÷
      DEL))-MU)+(2×DEL×XI×B2)-D1
[14]  E2←(Q×((1-MU)×(A1+B1÷DEL))-2)+DODZST+(GAM×XI)+(
      2×DEL×XI×B1)-D2
[15]  F1←(2×XI)-(R←(XI×MU×PSI*2)÷(1-MU)*2)×(2×A2-(MU×
      A2)+MU)÷1
[16]  F2←-DODZST+2×R×(A1×1-MU)-1
[17]  S←(E1-F2)÷2×F1
[18]  T←((S*2)+E2÷F1)*0.5
[19]  DVDZST1←S+T
[20]  DVDZST2←S-T
[21]  VS←1-DVDZST1×0.0001
[22]  THETAS←1-DODZST×0.0001
[23]  ZS←1-0.0001
[24]  XS←÷ZS
      ∇
```

```
      ∇SOLWIND2[□]∇
    ∇ SOLWIND2;X;Y;K;D;I;J;FV1;L;R1;R2;R3;R4;R5;R6
[1]   IV1←XS,VS,THETAS
[2]   ZF←VF←WF←THETAF←DODZF←PHIF←BETAF←⍳0
[3]   X←IV1[1],IC[1],(÷IC[2])
[4]   Y←IV1[3],IV1[2]
[5]   I←ZS
[6]   R1←ALPH×XI×(2○PHISTR)*2
[7]   R2←XI×ZETA*2
[8]   R3←ZETA*2
[9]   R4←GAM×XI
[10] CDP:K←(4,⍴,Y)⍴L←X[J←1] DER M←Y
[11] CEP:→(J<3+⍴⍴⍴K[J;]←JL←(X[1]+D) DER M←Y+K[
      ¯1+J←J+1;]×D←X[2]÷ 2 2 1[J])/CEP
[12]  →((L[1]=1)×(L[2]=0))/CHP
[13]  →((L[1]=0)×(L[2]=1))/CJP
[14]  FV1←(X[1]←+/X[⍳2]),Y←Y+(X[2]÷6)×+/[1] K[
      1 2 2 3 3 4 ;]
[15]  →((÷FV1[1])≤I)/CFP
[16] COP:→((X[2]×X[3]-X[1])>0)/CDP
[17]  MA←2
[18]  →CGP
[19] CFP:ZF←ZF,(÷FV1[1])
[20]  I←ZF[⍴,ZF]-IC[3]×ZF[⍴,ZF]
[21]  VF←VF,FV1[3]
[22]  THETAF←THETAF,FV1[2]
[23]  DODZF←DODZF,(-L[1]×FV1[1]*2)
[24] MHA:→COP
[25] CHP:'DVDZ<0;NUM.<0, DENOM.>0'
[26]  →CGP
[27] CJP:'DVDZ<0;NUM.>0, DENOM.<0'
[28] CGP:PHIF←(¯3○((ZETA×(SIG*2)-ZF*2)÷(VF×ZF)-MU÷ZF))
      +○1
[29]  WF←((VF×3○PHIF)+ZETA×ZF)÷DEL
[30]  BETAF←((BSTR×(1+PSI*2)×ZF*2)÷VF×(1+(3○PHIF)*
      2))×THETAF
    ∇
```

```
      ∇DER[□]∇
    ∇ Z←X DER M;M1;M2;Y1;Y2;T;P;A;B;C;Q
[1]   Q←1×U×(X>2)
[2]   →(M[1]<0)/D1
[3]   P←-(ZETA÷M[2]×X)×(A←1-X×X×SIG*2)×B←÷1-MU×X×X÷M[
      2]
[4]   M1←-(R1×1+P×P)÷M[1]*2.5
[5]   M2←(0.5×(M[2]-VINF)×M[2]+VINF)+(
      2.5×M[1]÷XI)-(GAM×X)-C←0.5×R3×X×X×B×B×((SIG*
      2)-MU÷M[2])*2
[6]   M2←M2+MU×R3×(A×B÷M[2])-÷VINF
[7]   Y1←(2×C×XI)+((2×MU×R2÷M[2])×(A×A×B*3)-A×B×B)+(X×
      M1×M2)+(2×M[1])-X×R4
[8]   Y2←(XI×M[2]×M[2])-M[1]+R2×MU×A×A×(B*3)÷M[
      2]
[9]   Z←(M1×M2),(-Y1×M[2]÷X×Y2)
[10]  →((Y1≤0)×(Y2≤0)×(Q=1))/D2
[11] D3:→((Y1÷Y2)>0)/0
[12]  Z←(Y1<0),(Y2<0)
[13]  →0
[14] D1:Z← 0 0
[15] D2:'R1    ';(÷X)×RST÷69600000000
[16]  U←0
[17]  →D3
    ∇


      ∇DBQ[□]∇
    ∇ DBQ
[1]   'ENTER K'
[2]   K←□
[3]   NST←(ALPH×K×(TST*2.5)×(2○PHISTR)*2)÷2×UST×RST×BC
[4]   NF←NST÷VF×ZF*2
[5]   BF←((MU×○4×MASS×NST×UST*2)*
      0.5)÷(ZF*2)×(2○PHIF)
[6]   QF←-K×((THETAF×TST)*2.5)×DODZF×TST÷RST
[7]   PRF←(((ZF×RST×BF)*2)×(UST×VF×(1○PHIF)*2)-DEL×UST
      ×WF×(1○PHIF)×(2○PHIF))÷○4
[8]   KEF←(MASS×NF×VF×UST×(ZF×RST)*2)×
      0.5×((VF×UST)+WF×DEL×UST)*2
[9]   F←H×NST×UST×(RST*2)×MASS×UST*2
[10]  'TOTAL ENERGY FLUX';F
[11]  NBQI← 2 1 ⍉(6,(⍴ZF))⍴(ZF×RST÷
      69600000000),NF,BF,QF,PRF,KEF
    ∇
```

```
      ∇ASOL[□]∇
    ∇ ASOL;P;S;A
[1]   PARAM1
[2]   PARAM
[3]   P←(1.5×VINF*2)-H
[4]   S←(1.5×VINF*2)+H
[5]   C10←GAM÷P
[6]   A←(TSOL[3]-(XI×C10×(S×C10)-GAM)×TSOL[1]*
      ¯2)÷(TSOL[1]*¯4÷3)+((TSOL[1]*¯7÷3)×(29×GAM)-
      35×S×C10)÷9×P
[7]   C11←-5×A÷2×XI×P
[8]   C12←0
[9]   C13←-(5×C10×(S×C10)-GAM)÷2×P
[10]  C14←((15×GAM×XI×C11)-35×C10×(XI×S×C11)+A)÷
      9×XI×P
[11]  C21←0
[12]  C22←(XI×C10×(S×C10)-GAM)÷A
[13]  C23←((14×C10×(XI×S×C11)+A)-6×GAM×XI×C11)÷
      9×A
[14]  VVEC←1,C10,C11,C12,C13,C14,0,0,0
[15]  TVEC←0,0,1,C21,C22,C23,0,0,0
[16]  DTZVEC←0,0,0,0,0,4,(5×C21),(6×C22),(7×C23)
[17]  'ENTER MAX. Z  AND PRINTOUT INTERVAL'
[18]  IV←□
[19]  ZF←VF←WF←THETAF←DODZF←PHIF←BETAF←ι0
[20]  ET←TSOL[1]*-÷3
[21] COL:EPN←1,ET*2+ι8
[22]  V←+/VINF×VVEC×EPN
[23]  T←+/A×TVEC×EPN
[24]  DT←+/(-A÷3)×DTZVEC×EPN
[25]  ZF←ZF,(ET*¯3)
[26]  VF←VF,V
[27]  DODZF←DODZF,DT
[28]  THETAF←THETAF,T
[29]  ET←(ZF[ρ,ZF]×1+IV[2])*-÷3
[30]  →(ZF[ρ,ZF]≤IV[1])/COL
[31]  PHIF←(¯3○((ZETA×(SIG*2)-ZF*2)÷(VF×ZF)-MU÷ZF))+○1
[32]  WF←((VF×3○PHIF)+ZETA×ZF)÷DEL
[33]  BETAF←((BSTR×(1+PSI*2)×ZF*2)÷VF×(1+(3○PHIF)*
      2))×THETAF
[34]  MAT← 2 1 ⍉(7,(ρZF))ρ(ZF×RST÷
      69600000000),(VF×UST),(WF×DEL×UST),(THETAF×TST),
      DODZF,(PHIF×360÷○2),BETAF
    ∇
```

```
      ∇PARAM1[□]∇
    ∇ PARAM1
[1]   GAM←TP[1]
[2]   BSTR←TP[2]
[3]   ZETA←TP[3]
[4]   H←TP[4]
[5]   PHISTR←TP[5]
    ∇

      ∇PARAM[□]∇
    ∇ PARAM;A;B;OME;GMSN;XP;BP
[1]   OME←2.92E¯6
[2]   GMSN←1.33E26
[3]   XI←((÷2)+÷BSTR)+((((÷2)+÷BSTR)*2)-(2×(2○PHISTR)*
      2)÷BSTR)*0.5
[4]   UST←(GMSN×OME÷GAM×ZETA)*÷3
[5]   RST←((GMSN×ZETA*2)÷GAM×OME*2)*÷3
[6]   PSI←3○PHISTR
[7]   DEL←PSI+ZETA
[8]   MU←(1-XI)÷(1-(XI÷((2○PHISTR)*2)))
[9]   SIG←(1+(PSI×1-MU)÷ZETA)*0.5
[10]  A←2+(XI×DEL*2)+(2×DEL×XI×MU×PSI÷1-MU)-GAM×XI
[11]  B←XI×(0.5×1+DEL*2)+(MU×PSI*2)+(5÷2×XI)-H+GAM+DEL
      ×MU×PSI
[12]  ALPH←A÷B
[13]  MASS←(1836×9.1066E¯28)+(0.05×
      6.6442E¯24)
[14]  BC←1.38E¯16
[15]  TST←(MASS×UST*2)÷(2×BC×XI)
[16]  XP←0,(-2×H),(2×MU×ZETA*2)
[17]  VINF←(CUBIC XP)[1]
    ∇

      ∇DBQ[□]∇
    ∇ DBQ
[1]   'ENTER K'
[2]   K←□
[3]   NST←(ALPH×K×(TST*2.5)×(2○PHISTR)*2)÷2×UST×RST×BC
[4]   NF←NST÷VF×ZF*2
[5]   BF←((MU×○4×MASS×NST×UST*2)*
      0.5)÷(ZF*2)×(2○PHIF)
[6]   QF←-K×((THETAF×TST)*2.5)×DODZF×TST÷RST
[7]   PRF←(((ZF×RST×BF)*2)×(UST×VF×(1○PHIF)*2)-DEL×UST
      ×WF×(1○PHIF)×(2○PHIF))÷○4
[8]   KEF←(MASS×NF×VF×UST×(ZF×RST)*2)×
      0.5×((VF×UST)+WF×DEL×UST)*2
[9]   F←H×NST×UST×(RST*2)×MASS×UST*2
[10]  'TOTAL ENERGY FLUX';F
[11]  NBQA← 2 1 ⍴(6,(⍴ZF))⍴(ZF×RST÷
      69600000000),NF,BF,QF,PRF,KEF
    ∇
```

APPENDIX B

The divergence of the anisotropic proton pressure tensor

$$\underline{\underline{P}}_p = p_\perp \underline{\underline{I}} + \frac{\underline{B}\underline{B}}{B^2}(p_\parallel - p_\perp) \tag{B1}$$

may be obtained as follows. In index notation we may write (B1) as

$$\frac{\partial P_{ij}}{\partial x_j} = \frac{\partial}{\partial x_j}(p_\perp \delta_{ij}) + \frac{\partial}{\partial x_j}\left[\frac{(p_\parallel - p_\perp)}{B^2} B_i B_j\right] \tag{B2}$$

where δ_{ij} is the Kronecker's delta.

It follows that

$$\frac{\partial P_{ij}}{\partial x_j} = \frac{\partial p_\perp}{\partial x_j} + B_i B_j \frac{\partial}{\partial x_j}\left(\frac{p_\parallel - p_\perp}{B^2}\right) + \frac{(p_\parallel - p_\perp)}{B^2}\left[B_i \frac{\partial B_j}{\partial x_j} + \frac{\partial B_i}{\partial x_j} B_j\right] \tag{B3}$$

but from Maxwell's equations

$$\frac{\partial B_j}{\partial x_j} = 0 \tag{B4}$$

hence we obtain

$$\nabla \cdot \underline{\underline{P}}_p = \nabla p_\perp + \underline{B}\left[\underline{B} \cdot \nabla\left(\frac{p_\parallel - p_\perp}{B^2}\right)\right] + \frac{(p_\parallel - p_\perp)}{B^2}\left[(\underline{B} \cdot \nabla)\,\underline{B}\right] \tag{B5}$$

which is the desired result.

APPENDIX C

The numerical integration process is optimized by expressing the system of governing equations in reciprocal space. Thus we introduce the new independent variable X, where

$$X = Z^{-1} \tag{C1}$$

and it follows that for any function $\varphi(z)$ we have

$$\frac{d\varphi(z)}{dz} = -X^2 \frac{d\varphi}{dx} \tag{C2}$$

The system of equations (III.2.25) then becomes

$$b_{i1}\frac{dV}{dx} + b_{i2}\frac{d}{dx}(Wx) + b_{i3}\frac{d\theta_{11}}{dx} + b_{i4}\frac{d\theta_{\perp}}{dx}$$

$$+ b_{i6}\frac{dQ_{11}}{\partial x} + b_{i6}\frac{dQ_{\perp}}{dx} + b_{i7}\frac{d\theta_e}{dx} = b_{i8} \tag{C3}$$

where the coefficients b_{ij}, (j=1,8) are given by the following expressions:

$$b_{11} = \xi V^2 - \frac{1}{2}\left[\theta_{\perp}\sin^2\phi(1+2\cos^2\phi) + \theta_{11}\cos^2\phi(1-2\sin^2\phi) + \theta_e\right] -$$

$$\xi\mu V X^2 + an^2\phi \tag{C4}$$

$$b_{12} = -(\delta/x)\left[\frac{1}{2}(\theta_{11}-\theta_{\perp})\sin 2\phi\cos^2\phi - \xi\mu V X^2 + an\phi\right] \tag{C5}$$

$$b_{13} = V\cos^2\phi/2 \quad ; \quad b_{14} = V\sin^2\phi/2 \tag{C6}$$

$$b_{15} = b_{16} = 0 \quad ; \quad b_{17} = V/2 \tag{C7}$$

$$b_{18} = -\frac{V}{X}\left[\theta_e + \theta_\perp + \frac{1}{2}(\theta_{11}-\theta_\perp)\sin^2\phi\,(1+2\cos^2\phi) - \gamma\xi X + \right.$$

$$\left. \xi\delta^2 W^2 \right] \qquad \text{(C8)}$$

$$b_{21} = \frac{1}{2}(\theta_{11}-\theta_\perp)\sin 2\phi\cos^2\phi - \xi\mu V X^2 \tan\phi \qquad \text{(C9)}$$

$$b_{22} = -\frac{\delta}{X}\left[\xi V^2 + \frac{1}{2}(\theta_{11}-\theta_\perp)\cos 2\phi\cos^2\phi - \xi\mu V X^2\right] \qquad \text{(C10)}$$

$$b_{23} = -\frac{V}{2}\cos\phi\sin\phi \quad ; \quad b_{24} = -b_{23} \qquad \text{(C11)}$$

$$b_{25} = b_{26} = b_{27} = 0 \qquad \text{(C12)}$$

$$b_{28} = -\frac{V}{2X}(\theta_{11}-\theta_\perp)\sin 2\phi\cos^2\phi - \frac{2\delta}{X}\xi W V^2 \qquad \text{(C13)}$$

$$b_{31} = \frac{2\cos\phi}{V}\left[\theta_{11}\cos\phi\left(1-3\theta_\perp\sin^2\phi/4\xi V^2\right) - 4Q_{11}\cos^2\phi/X^2\right] \qquad \text{(C14)}$$

$$b_{32} = \frac{\delta}{VX}\cos\phi\sin\phi\left[\theta_{11}\left(1+6\theta_\perp\cos^2\phi/4\xi V^2\right) - 8Q_{11}\cos\phi/X^2\right] \qquad \text{(C15)}$$

$$b_{33} = 1 - 6\theta_{11}\cos^2\phi/4\xi V^2 \qquad \text{(C16)}$$

$$b_{34} = b_{35} = b_{36} = b_{37} = 0 \qquad \text{(C17)}$$

$$b_{38} = -\frac{2\theta_{11}}{X}\left[\frac{3\theta_\perp\cos^2\phi(1+\cos^2\phi)}{4\xi V^2} - \sin^2\phi\right] - \frac{8\cos\phi\sin^2\phi\,Q_{11}}{X^3} \qquad \text{(C18)}$$

$$b_{41} = (Q_\perp \cos\phi/\sqrt{X^2})(1+\cos^2\phi)+(Q_\perp \sin^2\phi/\sqrt{})\left[(\theta_\perp \cos^2\phi/2\xi V^2)-1\right] \quad \text{(C19)}$$

$$b_{42} = \frac{\delta}{VX}\cos\phi\sin\phi\left[\frac{Q_\perp\cos\phi}{X^2}+\theta_\perp(1-\theta_\perp\cos^2\phi/2\xi V^2)\right] \quad \text{(C20)}$$

$$b_{43} = 0 \quad ; \; b_{44} = (\theta_{11}\cos^2\phi/2\xi V^2)-1 \quad \text{(C21)}$$

$$b_{45} = b_{46} = b_{47} = 0 \quad \text{(C22)}$$

$$b_{48} = -(Q_\perp\cos\phi/X^3)(\cos^2\phi-3)-(\theta_\perp/X)(1+\cos^2\phi)(1-\theta_\perp\cos^2\phi/2\xi V^2) \quad \text{(C23)}$$

$$b_{51} = \frac{2\cos\phi}{V}(\theta_{11}\cos\phi+Q_{11}\sin^2\phi/X^2) \quad \text{(C24)}$$

$$b_{52} = \frac{\delta}{VX}\cos\phi\sin\phi\,(\theta_{11}-2Q_{11}\cos\phi/X^2) \quad \text{(C25)}$$

$$b_{53} = 1 \quad ; \; b_{54} = 0 \quad ; \; b_{55} = \frac{2\cos\phi}{X^2} \quad \text{(C26)}$$

$$b_{56} = b_{57} = 0 \quad \text{(C27)}$$

$$b_{58} = \frac{2}{X}\left[\theta_{11}\sin^2\phi+Q_{11}\cos\phi(1+\cos^2\phi)/X^2\right] \quad \text{(C28)}$$

$$b_{61} = \frac{\sin^2\phi}{V}(\theta_\perp+Q_\perp\cos\phi/X^2) \quad \text{(C29)}$$

$$b_{62} = -\frac{\delta}{VX}\cos\phi\sin\phi\,(\theta_\perp+Q_\perp\cos\phi/X^2) \quad \text{(C30)}$$

$$b_{63} = 0 \; ; \quad b_{64} = 1 \quad ; \; b_{65} = 0 \tag{C31}$$

$$b_{66} = \frac{\cos\phi}{X^2} \quad ; \; b_{67} = 0 \tag{C32}$$

$$b_{68} = \frac{1}{X}(1+\cos^2\phi)(\theta_\perp + Q_\perp \cos\phi/X^2) \tag{C33}$$

$$b_{71} = b_{72} = b_{73} = b_{74} = b_{75} = b_{76} = 0 \tag{C34}$$

$$b_{77} = -\theta_e^{5/2}\cos^2\phi \tag{C35}$$

$$b_{78} = \alpha_e \cos^2\phi_3 \left[\frac{\xi}{2}(v^2+\delta^2 w^2) + \frac{1}{4}(5\theta_e + 4\theta_\perp + \theta_{11}) + \right.$$

$$\frac{1}{2}\cos^2\phi(\theta_{11}-\theta_\perp) + \frac{\delta w}{2v}\cos\phi\sin\phi(\theta_{11}-\theta_\perp) - \zeta\xi\mu\tan\phi\, X -$$

$$\left. \gamma\xi X - 4\xi + (Q_{11}+Q_\perp)\cos\phi/2X^2\right] \tag{C36}$$

and

$$\tan\phi = \frac{1}{vX}(\delta w X - \zeta) \tag{C37}$$

APPENDIX D

The computer programs developed to obtain solutions to the two-fluid, two-region model are listed below. In the inner region the programs listed in Appendix A are used to compute the solutions up to the transition point.

The outward two-fluid integration program is "MAIN" with subprograms "PARAM", "PARAM1", "START", "SOLWIND2", "DER", "SOLWIND3" and "DERA". The asymptotic solutions are obtained with the program "ASOLAN" and subprograms "PARAM1", "PARAM" and "COEFF".

The heat fluxes, density, magnetic field intensity and energy flows are computed with the "NQTF" program. The program "RATIOS" calculates the proton temperature anisotropy and proton-electron temperature ratio. "DFP" computes the parameter values that determine the proton velocity distribution function.

The constant contour curves of the distribution function may be obtained with the program "FUN" and subprograms "F", "G", "ZERO" and "ZEROP".

```
      ∇MAIN[□]∇
    ∇ MAIN;IC;FG;XM;KM;KL
[1]   'ENTER BETASTAR'
[2]   BSTR←□
[3]   KL←KM←0
[4]   'ENTER ZETA'
[5]   ZETA←□
[6]   'ENTER PHISTR IN DEGREES'
[7]   PHISTR←□×(○2÷360)
[8]   'ENTER GAMMA'
[9]   GAM←□
[10]  'ENTER RATIO OF GAMPAR TO GAMPER'
[11]  G←□
[12]  'ENTER H'
[13]  H←□
[14]  'ENTER STEP SIZE, TRANSITION  Z, PRINTOUT INTERV
      AL AND MAX.Z'
[15]  IC←□
[16]  'ENTER DGAM AND NO. OF EXECUTIONS'
[17]  AL←□
[18]  IJ←1
[19]  XM←1
[20] M11:PARAM
[21]  START
[22] M12:SOLWIND2
[23]  FG←(7,(⍴ZF))⍴(ZF×RST÷69600000000),(VF×UST),(WF×
      DEL×UST),(THETAF×TST),DODZF,(PHIF×360÷○
      2),BETAF
[24]  TSOL←ZF[⍴,ZF],VF[⍴,VF],THETAF[⍴,THETAF],WF[⍴,WF]
      ,PHIF[⍴,PHIF],DODZF[⍴,DODZF]
[25]  MAT← 2 1 ⍉FG
[26]  →(MA=2)/M20
[27] M21:→(MA=1)/M13
[28]  KM←1
[29]  →M14
[30] M13:KL←1
[31] M14:→((KL=1)×(KM=1))/M15
[32]  →M16
[33] M15:AL[1]←AL[1]÷2
[34] M16:→(MA=1)/M17
[35]  GAM←GAM-AL[1]
[36]  →M18
[37] M17:GAM←GAM+AL[1]
[38] M18:IJ←IJ+1
[39]  →(IJ=AL[2])/M19
[40]  →M11
[
```

```
[41] M19:'PROGRAM EXECUTED      ';IJ;'   TIMES;WISH TO
     SAVE?'
[42]  →M11
[43] M20:SOLWIND3
[44]  FGA←(11,ρZF)ρ(ZF×RST÷69600000000),(VF×UST),(WX×
     DEL×UST×ZF),(TPL×TST),(TPR×TST),QPL,QPR,(TE×TST)
     ,DTEDZ,(PHIF×360÷○2),BETAF
[45]  TSOLA←ZF[ρZF],VF[ρVF],TPL[ρTPL],TPR[ρTPR],QPL[ρ
     QPL],QPR[ρQPR],TE[ρTE],PHIF[ρPHIF],WX[ρWX]
[46]  →(MA=2)/0
[47]  →M21
      ∇

      ∇PARAM[□]∇
    ∇ PARAM;A;B;OME;GMSN;XP;PP
[1]   OME←2.92E¯6
[2]   GMSN←1.33E26
[3]   XI←((÷2)+÷BSTR)+((((÷2)+÷BSTR)*2)-(2×(2○PHISTR)*
     2)÷BSTR)*0.5
[4]   UST←(GMSN×OME÷GAM×ZETA)*÷3
[5]   RST←((GMSN×ZETA*2)÷GAM×OME*2)*÷3
[6]   PSI←3○PHISTR
[7]   DEL←PSI+ZETA
[8]   MU←(1-XI)÷(1-(XI÷((2○PHISTR)*2)))
[9]   SIG←(1+(PSI×1-MU)÷ZETA)*0.5
[10]  A←2+(XI×DEL*2)+(2×DEL×XI×MU×PSI÷1-MU)-GAM×XI
[11]  B←XI×(0.5×1+DEL*2)+(MU×PSI*2)+(5÷2×XI)-H+GAM+DEL
     ×MU×PSI
[12]  ALPH←A÷B
[13]  MASS←(1836×9.1066E¯28)+(0.05×
     6.6442E¯24)
[14]  BC←1.38E¯16
[15]  TST←(MASS×UST*2)÷(2×BC×XI)
[16]  XP←0,(-2×H),(2×MU×ZETA*2)
[17]  VINF←(CUBIC XP)[1]
[18]  'GAMMA:    ';GAM;'  RSTAR:     ';(RST÷
     69600000000);'  BETASTAR:    ';BSTR
[19]  ' PHISTAR:     ';PHISTR×(360÷○2);'  XI:    ';XI
[20]  ' H:    ';H;' USTAR:     ';UST
[21]  'ZETA:     ';ZETA;'      PSI:     ';PSI
[22]  'DELTA:    ';DEL;'      MU:    ';MU
[23]  'SIGMA:     ';SIG
[24]  ' ALPHA:     ';ALPH;'   TSTAR:      ';TST;'       U
     INF:      ';(VINF×UST)
    ∇
```

```
      ∇START[□]∇
    ∇ START;A1;A2;B1;B2;C1;C2;C3;C4;C5;D1;D2;P;E1;Q;F1
      ;F2;R;S;T
[1]   DODZST←2+(XI×DEL*2)+(2×DEL×XI×MU×PSI÷1-MU)-GAM×
      XI
[2]   A1←((3×MU)-1+(1+MU)×SIG*2)÷(1-MU)×(¯1+SIG*
      2)
[3]   A2←-÷(1-MU)
[4]   B1←ZETA+A1×PSI
[5]   B2←PSI×1+A2
[6]   C1←1+MU×PSI*2
[7]   C2←(DEL*2)-DEL×MU×PSI
[8]   C3←(2×MU×PSI)-DEL×MU
[9]   C4←5÷2×XI
[10]  C5←(2×DEL×MU×PSI)+GAM-2×MU×PSI*2
[11]  D1←(ALPH×XI×C1)+(B2×C2×ALPH×XI÷DEL)+A2×(P←(ALPH×
      XI×C3×PSI)+DODZST×2×(10PHISTR)*2)
[12]  D2←(ALPH×XI×C2×B1÷DEL)+(A1×P)+(((ALPH×XI×C4)-
      2)×DODZST)+(ALPH×XI×C5)-2.5×DODZST*2
[13]  E1←((Q←2×DEL×XI×MU×PSI÷(1-MU)*2)×((1-MU)×(A2+B2÷
      DEL))-MU)+(2×DEL×XI×B2)-D1
[14]  E2←(Q×((1-MU)×(A1+B1÷DEL))-2)+DODZST+(GAM×XI)+(
      2×DEL×XI×B1)-D2
[15]  F1←(2×XI)-(R←(XI×MU×PSI*2)÷(1-MU)*2)×(2×A2-(MU×
      A2)+MU)+1
[16]  F2←-DODZST+2×R×(A1×1-MU)-1
[17]  S←(E1-F2)÷2×F1
[18]  T←((S*2)+E2÷F1)*0.5
[19]  DVDZST1←S+T
[20]  DVDZST2←S-T
[21]  'DVDZST1     ';DVDZST1
[22]  'DVDZST2     ';DVDZST2
[23]  'DODZST      ';DODZST
[24]  VS←1+DVDZST1×0.0001
[25]  THETAS←1+DODZST×0.0001
[26]  ZS←1+0.0001
[27]  XS←÷ZS
[28]  TP←GAM,BSTR,ZETA,H,PHISTR
[29]  TN←MU,XI,DEL,SIG,ALPH,UST,TST,RST
      ∇
```

```
      ∇SOLWIND2[□]∇
    ∇ SOLWIND2;X;Y;K;D;I;J;FV1;L;R1;R2;R3;R4;R5;R6
[1]   IV1←XS,VS,THETAS
[2]   ZF←VF←WF←THETAF←DODZF←PHIF←BETAF←ι0
[3]   X←IV1[1],IC[1],(÷IC[2])
[4]   Y←IV1[3],IV1[2]
[5]   I←ZS
[6]   R1←ALPH×XI×(2○PHISTR)*2
[7]   R2←XI×ZETA*2
[8]   R3←ZETA*2
[9]   R4←GAM×XI
[10] CDP:K←(4,ρ,Y)ρL←X[J←1] DER M←Y
[11]  →((L[1]=0)×(L[2]=0))/CJP
[12]  →(L[1]<0)/CHP
[13] CEP:→(J<3+ρρρK[J;]←JL←(X[1]+D) DER M←Y+K[
      ¯1+J←J+1;]×D←X[2]÷ 2 2 1[J])/CEP
[14]  FV1←(X[1]←+/X[ι2]),Y←Y+(X[2]÷6)×+/[1] K[
      1 2 2 3 3 4 ;]
[15] CKP:→((÷FV1[1])≥I)/CFP
[16] COP:→((X[2]×X[3]-X[1])>0)/CDP
[17]  MA←2
[18]  →CGP
[19] CFP:ZF←ZF,(÷FV1[1])
[20]  I←ZF[ρ,ZF]×1+IC[3]
[21]  VF←VF,FV1[3]
[22]  THETAF←THETAF,FV1[2]
[23]  DODZF←DODZF,(-L[1]×FV1[1]*2)
[24]  →((ρDODZF)=1)/MHA
[25]  →((|DODZF[ρDODZF])>(|DODZF[(ρDODZF)-1]))/CJP
[26] MHA:→COP
[27] CHP:'DODZ POS.'
[28]  MA←1
[29]  →CGP
[30] CJP:'TEMP.<0 OR DODZ INCREASING'
[31]  MA←0
[32]  →CGP
[33] CGP:PHIF←(¯3○((ZETA×(SIG*2)-ZF*2)÷(VF×ZF)-MU÷ZF))
      +○1
[34]  WF←((VF×3○PHIF)+ZETA×ZF)÷DEL
[35]  BETAF←((BSTR×(1+PSI*2)×ZF*2)÷VF×(1+(3○PHIF)*
      2))×THETAF
    ∇
```

```
      ∇DER[□]∇
    ∇ Z←X DER M;M1;M2;Y1;Y2;T;P;A;B;C
[1]   →(M[1]<0)/D1
[2]   P←-(ZETA÷M[2]×X)×(A←1-X×X×SIG*2)×B←÷1-MU×X×X÷M[
      2]
[3]   M1←-(R1×1+P×P)÷M[1]*2.5
[4]   M2←(0.5×(M[2]-VINF)×M[2]+VINF)+(
      2.5×M[1]÷XI)-(GAM×X)-C←0.5×R3×X×X×B×B×((SIG*
      2)-MU÷M[2])*2
[5]   M2←M2+MU×R3×(A×B÷M[2])-÷VINF
[6]   Y1←(2×C×XI)+((2×MU×R2÷M[2])×(A×A×B*3)-A×B×B)+(X×
      M1×M2)+(2×M[1])-X×R4
[7]   Y2←(XI×M[2]×M[2])-M[1]+R2×MU×A×A×(B*3)÷M[
      2]
[8]   Z←(M1×M2),(-Y1×M[2]÷X×Y2)
[9]   →0
[10] D1:Z← 0 0
      ∇
```

```
      ∇SOLWIND3[□]∇
    ∇ SOLWIND3;X;Y;AN;K;I;L;JL;FV;D
[1]   GPER←(TSOL[2]×TSOL[1]*2)×(XI*0.5)×TSOL[3]×2×
      0.03914713205×(2○TSOL[5])×TSOL[6]÷ALPH×((2○PHISTR)*
      2)×1+G÷2
[2]   GPAR←G×GPER
[3]   'GPAR     ';GPAR;'  GPER     ';GPER
[4]   QPL1←GPAR×TSOL[3]×((TSOL[3]÷XI)*0.5)÷2×TSOL[2]×TSOL[1]*
      2
[5]   QPR1←QPL1×2×GPER÷GPAR
[6]   ZF←VF←WX←TPL←TPR←QPL←QPR←TE←DTEDZ←BETAF←PHIF←DODZF←THETAF←
      WF←⍳0
[7]   X←(÷TSOL[1]),IC[1],(÷IC[4])
[8]   Y←TSOL[2],(TSOL[4]÷TSOL[1]),(2⍴TSOL[3]),QPL1,QPR1,TSOL[
      3]
[9]   I←TSOL[1]
[10]  ALPHE←ALPH×1.04074206
[11]  AN←(ALPHE×(2○PHISTR)*2),(0.5×XI×DEL*2),(H×XI),(GAM×XI),(
      ZETA×XI×MU),(XI×MU),(XI×DEL*2),(2×DEL)
[12] CDP:K←(4,⍴,Y)⍴L←X[J←1] DERA M←Y
[13]  →((+/L)=0)/CJP
[14]  →(L[7]<0)/CHP
[15] CEP:→(J<3+⍴⍴⍴X[J;]←JL←(X[1]+D) DERA M←Y+K[¯1+J←J+1;]×D←X[
      2]÷ 2 2 2 1[J])/CEP
[16]  FV←(X[1]←+/X[⍳2]),Y←Y+(X[2]÷6)×+/[1] X[1 2 2 3 3
      4 ;]
[17] CKP:→((÷FV[1])≥I)/CFP
[18] COP:→((X[2]×X[3]-X[1])>0)/CDP
[19]  MA←2
[20]  →CGP
[21] CFP:ZF←ZF,(÷FV[1])
[22]  VF←VF,FV[2]
[23]  I←ZF[⍴,ZF]×1+IC[3]
[24]  WX←WX,FV[3]
[25]  TPL←TPL,FV[4]
[26]  TPR←TPR,FV[5]
[27]  QPL←QPL,FV[6]
[28]  QPR←QPR,FV[7]
[29]  TE←TE,FV[8]
[30]  DTEDZ←DTEDZ,(-L[7]×FV[1]*2)
[31]  →((⍴DTEDZ)=1)/MHA
[32]  →((|DTEDZ[⍴DTEDZ])>(|DTEDZ[¯1+⍴DTEDZ]))/CJP
[33] MHA:→COP
[34] CHP:'DTEDZ POS.'
[35]  MA←1
[36]  →CGP
[37] CJP:'TEMP<0 OR DTEDZ INCR.'
[38]  MA←0
[39]  →CGP
[40] CGP:PHIF←(¯3○(ZF÷VF)×(DEL×WX)-ZETA)+○1
[41]  BETAF←0.5×((BSTR×(1+PSI*2)×ZF*2)÷VF×(1+(3○PHIF)*2))×TE+((
      2×TPR)+TPL)÷3)
    ∇
```

```
      ∇DERA[□]∇
    ∇ Z←X DERA M;M1;M2;A;B;C;D;E;F;MX;SL;MX1;MX2;MX3;MX4;MX5;MX6
      ;MX7
[1]   →(M[7]<0)/D11
[2]   C2FI←1-2×SFI2←1-CFI2←÷1+TFI2←TFI×TFI←(÷M[1]×X)×(DEL×M[
      2])-ZETA
[3]   S2FI←2×(SFI←SFI2*0.5)×(CFI←-CFI2*0.5)
[4]   M1←-(AN[1]×1+TFI2)÷M[7]*2.5
[5]   M2←(0.5×A←XI×M[1]*2)+(AN[2]×(M[2]*2)÷B←X*2)+(
      0.25×(5×M[7])+(4×M[4])+M[3])+0.5×CFI2×M[3]-M[4]
[6]   M2←M2+(((C←DEL×S2FI÷M[1]×X)×M[2]×M[3]-M[4])÷4)+((M[
      5]+M[6])×|CFI÷2×B)-AN[3]+(AN[4]×X)+AN[5]×TFI×X
[7]   A11←A-((D←AN[6]×M[1]×B)×TFI2)+0.5×(M[4]×SFI2×1+2×CFI2)+(M[
      3]×CFI2×1-2×SFI2)+M[7]
[8]   A12←-(DEL÷X)×(0.5×(M[3]-M[4])×S2FI×CFI2)-D×TFI
[9]   A13←M[1]×CFI2÷2
[10]  A14←M[1]×SFI2÷2
[11]  A17←-(M[1]÷X)×(X×M1×M2÷2)+M[7]+M[4]+(
      0.5×SFI2×(1+2×CFI2)×M[3]-M[4])+(AN[7]×(M[2]÷X)*2)-AN[
      4]×X
[12]  MX1←A11,A12,A13,A14,0,0
[13]  A21←(0.5×S2FI×CFI2×M[3]-M[4])-D×TFI
[14]  A22←-(DEL÷X)×A+(0.5×C2FI×CFI2×M[3]-M[4])-D
[15]  A24←¯1×A23←-M[1]×S2FI÷4
[16]  A27←-((M[1]×S2FI×CFI2×M[3]-M[4])÷2×X)+AN[8]×A×M[2]÷B
[17]  MX2←A21,A22,A23,A24,0,0
[18]  A31←(2×CFI÷M[1])×(M[3]×CFI×1-3×M[4]×SFI2÷4×A)-CFI2×E←
      4×M[5]÷B
[19]  A32←(C÷2)×(M[3]×1+6×M[4]×CFI2÷4×A)-2×E×CFI
[20]  A33←1-6×M[3]×CFI2÷4×A
[21]  A37←-((2×M[3]÷X)×((3×M[4]×CFI2×1+CFI2)÷4×A)-SFI2)+
      2×E×CFI×SFI2÷X
[22]  MX3←A31,A32,A33,0,0,0
[23]  A41←((M[6]×CFI×1+CFI2)÷M[1]×B)+(M[4]×SFI2×(M[4]×CFI2÷
      2×A)-1)÷M[1]
[24]  A42←(C÷2)×(M[6]×CFI÷B)+M[4]×1-M[4]×CFI2÷2×A
[25]  A44←(M[3]×CFI2÷2×A)-1
[26]  A47←-((M[6]×CFI×CFI2-3)÷X×B)+(M[4]×(1+CFI2)×1-M[4]×CFI2÷
      2×A)÷X
[27]  MX4←A41,A42,0,A44,0,0
[28]  A51←(2×CFI÷M[1])×(M[3]×CFI)+M[5]×SFI2÷B
[29]  A52←(C÷2)×M[3]-CFI×E÷2
[30]  A53←1
[31]  A55←2×CFI÷B
[32]  A57←(2÷X)×(M[3]×SFI2)+(M[5]×CFI×1+CFI2)÷B
[33]  MX5←A51,A52,A53,0,A55,0
[34]  A61←(SFI2÷M[1])×F←M[4]+M[6]×CFI÷B
[35]  A62←-C×F÷2
[36]  A64←1
[37]  A66←CFI÷B
[38]  A67←(1+CFI2)×F÷X
[39]  MX6←A61,A62,0,A64,0,A66
[40]  MX7←A17,A27,A37,A47,A57,A67
```

```
[41]   SL←⎕MX←(6,6)ρMX1,MX2,MX3,MX4,MX5,MX6
[42]   Z←(SL+.×MX7),(M1×M2)
[43]   →0
[44] D11:Z←7ρ0
       ∇


       ∇NQTF[□]∇
     ∇ NQTF K;Z1;V1;PHI1;Z;V;PHI;NST;NF;BF;Q1;QE;F;A;QL;QR;PRF;W;
       KEF
[1]    Z1←MAT[;1]×69600000000÷RST
[2]    BNQ←⍳0
[3]    V1←MAT[;2]÷UST
[4]    PHI1←○2×MAT[;6]÷360
[5]    Z←Z1,ZF
[6]    V←V1,VF
[7]    W←MAT[;3],FGA[3;]
[8]    PHI←PHI1,PHIF
[9]    NST←(ALPH×K×(TST*2.5)×(2○PHISTR)*2)÷2×UST×RST×BC
[10]   NF←NST÷V×Z*2
[11]   BF←((MU×○4×MASS×NST×UST*2)*0.5)÷(Z*2)×|2○PHI
[12]   Q1←-K×(MAT[;4]*2.5)×MAT[;5]×TST÷RST
[13]   QE←-K×((TE×TST)*2.5)×DTEDZ×TST÷RST×1.04
[14]   F←H×NST×UST×(RST*2)×MASS×UST*2
[15]   'TOTAL ENERGY FLUX        ';F;'       F/R *2     :     ';F÷(
       214×69600000000)*2
[16]   QL←QPL×A←NST×BC×TST×UST
[17]   QR←QPR×A
[18]   PRF←(((Z×RST×BF)*2)×(UST×V×(1○PHI)*2)-W×(1○PHI)×(
       2○PHI))÷○4
[19]   KEF←(MASS×NF×V×UST×(Z×RST)*2)×0.5×((V×UST)+W)*2
[20]   BNQ← 2 1 ⍉(8,ρZ)ρ(Z×RST÷69600000000),NF,BF,Q1,QE,P,QL,(P←(
       ρQ1)ρ0),QR,PRF,KEF
     ∇

       ∇RATIOS[□]∇
     ∇ RATIOS
[1]    PL←□← 2 1 ⍉(4,ρTPL)ρFGA[1;],(TPL÷TPR),((TPL+2×TPR)×TST÷
       3),((TPL+2×TPR)÷3×TE)
     ∇

       ∇DFP[□]∇
     ∇ DFP;GPL;GPR
[1]    GPL←(2×QPL×(VF×ZF*2)×(XI÷TPL)*0.5)÷TPL
[2]    GPR←(QPR×(VF×ZF*2)×(XI÷TPL)*0.5)÷TPR
[3]    □← 2 1 ⍉(5,ρGPL)ρFGA[1;],GPL,GPR,(TPL÷TPR),(TPL×TST)
     ∇
```

```
      ∇ASOLAN[□]∇
    ∇ ASOLAN;P;S
[1]     PARAM1
[2]     PARAM
[3]     P←(1.5×VINF*2)-H
[4]     S←(1.5×VINF*2)+H
[5]     EO←TSOLA[1]*-÷3
[6]     TSOLA[9]←TSOLA[9]×TSOLA[1]
[7]     A←0,A←TSOLA[7 3 4 5 6 9]÷EO* 4 6 3 15 12 3
[8]   BOL:COEFF
[9]     EOV←EO*0,⍳8
[10]    VV←C10,C11,0,C13,C14,C15,C16,C17,C18
[11]    TEV←1,0,C22,C23,C24,C25,C26,C27,0
[12]    TPLV←1,0,0,0,0,0,C36,0,0
[13]    TPRV←1,0,0,C43,C44,0,C46,C47,C48
[14]    QPLV←1,0,0,C53,C54,0,C56,C57,C58
[15]    QPRV←1,0,0,C63,C64,0,C66,C67,C68
[16]    DTV←4,0,(6×C22),(7×C23),(8×C24),(9×C25),(10×C26),(
        11×C27),0
[17]    WV←1,0,0,C73,C74,0,C76,C77,C78
[18]    A2←TSOLA[7]÷(EO*4)×+/TEV×EOV
[19]    A3←TSOLA[3]÷(EO*6)×+/TPLV×EOV
[20]    A4←TSOLA[4]÷(EO*3)×+/TPRV×EOV
[21]    A5←TSOLA[5]÷(EO*15)×+/QPLV×EOV
[22]    A6←TSOLA[6]÷(EO*12)×+/QPRV×EOV
[23]    A7←TSOLA[9]÷(EO*3)×+/WV×EOV
[24]    →((A2-A[2])≤0.001×A2)/BUR
[25]    A←0,A2,A3,A4,A5,A6,A7
[26]    →BOL
[27]  BUR:'ENTER MAX. Z AND PRINTOUT INTERVAL'
[28]    IV←□
[29]    'A VECTOR     ';A
[30]    ZF←VF←WF←BETAF←TPL←TPR←QPL←QPR←TE←DTEDZ←PHIF←⍳0
[31]    ET←TSOLA[1]*-÷3
[32]  COL:EPN←ET*0,⍳8
[33]    V←VINF×1+EPN[4]×+/VV×EPN
[34]    T←A2×EPN[5]×+/TEV×EPN
[35]    TPAR←A3×EPN[7]×+/TPLV×EPN
[36]    TPER←A4×EPN[4]×+/TPRV×EPN
[37]    QPAR←A5×(EPN[2]*15)×+/QPLV×EPN
[38]    QPER←A6×(EPN[2]*12)×+/QPRV×EPN
[39]    DT←-(A2÷3)×EPN[8]×+/DTV×EPN
[40]    W←A7×EPN[4]×+/WV×EPN
[41]    ZF←ZF,(ET*¯3)
[42]    VF←VF,V
[43]    DTEDZ←DTEDZ,DT
[44]    TE←TE,T
[45]    TPL←TPL,TPAR
[46]    TPR←TPR,TPER
```

```
[47]  QPL←QPL,QPAR
[48]  QPR←QPR,QPER
[49]  WF←WF,W
[50]  ET←(ZF[⍴,ZF]×1+IV[2])*-÷3
[51]  →(ZF[⍴,ZF]≤IV[1])/COL
[52]  PHIF←(¯3○((ZETA×(SIG*2)-ZF*2)÷(VF×ZF)-MU÷ZF))+○1
[53]  BETAF←0.5×((BSTR×(1+PSI*2)×ZF*2)÷VF×(1+(3○PHIF)*2))×TE+(((
      2×TPR)+TPL)÷3)
[54]  □← 2 1 ⍉FGA←(11,⍴ZF)⍴(ZF×RST÷69600000000),(VF×UST),(WF×DEL
      ×UST),(TPL×TST),(TPR×TST),QPL,QPR,(TE×TST),DTEDZ,(PHIF×
      360÷○2),BETAF
      ∇
```

```
      ∇PARAM1[□]∇
    ∇ PARAM1
[1]   GAM←TP[1]
[2]   BSTR←TP[2]
[3]   ZETA←TP[3]
[4]   H←TP[4]
[5]   PHISTR←TP[5]
    ∇
```

```
      ∇PARAM[□]∇
    ∇ PARAM;A;B;OME;GMSN;XP;BP
[1]   OME←2.92E¯6
[2]   GMSN←1.33E26
[3]   XI←((÷2)+÷BSTR)+((((÷2)+÷BSTR)*2)-(2×(2○PHISTR)*2)÷BSTR)*
      0.5
[4]   UST←(GMSN×OME÷GAM×ZETA)*÷3
[5]   RST←((GMSN×ZETA*2)÷GAM×OME*2)*÷3
[6]   PSI←3○PHISTR
[7]   DEL←PSI+ZETA
[8]   MU←(1-XI)÷(1-(XI÷((2○PHISTR)*2)))
[9]   SIG←(1+(PSI×1-MU)÷ZETA)*0.5
[10]  A←2+(XI×DEL*2)+(2×DEL×XI×MU×PSI÷1-MU)-GAM×XI
[11]  B←XI×(0.5×1+DEL*2)+(MU×PSI*2)+(5÷2×XI)-H+GAM+DEL×MU×PSI
[12]  ALPH←A÷B
[13]  MASS←(1836×9.1066E¯28)+(0.05×6.6442E¯24)
[14]  BC←1.38E¯16
[15]  TST←(MASS×UST*2)÷(2×BC×XI)
[16]  XP←0,(-2×H),(2×MU×ZETA*2)
[17]  VINF←(CUBIC XP)[1]
    ∇
```

```
      ∇COEFF[□]∇
    ∇ COEFF;M
[1]   C10←((GAM×XI)-A[4])÷M←XI×P
[2]   C11←-5×A[2]÷4×M
[3]   C22←(2×C10×A[4]+(XI×S×C10)-GAM×XI)÷A[2]
[4]   C13←((4×A[4]×C10)-A[3]+5×A[2]×C22)÷4×M
[5]   C23←((C11×(6×A[4]))+(14×XI×C10×S)-6×GAM×XI)-A[2]×C10)×
      11÷42×A[2]
[6]   C14←(-(5×A[2]×C23)-4×A[4]×C11)÷4×M
[7]   C24←C11×1+4×XI×C11×S÷3×A[2]
[8]   C15←-5×A[2]×C24÷4×M
[9]   C36←((4×A[5]÷A[3])-VINI÷ZETA)×VINF÷ZETA
[10]  C43←-C10
[11]  C44←-C11
[12]  C46←(C10*2)+(((1.5×A[6]÷A[4])+VINF÷2×ZETA)×VINF÷ZETA)-C13
[13]  C47←(2×C10×C11)-C14
[14]  C48←(C11*2)-C15
[15]  C25←((2×A[4]×C46)+((2×VINF÷ZETA)×(A[4]×VINF÷ZETA)-
      3×A[6])+2×C10×(6×XI×S×C13)+(3×A[2]×C22)+A[3]-2×A[
      4]÷C10)÷5×A[2]
[16]  C16←(((2×VINF÷ZETA)×A[6]-A[4]×VINF÷ZETA)-(4×A[4]×C46)+
      5×A[2]×C25)÷4×M
[17]  C26←(¯7×A[4]×C47)+(20×C10×(A[4]×(VINF*2)÷(ZETA*2))+(XI×S×
      C14)+A[2]×C23÷2)
[18]  C26←C26+(C11×(3×A[3])+(20×XI×S×C13)+(¯5×A[4]×C10)+
      8×A[2]×C22)+(4×A[2]×C13)-C14×(6×GAM×XI)+A[4]
[19]  C26←C26÷9×A[2]
[20]  C17←((¯5×A[2]×C26÷4)+(VINF*2)×A[4]×C10÷ZETA*2)÷M
[21]  C27←(¯16×A[4]×C48)+(¯2×C11×(22×A[4]×(VINF*2)÷(ZETA*
      2))+(22×XI×S×C14)+(¯6×A[4]×C11)+9×A[2]×C23)
[22]  C27←C27+(4×C15×A[4]+3×GAM×XI)-(C10×(44×XI×S×C15)+
      1650×A[2]×C24÷61)+4×A[2]×C14
[23]  C27←C27÷21×A[2]
[24]  C18←((¯5×A[2]×C27÷4)+(C11×A[4]×(VINF*2)÷(ZETA*2))-A[
      4]×C48)÷M
[25]  C53←-C10+3×A[3]×A[4]÷4×XI×ZETA×VINF×A[5]
[26]  C54←-C11
[27]  C56←(3×(A[3]*2)÷4×XI×ZETA×VINF×A[5])+(3×(VINF*2)÷
      2×ZETA*2)-C13+C10×C10+2×C53
[28]  C57←-C14+2×C11×C53
[29]  C58←(C11*2)-C15
[30]  C63←-(2×C10)+(A[4]*2)÷2×XI×ZETA×VINF×A[6]
[31]  C64←-2×C11
[32]  C66←(¯2×C10×(2×C63)+C10)+(¯2×C13)+A[3]×A[4]÷4×XI×ZETA×VINF
      ×A[6]
[33]  C67←(6×C10×C11÷7)+(¯2×C14)-18×C11×C63÷7
[34]  C68←(¯3×C11×C64÷2)-2×C15
[35]  C73←((C10×MU×ZETA÷VINF)-A[4]÷2×XI×ZETA)÷DEL×A[7]
[36]  C74←C11×MU×ZETA÷DEL×VINF×A[7]
[37]  C76←(C13×MU×ZETA÷DEL×VINF×A[7])+(MU÷VINF)+(A[3]÷2×DEL×ZETA
      ×XI×A[7])-C10×C73
[38]  C77←(C14×MU×ZETA÷DEL×VINF)+(A[4]÷14×DEL×ZETA×XI×A[
      7])-(6×C11×C73÷7)+8×C74×C10÷7
[39]  C78←(C15×MU×ZETA÷DEL×VINF×A[7])-C11×C74
    ∇
```

```
      ∇NQTF[□]∇
    ∇ NQTF K;Z1;V1;PHI1;Z;V;PHI;NST;NF;BF;Q1;QE;F;A;QL;QR;PRF;W;
      KEF
[1]   Z1←⍳0
[2]   BNQ←⍳0
[3]   V1←⍳0
[4]   PHI1←⍳0
[5]   Z←Z1,ZF
[6]   V←V1,VF
[7]   W←,FGA[3;]
[8]   PHI←PHI1,PHIF
[9]   NST←(ALPH×K×(TST*2.5)×(2○PHISTR)*2)÷2×UST×RST×BC
[10]  NF←NST÷V×Z*2
[11]  BF←((MU×○4×MASS×NST×UST*2)*0.5)÷(Z*2)×|2○PHI
[12]  Q1←⍳0
[13]  QE←-K×((TE×TST)*2.5)×DTEDZ×TST÷RST×1.04
[14]  F←H×NST×UST×(RST*2)×MASS×UST*2
[15]  'TOTAL ENERGY FLUX        ';F
[16]  QL←QPL×A←NST×BC×TST×UST
[17]  QR←QPR×A
[18]  PRF←(((Z×RST×BF)*2)×(UST×V×(1○PHI)*2)-W×(1○PHI)×(
      2○PHI))÷○4
[19]  KEF←(MASS×NF×V×UST×(Z×RST)*2)×0.5×((V×UST)+W)*2
[20]  BNQA← 2 1 ⍉(8,⍴Z)⍴(Z×RST÷69600000000),NF,BF,Q1,QE,P,QL,(P←
      (⍴Q1)⍴0),QR,PRF,KEF
    ∇


      ∇RATIOS[□]∇
    ∇ RATIOS
[1]   PL←□← 2 1 ⍉(4,⍴TPL)⍴FGA[1;],(TPL÷TPR),((TPL+2×TPR)×TST÷
      3),((TPL+2×TPR)÷3×TE)
    ∇


      ∇DFP[□]∇
    ∇ DFP;GPL;GPR
[1]   GPL←(2×QPL×(VF×ZF*2)×(XI÷TPL)*0.5)÷TPL
[2]   GPR←(QPR×(VF×ZF*2)×(XI÷TPL)*0.5)÷TPR
[3]   □← 2 1 ⍉(5,⍴GPL)⍴FGA[1;],GPL,GPR,(TPL÷TPR),(TPL×TST)
    ∇
```

```
      ∇FUN[□]∇
    ∇ FUN;H;I;J;PHI;M;XIO;K
[1]   'ENTER GPAR, GPER, TPAR, TPER'
[2]   IN←□
[3]   M←IN[3]÷IN[4]
[4]   XIO←0.001 ZERO ¯1 0.001
[5]   H←(*-XIO*2)×1+(IN[1]×XIO×((2×XIO*2)÷3)-1)-2×IN[2]×XIO
[6]   K←H×0.1×ι9
[7]   PHI←(-○1÷2)+○1×(÷18)×ι18
[8]   LP←((ρK),ρPHI)ρ0
[9]   I←J←1
[10] CO1:LP[I;J]←0.001 ZEROP 4 0
[11]  J←J+1
[12]  →(J≤ρPHI)/CO1
[13]  I←I+J←1
[14]  →(I≤ρK)/CO1
[15]  LP← 2 1 ⍉((1+ρK),ρPHI)ρ(PHI×360÷○2),,LP
[16]  'SCALE FACTOR'
[17]  □←S←(2×1.38E¯16×IN[3]÷MASS)*0.5
[18]  □←S×(÷M)*0.5
[19]  LP
    ∇

      ∇F[□]∇
    ∇ Z←F X
[1]   Z←(((4÷3)×GAM[1])×X*4)+(X×2-GAM[1])+GAM[1]+(2×GAM[
      2])-(X*2)×(2×GAM[1])+4×GAM[2]
    ∇

      ∇G[□]∇
    ∇ Z←G X;A;B
[1]   Z←K[I]-(*-(A*2)+B)×1+(IN[1]×A×(¯1+2×(A*2)÷3))+2×IN[
      2]×(A←XIO+X×1○PHI[J])×(¯1+B←M×(X×2○PHI[J])*2)
    ∇

      ∇ZERO[□]∇
    ∇ Z←TOL ZERO B;T
[1]   →0×ιTOL≥|T←F Z←0.5×+/B
[2]   →1,B[2⊥(0<T)≠0<F B]←Z
    ∇

      ∇ZEROP[□]∇
    ∇ Z←TOL ZEROP B;T
[1]   →0×ιTOL≥|T←G Z←0.5×+/B
[2]   →1,B[2⊥(0<T)≠0<G B]←Z
    ∇
```

REFERENCES

Axford, W.I., 1968, Space Sci. Rev., 8, 331.

Axford, W.I., Dessler, A.J. and Gottlieb, B., 1963, Astrophys. J., 137 1268.

Barnes, A., 1968, Astrophys. J., 154, 751.

Barnes, A., Hartle R.E., and Bredekamp, J.H., 1971, Astrophys. J., 166 L53.

Belcher, J.W., 1971, Astrophys. J., 168, 509.

Biermann, L., 1951, Z. Astrophys., 29, 274.

Braginskii, S.I., 1965, Reviews of Plasma Physics, Vol. 1, Consultants Bureau, New York.

Brandt, J.C. and Casinelli, J.P., 1966, Icarus, 5, 47.

Burlaga, L.F., 1971, The Solar Envelope, NASA-GSFC X-692-71-400.

Chamberlain, J.W., 1960, Astrophys. J., 131, 47.

Chen, W.M., Lai, C.S., Lin, H.E. and Lin, W.C., 1972, J. Geophys. Res., 77, 1.

Chew, G.F., Goldberger, M.L. and Low, F.E., 1956, Proc. Roy. Soc. London, A236, 112.

Clauser, F.H., 1960, John Hopkins University Lab. Report, AFOSR TN 60-1386.

Clemmow, P.C., and Dougherty, J.P., 1969, Electrodynamics of Particles and Plasmas, Addison-Wesley, London

Dessler, A.J., 1967, Rev. Geophys., 5, 1.

Durney, B., 1971, Astrophys. J., 166, 669.

Gentry, R.A. and Hundhausen, A.J., 1969, Trans. AGU, 50, 302.

Hartle, R.E. and Sturrock, P.A., 1968, Astrophys. J., 151, 1155.

Hollweg, J.V., 1970, J. Geophys. Res., 75, 2403.

Hollweg, J.V., 1971, J. Geophys. Res., 76, 7491.

Hollweg, J.V., 1972, Max Planck Institut fur Physik und Astrophysik, internal report.

Hollweg, J.V., and Jokipii, J.R., 1972, J. Geophys. Res., 77, 3311.

Hundhausen, A.J., 1968, Space Sci. Rev., 8, 690.

Hundhausen, A.J., 1970, Rev. Geophys. Space Phys., 8, 729.

Hundhausen, A.J., 1971, Proc. of the Fourth Summer Institute for Astronomy and Astrophysics, Stony Brook.

Hundhausen, A.J., 1972, Coronal Expansion and Solar Wind, Springer-Verlag, New York.

Hung, R.J., and Barnes, A., 1973, Astrophys. J., 180, 253.

Iverson, K.E., 1962, A Programming Language, John Wiley, New York.

Jockers, K., 1970, Astron, Astrophys., 6, 219.

Jokipii, J.R., 1972, Ann. Rev. Astron. Astrophys., Vol. II, in press.

Krall, N.A. and Trivelpiece, A.W., 1973, Principles of Plasma Physics, McGraw-Hill, New York.

Leer, E. and Holzer, T.E., 1972, J. Geophys. Res., 77, 4035.

Modisette, J.L., 1972, Astrophys. J., 174, 151.

Montgomery, M.D., 1971, Proc. of the Solar Wind Conference, Asilomar. Pacific Grove, Calif. NASA SP-308.

Ness, N.F., 1967, Ann. Rev. Astron. Astrophys., 6, 79.

Ness, N.F. and Wilcox, J.M., 1967, Solar Phys., 2, 351.

Neugebauer, M. and Snyder, C.W., 1962, Science, 138, 1095.

Newkirk, G., 1967, Ann. Rev. Astron. Astrophys., 5, 213.

Noble, L.M. and Scarf, F.L., 1963, Astrophys. J., 138, 1169.

Olvie, K.W., Burlaga, L.F. and Wilkerson, T.D., 1968, J. Geophys. Res., 73, 6809.

Papadopoulos, K., 1973, Astrophys. J., 179, 939.

Parker, E.N., 1958, Astrophys. J., 128, 664.

Parker, E.N., 1960, Astrophys. J., 132, 821.

Parker, E.N., 1965, Space Sci. Rev., 4, 666.

Parker, E.N., 1971, Rev. Geophys. Space Phys., 9, 825.

Perkins, F., 1973, Astrophys. J., 179, 637.

Pneuman, G.W., 1966, Astrophys. J., 145, 800.

Scarf, F.L. and Noble, L.M., 1964, AIAA J., 2, 1158.

Snyder, C.W., Neugebauer, M. and Rao, U.R., 1963, J. Geophys. Res., 68, 6361.

Spitzer, L., 1962, Physics of Fully Ionized Gases, Interscience, New York.

Spreiter, J.R. and Rizzi, A.W., 1972, Proc. of the Eighth International Symposium on Rarefied Gas Dynamics, in press.

Sturrock, P.A. and Hartle, R.E., 1966, Phys. Rev. Letters, 16, 628.

Toichi, T., 1971, Solar Phys. 18, 150.

Urch, I.H., 1969, Solar Phys. 10, 219.

Urch, I.H., 1972, Cosmic Electrodyn., 3, 316.

Weber, E.J. and Davis. L., 1967, Astrophys. J., 148, 217.

Weber, E.J., 1967, Ph.D. Thesis, California Institute of Technology.

Weber, E.J. and Davis, L., 1970, J. Geophys. Res., 75, 2419.

Whang, Y.C. and Chang, C.C., 1965, J. Geophys. Res., 70, 4175.

Whang, Y.C., Liu, C.K. and Chang, C.C., 1966, Astrophys. J., 145, 255.

Whang, Y.C., 1971a., Astrophys. J., 169, 369.

Whang, Y.C., 1971b., J. Geophys. Res., 76, 7503.

Whang, Y.C., 1971c., Private Communication.

Whang, Y.C., 1972, Astrophys. J., 178, 221.

Wolff, C.L., Brandt, J.C. and Southwick, R.G., 1971, Astrophys. J., 165, 181.